Nonlinear finite element simulation of non-local tension softening for high strength steel material.

Tong, F. M

Swansea University
Prifysgol Abertawe

Nonlinear Finite Element Simulation of Non-local Tension Softening for High Strength Steel Material

By

F.M. TONG

Supervisor:

Dr. R.Y.Xiao

Civil and Computational Engineering Centre (C^2EC)

School of Engineering

Singleton Park,

Swansea. SA2 8PP United Kingdom

The LORD is my shepherd; I shall not be in want.

He makes me lie down in green pastures,

He leads me beside quiet waters,

He restores my soul.

~ psalm 23:1-3 ~

DECLARATION

This work has not previously been accepted in substance for any degree and is not being currently submitted in candidature for any degree.

Signed..... (Candidate)

Date..... 01 SEPT 2008

STATEMENT 1

This dissertation is being submitted in partial fulfilment of the requirements for the degree of M.Phil. in the School of Engineering.

Signed..... (Candidate)

Date 01 SEPT 2008

STATEMENT 2

This dissertation is the result of my own independent work/investigation, expect where otherwise stated. Other sources are acknowledged by bracket '[]' giving explicit references. A bibliography is appended.

Signed..... (Candidate)

Date 01 SEPT 2008

STATEMENT 3

I hereby give consent for my thesis, if accepted, to be available for photocopying and for inter-library loan, and for the title and summary to be made available to outside organisations.

Signed..... (Candidate)

Date 01 SEPT 2008

Acknowledgements

First and foremost, utmost gratitude and love to my family back home who has been encouraging and supportive of my chosen path. Thank you for all the love and care you have shown to me throughout my life.

To my supervisor Dr. R.Y. Xiao, who has given all his support and motivation on my research subject, I reserved my appreciation to him. He and other colleagues particularly Dr. C.S. Chin, S. Baharom, S. Taufik and W. Almajed have been influential and helpful in my research. I thank them for all the supports, valuable hints and interests shown to my research.

Also not forgetting Professor X.L Zhao from Monash University for his patience contemplating my engineering queries and also for making experimental data available for my research. Thank you.

Last but not least, my family in Christ, whom we share and being part of the amazing grace; I treasure the time as we walk this journey of faith. And above all, to the One who has been ever so good to me, all glory to You!

Summary

The capability of current finite element softwares in simulating the stress – strain relation beyond the elastic-plastic region has been limited by the inability for non-positivity in the computational finite elements' stiffness matrixes. Although analysis up to the peak stress has been proved adequate for analysis and design, it provides no indication of the possible failure predicament that is to follow. Therefore an attempt was made to develop a modelling technique capable of capturing the complete stress-deformation response in an analysis beyond the limit point. This proposed model characterizes a cyclic loading and unloading procedure, as observed in a typical laboratory uniaxial cyclic test, along with a series of material properties updates. The Voce equation and a polynomial function were proposed to define the monotonic elasto-plastic hardening and softening behaviour respectively. A modified form of the Voce equation was used to capture the reloading response in the softening region. To accommodate the reduced load capacity of the material at each subsequent softening point, an optimization macro was written to control this optimum load at which the material could withstand. This preliminary study has ignored geometrical effect and is thus incapable of capturing the localized necking phenomenon that accompanies many ductile materials. The current softening model is sufficient if a global measure is considered. Several validation cases were performed to investigate the feasibility of the modelling technique and the results have been proved satisfactory. The ANSYS finite element software is used as the platform at which the modelling technique operates.

Notations

σ	-	Engineering stress
ε	-	Engineering strain
ε_p	-	Engineering strain at peak stress
σ_t	-	True stress
ε_t	-	True (logarithmic) strain
P	-	Applied load
A_0	-	Initial cross-sectional area of a tensile specimen
A		Final (current) cross-sectional area of tensile specimen
ΔL	-	Incremental (decrement) in specimen length
L_0	-	Initial length of tensile specimen
L	-	Final (current) length of tensile specimen
$[K]$	-	Stiffness matrix
$\left[K_i^T\right]$	-	Tangent (Jacobian) matrix
$\{u_i\}$	-	Displacement vector at *i*-step
$\{\Delta u_i\}$	-	Incremental displacement vector of *i*-step
$\{F^a\}$	-	Vector of applied loads
$\{F_i^{nr}\}$	-	Vector of restoring loads corresponding to the element internal loads
$D_{i,j}$	-	General form representing stiffness and element matrixes of row *i* and column *j*
r_1	-	Reference arc-length radius
σ_u	-	True stress at onset of necking
ε_u	-	True (logarithmic) strain at onset of necking
w	-	Weighted average constant

$\overset{\square}{f}$	-	Evolution function for the node separation method
C	-	Critical void volume fraction
k_0	-	Elastic limit
R_0	-	Plastic hardening modulus
R_∞	-	Asymptotic stress
b	-	Voce characteristic parameter
ε^{pl}	-	Equivalent plastic strain
f_t	-	Ultimate tensile strength of concrete
α, β	-	Characteristic parameters for FRC softening branch proposed by Zongjin Li and co.
ε_{ij}	-	Total strain tensor
ε_{ij}^{e}	-	Elastic strain tensor
ε_{ij}^{p}	-	Plastic strain tensor
σ_{ij}	-	Stress tensor
[D]	-	3-dimensional uniaxial isotropic elasticity matrix
υ	-	Poisson's ratio
$f(\sigma)$	-	Failure criterion
$\sigma_1, \sigma_2, \sigma_3$	-	Principle stress
κ_y	-	Maximum shear stress
k	-	Work hardening parameter
$d\lambda$	-	Plastic multiplier
Q	-	Plastic potential
σ_{eff}	-	Effective (Von Mises) stress
σ_{Y0}	-	Initial yield stress
H	-	Plastic hardening modulus (Equivalent to R_0 in the Voce function)
α	-	Evolution parameter in isotropic hardening
R	-	Strain ratio

σ_{ult} - Ultimate tensile strength

R_0^{soft} - Plastic softening modulus

R_∞^{soft} - Asymptotic softening modulus

b^{soft} - Modified Voce characteristic softening parameter

C_i - Nonlinear elasto-plastic polynomial constants; where $0 < i < 7$

E - Initial Young's modulus

E_T - Instantaneous elasto-plastic tangent modulus

k_0^* - Elastic limit for reloading

R_0^* - Plastic hardening modulus for reloading

R_∞^* - Asymptotic stress for reloading

b^* - Voce characteristic parameter for reloading

ψ - Ratio of elastic limit to ultimate strength

List of Figures

Figure 1.1 – A Typical Tensile Test Specimen

Figure 1.2 – A Typical Engineering Stress-Strain Curve with a Ductile Failure Mode from onset of Loading to Fracture [3]

Figure 1.3 – A Comparison between the True and Engineering Stress-Strain Curves of a Ductile Steel Material

Figure 1.4 – Newton-Raphson Solution Iteration

Figure 2.1 – The Arc-length Method Iteration Procedure

Figure 2.2 – True stress-true strain plot of a sample. The log-log presentation shows that the power law extrapolation tends to underestimate the true stress

Figure 2.3 – a) Load-engineering strain comparison between experimental and several applied weighted average constants, *w* used in FEA. b) The corresponding true stress-true plastic strain curve. Sample – C260 Extra Hd-Longitudinal Copper strip-shape test piece

Figure 2.4 – [Left] Experimental Fracture mode [Right] Node Separation Method Deformed Mesh of a) Steel; b) Copper; c) Aluminium

Figure 2.5 – The load-nominal strain relationship from experimental and the node separation approach for a) Steel b) Copper c) Aluminium

Figure 2.6 – Load-displacement diagram, with medium mesh of unregularized a) 5-teeth b) 10-teeth c) 20-teeth

Figure 2.7 – Load-displacement diagram, with unregularized 20-teeth of a) very coarse b) medium c) very fine meshes

Figure 2.8 – A load-displacement response captured by adopting 20 teeth, medium mesh and the mesh regularization procedure

Figure 2.9 – Experimental and Numerical models comparison of complete stress-deformation response of a) throated prismatic b) rectangular plate c) throated square plate specimens.

Figure 3.1 – a) Tresca and b) Von Mises Yield Surfaces

Figure 4.1 – Force-displacement diagram of a) monotonic and b) cyclic loaded steel bar

Figure 4.2 – A typical $\sigma_t - R$ curve, obtained from tensile tests on Electrolytic and Phosphorus Deoxidised Coppers

Figure 4.3 – Elasto-plastic hardening fillets due to variation of constant b

Figure 4.4 – Voce Nonlinear Hardening Stress- Plastic Strain Curve

Figure 4.5 – SOLID185 Structural solid geometry

Figure 5.1 – The Element Mesh of specimen G1X1A with its applied boundary condition(s).

Figure 5.2 – Stress-Deformation Response of specimen G1X1A Steel a) cyclic and b) monotonic representations

Figure 5.3 – The stress distribution of specimen G1X1A a) Time=1 @ peak stress and b) Time=9 @ fracture stress

Figure 5.4 – The Element Mesh of VHS FTS2A with its applied boundary condition(s).

Figure 5.5 – Stress-Deformation Response of VHS Circular Steel Tubes a) cyclic and b) monotonic representations

Figure 5.6 – The stress distribution of specimen VHS FTS2A a) Time=7 @ peak stress and b) Time=13 @ fracture stress

Figure 5.7 – The Element Mesh of NHT FTS1A with its applied boundary condition(s).

Figure 5.8 – Stress-Deformation Response of specimen NHT-FTS1A a) cyclic and b) monotonic representations

Figure 5.9 – The stress distribution of specimen NHT FTS1A a) Time=5 @ peak stress and b) Time=15 @ (near) fracture stress

Figure 5.10 – The Element Mesh of a Ductile Material (DUCMAT) with the applied boundary condition(s)

Figure 5.11 – Stress-Deformation Response of specimen DUCMAT a) cyclic and b) monotonic representations

Figure 5.12 – The stress distribution of specimen DUCMAT a) Time=2 @ peak stress and b) Time=10 @ fracture stress

Figure 5.13 – The Element Mesh of DP800 steel plate with the applied boundary condition(s)

Figure 5.14 – Stress-Deformation Response of specimen DP800 plate a) cyclic and b) monotonic representations

Figure 5.15 – The stress distribution of specimen DP800 steel a) Time=5 @ peak stress and b) Time=13 @ fracture stress

Figure 5.16 – The Element Mesh of specimen G1WA with the applied boundary condition(s)

Figure 5.17 – Stress-Deformation Response of specimen G1WA a) cyclic and b) monotonic representations

Figure 5.18 – The stress distribution of specimen G1WA a) Time=3 @ peak stress and b) Time=13 @ fracture stress

List of Tables

Table 5.1 – Material properties and gauge dimension of Circular Solid Steel Specimen G1X1A

Table 5.2 – Material properties and gauge dimension of Very High Strength (VHS) Circular Steel Tubes

Table 5.3 – Material properties and gauge dimension of Non-Heat-Treated (NHT) Circular Hollow Section (CHS) Specimen FTS1A

Table 5.4 – Material properties and gauge dimension of a Ductile Material (DUCMAT)

Table 5.5 – Material properties and gauge dimension of DP800 Dual Phase Steel Strip Specimen

Table 5.6 – Material properties and gauge dimension of a Circular Solid Copper Specimen G1WA

Table of Contents

1.0 Introduction **1**

1.1 Scope of Research ---------- 1

1.2 Fundamentals ---------- 1

1.2.1 Introduction to Tensile Test and Stress-strain Curves ---------- 1

1.2.2 Finite Element Analysis ---------- 6

1.2.3 The Newton-Raphson Solution Technique ---------- 7

1.2.4 Background of Problem ---------- 9

1.2.4.1 Overview of Current Capability of FEA 9

1.2.4.2 The Positive Definite Matrices and Limitation of N-R Procedure 9

1.3 Objectives ---------- 11

2.0 Literature Review **12**

2.1 Introduction ---------- 12

2.2 Displacement-Controlled Technique ---------- 13

2.3 The Arc-length Method ---------- 14

2.4 The Weighted-Average Method ---------- 16

2.5 Node Separation Method ---------- 19

2.6 Saw-Tooth Continuum Model ---------- 21

2.7 Tension Softening Material Model ---------- 25

2.8 Evaluation ---------- 28

3.0 Numerical Modelling **30**

3.1 Overview ---------- 30

3.2 The Elasto-Plastic (EP) Constitutive Relations for Plasticity ---------- 31

3.2.1 Additive split ---------- 31

3.2.2 Failure/yield criterion ----------32

3.2.3 Flow rule----------33

3.2.4 Loading/unloading conditions ----------33

3.2.5 Isotropic hardening----------34

3.2.6 Elasto-plastic stiffness matrix----------35

3.3 General purpose ANSYS® software package ----------38

3.3.1 Introduction ----------38

3.3.2 Preprocessing ----------38

3.3.3 Solver ----------39

3.3.4 Postprocessor----------39

4.0 Methodology of the Proposed Modelling Technique.....40

4.1 Introduction----------40

4.2 The Constitutive Theory of the Proposed Softening Model----------42

4.3 Determination of Parameters ----------44

4.4 Numerical Simulation: ANSYS® Input Commands and Solution Options ---------47

4.4.1 Element type ----------47

4.4.2 Material Properties ----------48

4.4.3 Loadings and Boundary Condition----------50

4.4.4 Solution Option ----------50

4.4.5 Reduced-load Optimization ----------52

5.0 Results: Validation Cases.....54

5.1 Introduction----------54

5.2 Case 1: Circular Solid Steel; Specimen G1X1A----------55

5.3 Case 2: VHS Circular Steel Tube; Specimen FTS2A----------59

5.4 Case 3: NHT CHS; Specimen FTS1A ----------62

5.5 Case 4: A Ductile Material; Specimen DUCMAT ----------65

5.6 Case 5: Dual Phase Steel Strip; Specimen DP800----------68

5.7 Case 6: Circular Solid Copper; Specimen G1WA----------71

6.0 Discussions.....**74**

6.1 The material stress-strain curve ----------74

6.2 Determination of parameters ----------75

6.3 Evaluations----------76

6.3.1 The capability of geometrical effect ----------76

6.3.2 Adaptability ----------77

7.0 Concluding Remarks.....**78**

8.0 Future Research.....**80**

References.....**82**

Appendix.....**88**

Appendix 1: True and engineering stress strain conversion ----------88

Appendix 2: The Ludwick power law relation ----------89

Appendix 3: The properties of Voce $\sigma_t - R$ curve ----------90

Appendix 4: Macros for the Setting of Analysis Environment----------92

1.0 Introduction

1.1 Scope of Research

This study utilizes the current capability of the ANSYS® finite element software package in an attempt to develop a modelling technique capable of simulating the post-limit softening response of a material under consideration albeit the limitation to attain solution through the direct solution approach. The proposed technique was validated against experimental data to provide an understanding of its feasibility and thence the confidence for further developments and applications.

1.2 Fundamentals

1.2.1 Introduction to Tensile Test and Stress-strain Curves

A tensile test is a common test performed on a particular material to determine its material properties and damage mechanism under certain load combinations. Although there are various forms of tensile tests, the uniaxial tensile test is the simplest form of its type whereby a slender material specimen is stretched along its central axis. These specimens normally have enlarged ends for gripping and a reduced cross sectional area in

the gauge section to allow localisation of stress and deformation in this region. Test piece of this shape, as shown in Figure 1.1 is also known as the dumbbell specimen. The cross section of the test piece may be circular, square or hexagonal. Some materials are also tested in different shapes e.g. flat plates, hollow sections etc. to compromise with their manufactured shapes. A detailed standard for metallic material tensile tests is discussed in (BSI 1992).

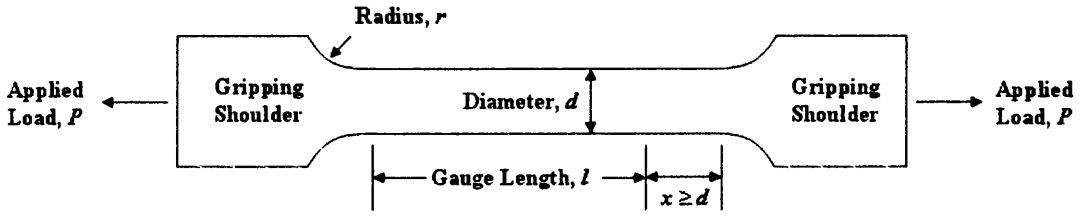

Figure 1.1 – A Typical Tensile Test Specimen

The output of such tensile test is the stress-strain curve, which is a graphical representation of the performance and strength of the specimen as applied load is increased monotonically or cyclically usually until fracture. Several important parameters that define the specific material are obtained from the curve, i.e. the Young's modulus, tensile yield stress, ultimate tensile strength, percentage elongation and reduction in cross sectional area.

Figure 1.2 presents a typical engineering stress-strain curve of a ductile steel material accompanied by some important terms. The shape of a stress –strain curve can be affected by several factors such as the material's composition, prior history of deformation, strain rate of test, temperature and size/shape of the test piece. The corresponding failure mode from the onset of loading till fracture is also presented.

The average engineering measures of the stress and strain, denoted by σ_e and ε_e, are therefore obtained from the applied force P and incremental length ΔL, divided respectively by the original cross sectional area of the gauge section A_0 and the length L_0. These simple arithmetic operations are as follow;

$$\sigma = \frac{P}{A_0}; \varepsilon = \frac{\Delta L}{L_0} = \frac{L - L_0}{L_0} \qquad \text{[Eq.1.1]}$$

At the elastic region of the curve, many materials obey the Hooke's law where the stress is proportional to strain. This proportionality is termed as the Young's modulus E, also known as the modulus of elasticity. It describes the stiffness of a material, i.e. the greater the slope is, the smaller the elastic strain and thus the stiffer it is. This modulus is an important design value in the structural field, used to compute the deflection of structural members (Arya 2003).

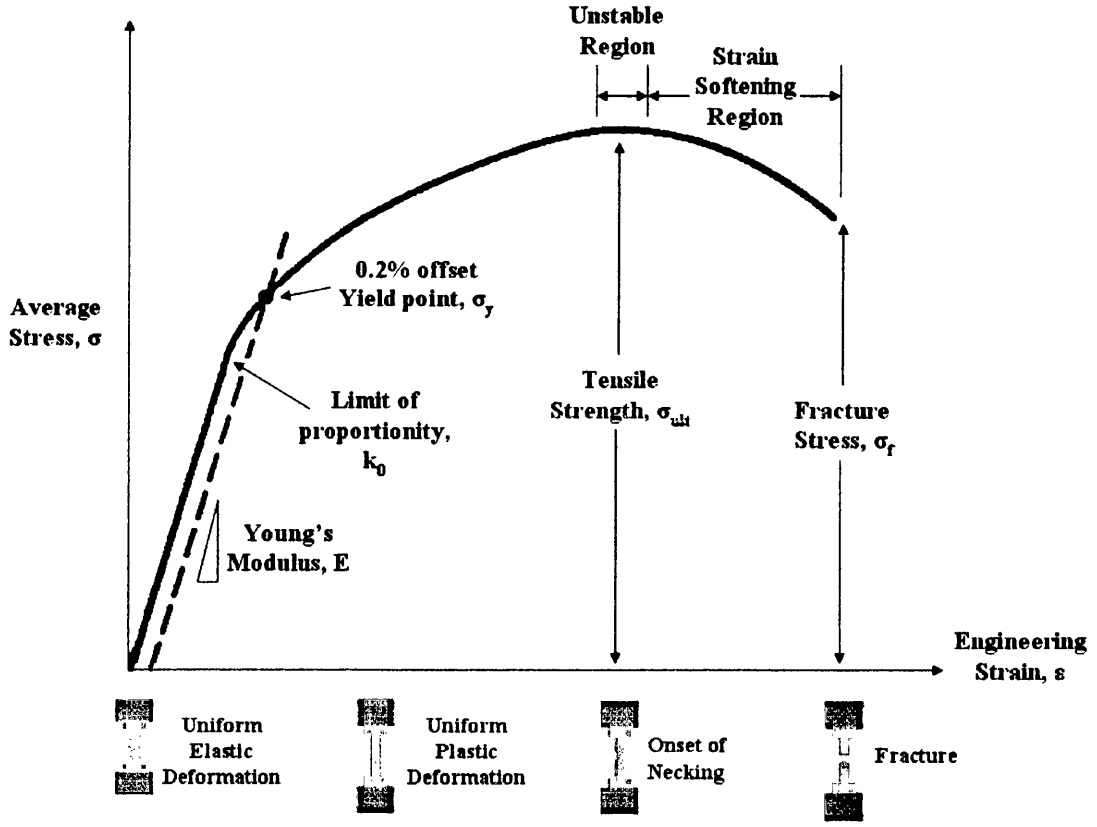

Figure 1.2 - A Typical Engineering Stress-Strain Curve with a Ductile Failure Mode from onset of Loading to Fracture (Key-to-Steel 2007)

The stress point at which the stress-strain curves starts to deviates from the Young's modulus or linearity as the strain is increased is called the limit of

proportionality. Beyond this limit, the stress-strain response will become nonlinear, though not necessary inelastic. Plastic deformation becomes imminent when stresses exceed the material's yield point which is characterized by non-recoverable strains. For smooth curves without a definite yield plateau (see Figure 1.2), the yield point can be approximated by the intersection of a line offset from the initial elastic slope by a required strain, typically 0.2%. There is usually very little difference between this yield point and elastic limit and it is therefore convenient in plasticity to assume that these points coincide.

These parameters are essential in the definition of a material characteristic. In the structural field, they are used for the selection of materials in the design process for various engineering applications (Arya 2003). In numerical simulations, the tensile properties are usually used for the prediction of material behaviour under various forms of loadings.

Strain softening, observed as the descending branch in the stress-strain curve occurs when the influence of the geometrical instability becomes more significant than the work hardening. This phenomenon results in the gradual decrease in the mechanical resistant under continuous increase of deformation on the material. The apparent change of the slope's sign convention from work (or strain) hardening to strain softening is due to the approach used to define stress. The definition of 'engineering' stress is based on an incorporated fixed reference quantity, i.e. the original cross sectional area A_0 as in equation [Eq.1.1a]. This quantity is used throughout the strain increment, ignoring the influence of its change in geometry. In fact, substantial reduction in the cross sectional area A can be observed, so that a new conception is borne where the 'true' stress measures the instantaneous value of the area A, giving more accurate representation of the current stress state, i.e.

$$\sigma_t = \frac{P}{A} \qquad \text{[Eq.1.2]}$$

Since A is a decreasing variable as the material is stretched and stress is inversely proportional to the cross sectional area, the value of true stress would always be greater

than the corresponding engineering stress. If the true stress-strain points are plotted at the critical reduced cross sectional area, no maximum would be observed in the curve. A comparison between the true and engineering stress-strain curves for the same material under the same tensile test can be observed in Figure 1.3.

The true strain on the other hand, is defined as the sum of all the instantaneous engineering strains given by equation [Eq.1.3] below.

$$\varepsilon_t = \ln\left(\frac{L}{L_0}\right) \qquad \text{[Eq.1.3]}$$

The derivation is shown in Appendix 1. Also demonstrated is the conversion from engineering to true values and vice versa.

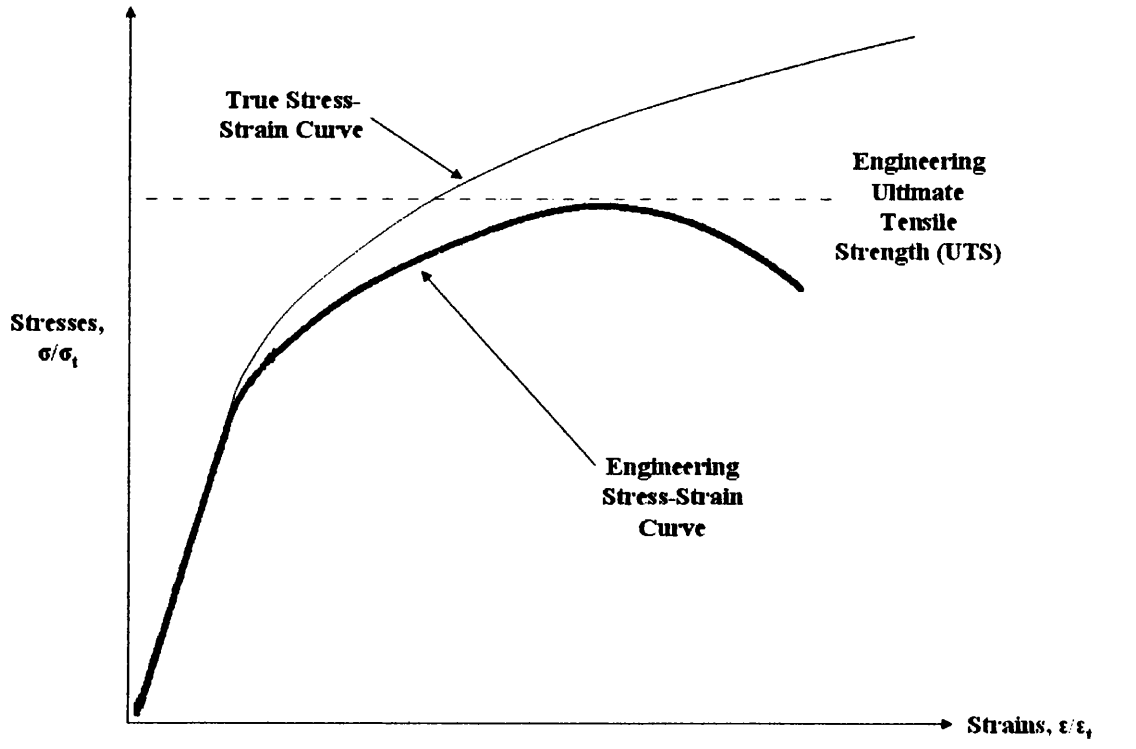

Figure 1.3 – A Comparison between the True and Engineering Stress-Strain Curves of a Ductile Steel Material

Although true stress-strain proves to be a much accurate representation of the stress and strain states, the engineering stress-strain provides a much easier way to present the material data. In the small strain region, the difference between the true and engineering stress-strain curve is negligible. The difference however becomes more significant when large strain analysis is involved.

In short, this research attempts to implement the complete stress-strain relation, which includes the softening branch into computational analysis that defines the material characteristic of the model.

1.2.2 Finite Element Analysis

The Finite Element Method (FEM) was first introduced to solve problems in structural mechanics by one of its pioneers, O.Zienkiewicz who published the first text book on the FEM in the 1960s. In fact, its development can be traced back to the work by several scholars (Hrennikoff 1941; R.Courant 1942; J.Argyris 1954; Turner, Clough et al. 1956; Clough 1960), although the approaches in the early era (Hrennikoff 1941; R.Courant 1942) are dramatically different from the modern methods. They however share one elementary concept, i.e. the mesh discretization of a continuous domain or system into discrete sub-domains on an unstructured grid called the finite elements, a term popularised by Clough (Clough 1960). This mesh discretization in a FEM model deals with a set of equilibrium equations which characterized the existing physical conditions for each element. A massive system of equation is assembled and solved with the available solver or solution techniques (Nour-Omid, Rodrigues et al. 1983).

The Finite Element Analysis (FEA) refers to computational-based simulation technique applying the FEM and is widely used in engineering analysis. Presently, it has been accepted as one of the most powerful technique of numerical solution of different variety of problems and has been expanded to cover various aspects in engineering analysis such as heat transfer, fluid dynamics etc (Bathe 1996). Advancement in computational technologies has enabled complex structural problems to be solved using the FEM which would otherwise be difficult to be obtained by any other means. The

general application of FEA in the structural field today includes the determination of stress distribution for critical elements, the prediction of the deformation under certain combinations of loadings, design optimization etc. While being an approximate method, the accuracy of FEA method can be enhanced by refining the mesh model and thus generating more elements.

Non-linearity material behaviour comes in two forms; material and geometric non-linearity (O.C.Zienkiewicz and Taylor 2000). Material non-linearity involves the diversion of linear behaviour due to the changes in the material's micro-structure in which the stress is not linearly proportional but a function of strain. A typical case would be the classical elasto-plastic behaviour which will be discussed in chapter 3.2. In the case of geometric non-linearity, it involves the change to the shape or geometric configuration due to large deformation, i.e. a state of finite deformation to an extent where it could not be neglected whereby the element stiffness matrix is then a function of displacement.

1.2.3 The Newton-Raphson Solution Technique

The Newton-Raphson (N-R) solution technique (Bathe 1996; O.C.Zienkiewicz and Taylor 2000; Kaw 2007) is employed in ANSYS® for the solution of nonlinear problems. Here, the overview of the procedure will be briefly presented.

This approach divides the total load into a series of load increments, which in turn could be applied through several loadsteps. The simultaneous equation for the finite element discretization process is

$$[K]\{u\} = \{F^a\} \qquad \text{[Eq.1.4]}$$

where; K - stiffness matrix, u - vector of the unknown degree of freedom (displacement), F^a - applied load.

Before each solution, the N-R evaluates the out-of-balance load vector. This out-of-balance load vector is the difference between the restoring force, which is the load corresponding to the element stress, and the applied load. It can be written as

$$\left[K_i^T\right]\{\Delta u_i\} = \{F^a\} - \{F_i^{nr}\} \qquad \text{[Eq.1.5]}$$

where; K_i^T - Jacobian (tangent) matrix, subscript i represents current iteration number, F_i^{nr} - restoring force. N-R solves for Eq.1.5 and computes the next approximation through Eq.1.6. A linear solution is performed using this out-of-balance load vector to attempt convergence.

$$\{u_{i+1}\} = \{u_i\} + \{\Delta u_i\} \qquad \text{[Eq.1.6]}$$

If solution is not attained in the first attempt, the out-of-balance load vector is re-evaluated and the stiffness matrix is updated. This process is repeated until convergence is achieved. Figure 1.4 illustrates the N-R solution procedure for two iterations.

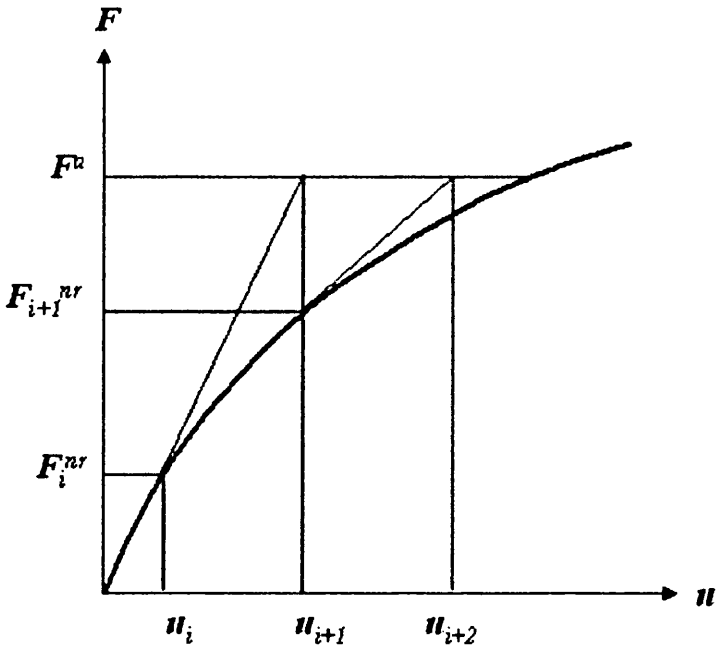

Figure 1.4 – Newton-Raphson Solution Iteration

The N-R solution procedure, though with its rapid convergence, has its own short comings; Firstly, the stiffness (Jacobian) matrix needs to be updated at each iteration point and secondly, the solution can diverge by oscillating between several potential solutions (O.C.Zienkiewicz and Taylor 2000; Crutchley and Zwonlinski 2004). Hence, several other solution techniques were developed based on the full (original) N-R procedure such as the modified N-R and the Initial Stiffness N-R solution techniques (Nayak and Zienkiewicz 1972; Simo and Taylor 1985; He 2004).

1.2.4 Background of Problem

1.2.4.1 Overview of Current Capability of FEA

The ANSYS® finite element software package provides several nonlinear material options for the derivation of the material properties for plastic analysis such as bilinear hardening, multilinear hardening, nonlinear hardening etc. for both isotropic and kinematic models (ANSYS 2007). These material options provide solutions up to the peak stress, i.e. until which the ultimate strength is attained. Beyond this point, the analysis will either stop due non-convergence or continue to follow the hardening paths depending on the material model adopted. Apparently, material softening capabilities are not presently available and this prevents the prediction of the damage mechanism beyond the peak stress.

Although analysis up to the peak stress has proved to be adequate for analysis and design, it provides no indication of the possible failure predicament that is to follow. On the other hand, a material softening model could provide a prediction on the failure behaviours and mechanism when the post limit stress state is exceeded.

1.2.4.2 The Positive Definite Matrices and Limitation of N-R Procedure

A matrix and its inverse [D] and $[D]^{-1}$ are positive definite if the determinants of the sub-matrices are of the series of $D_{i,j}$, e.g.

$$\left[D_{1,1}\right],\begin{bmatrix} D_{1,1} & D_{1,2} \\ D_{2,1} & D_{2,2} \end{bmatrix},\begin{bmatrix} D_{1,1} & D_{1,2} & D_{1,3} \\ D_{2,1} & D_{2,2} & D_{2,3} \\ D_{3,1} & D_{3,2} & D_{3,3} \end{bmatrix},etc$$

Thus two conditions for a symmetric matrix have to be fulfilled to maintain a state of matrix positivity, i.e.

$$\begin{aligned} D_{i,i} &> 0.0 \\ D_{i,j} &< \sqrt{D_{i,j}D_{j,j}} \end{aligned} \qquad \text{[Eq.1.7]}$$

If any of the determinants are zero, the matrix is said to be positive semidefinite, given that the rest of the matrixes are positive. If all of the determinants are negative, then the matrix is said to be negative definite.

A full structural matrix that combines the particular effects of the elements is normally a positive or a zero definite matrix. For exception where a negative definite element is connected to one which is positive definite, the resulting system would still remain a positive definite. Virtually for all cases, the complete structural element matrices must be in positive definite state, bounded by the appropriate boundary conditions. As for the element matrices, they are usually positive semidefinite, sometimes either positive or negative indefinite.

As the solution approached the unstable region, i.e. at peak stress proximity into material softening or compression post-buckling, the stiffness matrix becomes singular at the point when the matrix changes from a positive to negative definite and remains negative at the strain softening region. The softening analysis has therefore been made complicated with the inability of the conventional Newton-Raphson (N-R) solution techniques, including the modified N-R and the Initial Stiffness N-R (which are generally available in most of the commercial finite element softwares) to handle the matrix singularity and negativity in the softening region. Subsequently, the solution will encounter convergence difficulties and abort.

1.3 Objectives

The ultimate goal of this research field is to develop a complete softening model which could be implemented into the ANSYS® finite element software for both material and structural softening analysis. This study thus serves as a preliminary study towards achieving that goal whereby a modelling technique is proposed and discussed.

Therefore, the objectives of this study can be subdivided into the following divisions;

a) To develop a preliminary computational method capable of numerically simulating the material softening behaviour of materials, including the post limit stress distribution such that the critical region or elements could be identified. The ANSYS® finite element software will be used as the platform at which the modelling technique is built upon.

b) To perform validation tests on the proposed modelling technique against several experimental tensile test data. This is necessary to determine the feasibility of the modelling technique and also the prospect for further developments.

2.0 Literature Review

2.1 Introduction

There is considerably much research in the recent time in developing softening models for fracture simulation which could be implemented into the FEA. Many of the targeted materials in which these models were developed are quasi-brittle cementitious materials such as concrete and masonry (Suidan and Schnobrich 1973; Borst and Nauta 1986; Pimanmas and Maekawa 2001; Rots and Invernizzi 2004; Xiao and Chin 2004). The smeared crack approach, where cracks were represented by an infinite number of parallel cracks of infinitely small openings followed by reduction in stiffness and strength due to crack propagation, is widely popular among scholars. A plastic-damage-contact model for concrete called the Craft model, developed by Jefferson (2003) is currently the only softening model known to be implemented into commercial FE program (LUSAS).

Softening models for ductile materials gained latter attention as compared to cementitious materials. In the 2000s, significant increase in interest towards the post limit characteristic for both tension softening and post buckling response has resulted in softening model such as the works of Komori (2002), Ponthot (2002), D.J. Celentano et al. (2004), Ling (2004) and Belnoue et al. (2007). Most of these are non-local models,

whereby deformation is taken as a global measure. The capability of capturing the localized deformation provides yet another challenge due to geometrically perfect finite element model.

Sub-chapters 2.2 and 2.3 discuss two options readily available in many commercial finite element softwares that could be exploited to simulate the post limit analysis. The following sub-chapters (2.4 – 2.7) present several of the author's favourite softening models in terms of the contributions to the flow of ideas acquired from extensive literature search. The basis of the methodologies, if known, will be briefly introduced along with some corresponding validation results. Some of the capabilities of the models are discussed based on the author's point of view on neutral ground. Neither completeness nor originality is claimed.

2.2 Displacement-Controlled Technique

The limitation on the load-controlled N-R procedure to traverse the limit point has stimulated various researches to attempt alternatives to capture the post limit softening region. Subsequently many scholars explore the use of displacement as the governing parameter for the post limit incremental algorithm (Zienkiewicz 1971; Haisler and Stricklin 1977; Batoz and Dhatt 1979). One of the earliest methods to achieve this was by incrementing the load parameter to the limit point to solve the displacement and then assigning a characteristic displacement value beyond that point to solve the load parameter. However, this approach leads to a problem due to non-symmetric equations, resulting in high cost and numerical instability (Crisfield 1991).

Several displacement-controlled based alternatives were introduced by Zienkiewicz (1971), Haisler and Stricklin (1977) and Batoz (1979) to traverse the limit point. These methods usually involve a stage at which the load multiplier is computed, followed by a backward substitution to solve the displacement vector. Zheng et al. (2005) further introduced an improved procedure characterized by its efficiency and good numerical stability. The structure of the algorithm is also similar to the load-controlled program whereby no spurious constraint is introduced into the global stiffness matrix.

Displacement-controlled techniques have proved to be a more stable, efficient and exhibit more abilities than the conventional load-controlled analysis. It is much easier for convergence to be achieved with a displacement-controlled analysis than a conventional load-controlled analysis for a similar problem especially for highly nonlinear analysis and when the tangent modulus is small.

There are occasions, however, when the application of this method is either difficult or impossible. Analysis involving the snap back or snap through behaviour will lead to solution error (Crisfield 1991; Memon and Su 2004 Zheng et al. 2005). Even in the 1970s, researchers acknowledged this problem and responded by proposing several solutions; using artificial springs (Wright and Gaylord 1968), switching between load and displacement controls (Sabir and Lock 1972), abandoning equilibrium iterations in the close vicinity of the limit point (Bergan and Soreide 1978), etc. Arguably the most significant is the arc-length method which was originally developed by Riks (1972, 1979) and Wemper (1971). This method will be discussed in the next sub-chapter.

2.3 The Arc-length Method

The arc-length method, which is available in many commercial finite element softwares including ANSYS®, offers another alternative of tracing the complex load-displacement response of an instable structure. This method has become a widely established solution technique for nonlinear structural behaviour and is ever-improved by continuous research interest shown by researchers (Teng and Luo 1988; May and Duan 1997; Zhu and Chu 2002; Mallardo and Alessandri 2004; Cerini and Falzon 2005). This option is capable of passing through the unstable region of the stress-strain curve and beyond into the strain softening region, thus preventing divergence by avoiding the numerical complexities that accompanies the N-R solutions. In FEA however, this option is restricted for static and rate-independent problems only.

This method uses explicit spherical iterations to maintain the orthogonality between the arc-length radius and orthogonal directions (Forde and Stiemer 1987). The reference arc-length radius, computed for the first iteration of the first substep, is given by

$$\text{Reference Arc - length radius, } r_1 = \frac{\text{Total Load or Displacement}}{MNSBSTP} \qquad \text{[Eq.2.1]}$$

where *MNSBSTP* being the (minimum) number of substeps specified by the user. It is assumed that all load magnitudes are controlled by a single scalar parameter, i.e. the total load factor. The load factor at each iteration is modified so that the solution follows some specific path until convergence is achieved. Mathematically, the arc-length method can be viewed as tracing a single equilibrium curve in a space spanned by the nodal displacement variables and the total load factor.

The N-R solution options are still employed for the solution of the arc-length method. Figure 2.1 below demonstrates the iteration procedure at the first and subsequent loadsteps. The arc-length causes the N-R method to converge along an arc and thus allows convergence to be attained even if the load-displacement slope is zero or negative.

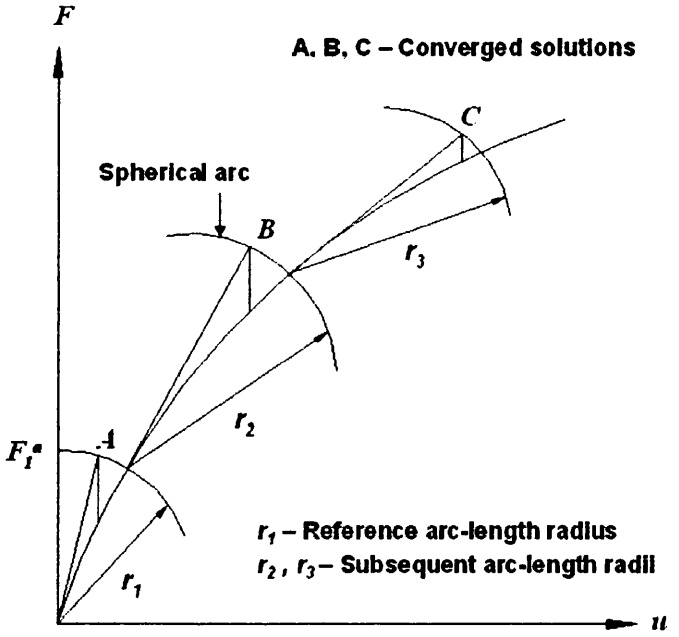

Figure 2.1 – The Arc-length Method Iteration Procedure

Although the arc-length method has proved to be a powerful method to trace the complete load-deformation response, it is still incapable of simulating the post-peak stress distribution response. Beyond this peak point, the solution will continue to follow

an increasing stress path even when the load-deformation response descends down a negative slope. This gives an incorrect representation of the stress states of the solution in the softening and post-buckling region.

2.4 The Weighted-Average Method

A computational procedure, called the weighted average method (Ling 2004), built upon the ABAQUS finite element software was developed in 1996. This method was one of the earliest modern attempts to predict the post limit softening response and was achieved by adopting the uniaxial true stress-true strain relation, with modifications when necking is attained. The necking phenomenon was governed by two characteristic equations, each representing the lower and upper bound of the true stress-true strain relation after necking. The extended (extrapolated) power law (see Appendix 2), very often underestimates the stress states beyond the neck region (refer Figure 2.2) (Ling 2004), is used as the governing equation as the lower bound. The upper bound was characterized by a linear equation (not in the figure) beginning from the onset of necking, which was found to fit the true stress-strain relation for many copper alloys.

The assembled relation of true stress-true strain relationship is therefore computed as a fraction of both the lower and upper limits given by

$$\sigma_t = \sigma_u \left[w\left(1+\varepsilon-\varepsilon_u\right)+\left(1-w\right)\left(\frac{\varepsilon^{\varepsilon_u}}{\varepsilon_u^{\varepsilon_u}}\right)\right] \qquad \text{[Eq.2.2]}$$

where ε_u - true strain at which necking initiates, σ_u - the corresponding true stress, ε - current true strain, w - weighted average constant; $0 \le w \le 1$.

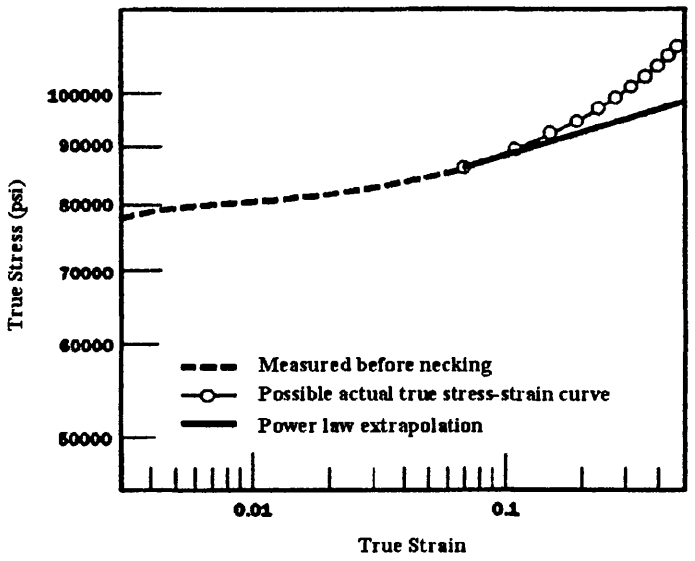

Figure 2.2 – True stress-true strain plot of a sample. The log-log presentation shows that the power law extrapolation tends to underestimate the true stress

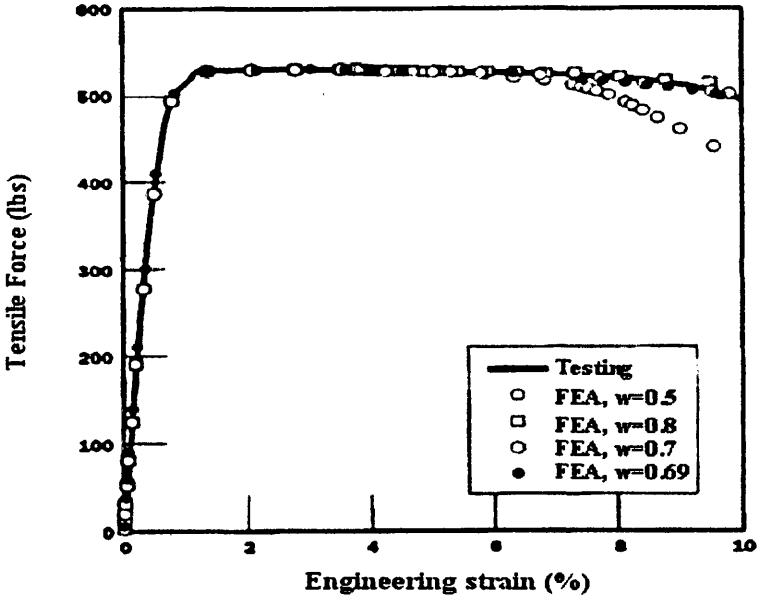

a)

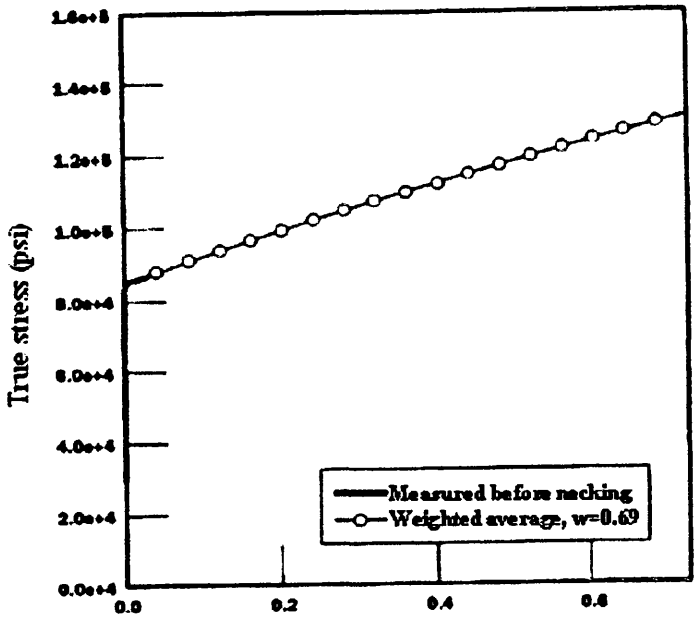

b)

Figure 2.3 – a) Load-engineering strain comparison between experimental and several applied weighted average constants, *w* used in FEA. b) The corresponding true stress-true plastic strain curve. Sample – C260 Extra Hd-Longitudinal Copper strip-shape test piece

This constant can be determined by Zhang and Li's (1994) approach i.e. through an optimization procedure in which the engineering curve is considered to be the target. The weight constant is searched until the calculated load-extension relation agrees with the predefined limits. Figure 2.3 presents one selected results whereby the load-strain response was plotted with different *w* values. Note that in this case, the FEA run best matches the experimental data with a weight constant of 0.69. The corresponding true stress-true strain relationship is also presented.

This method has indeed provided a way of predicting the complete load-extension and true stress-true strain curves. Good accuracy can be achieved with proper selection of the weight constant.

2.5 Node Separation Method

The node separation method developed by K.Komori (2002), presents another softening model with the intention of simulating the crack growth after ductile fracture in bulk metal forming processes, as an extension to FEA of metal forming processes which has been studied substantially (Clift et al. 1990; Wifi et al. 1998; Kim et al. 1999; Reddy et al. 2000). One characteristic of the node separation method is whereby a material is divided into two separate materials upon reaching the ductile fracture as observed in a material tensile test. This method adopts the anisotropic Gurson yield function which was initially developed for porous ductile materials (Gurson 1977) and is widely utilized in the fracture mechanics field. Komori's softening model uses this criterion along with two proposed evolution equations, which govern the void volume fractions (i.e. void growth and void nucleation) of the model under consideration. Crack is assumed to propagate when the evolution equation satisfied a constant C given by;

$$\int \dot{f} dt \geq C \qquad \text{[Eq.2.3]}$$

where; $\dot{f}$ - evolution equation, t - time, C - critical void volume fraction. At this stage, the material starts to deviates from homogeneity and deforms heterogeneously, i.e. necking initiates, in the axial direction until fracture; see Figure 2.4 [Left]. The computational procedures were explained in details in the K.Komori's previous publications (Komori 1999, 2001). The deformed mesh is demonstrated in Figure 2.4 [Right]. It can be observed that the deformation mode was clearly captured.

It is surprising that the validation of the node separation approach was carried out without the second half of the experimental load-nominal strain curve; see graphical representation of results in Figure 2.5. The intention of K.Komori to omit the softening branch of the experimental curve remains unknown and this could only demonstrate the capability of the approach to capture the softening branch yet without experimental validations. Furthermore, the ascending branch does not seem to agree although the elasto-plastic hardening analysis does not present a major issue. Nevertheless, the

strength of this method is its ability to simulate the necking phenomenon beyond the limit point and upon reaching fracture.

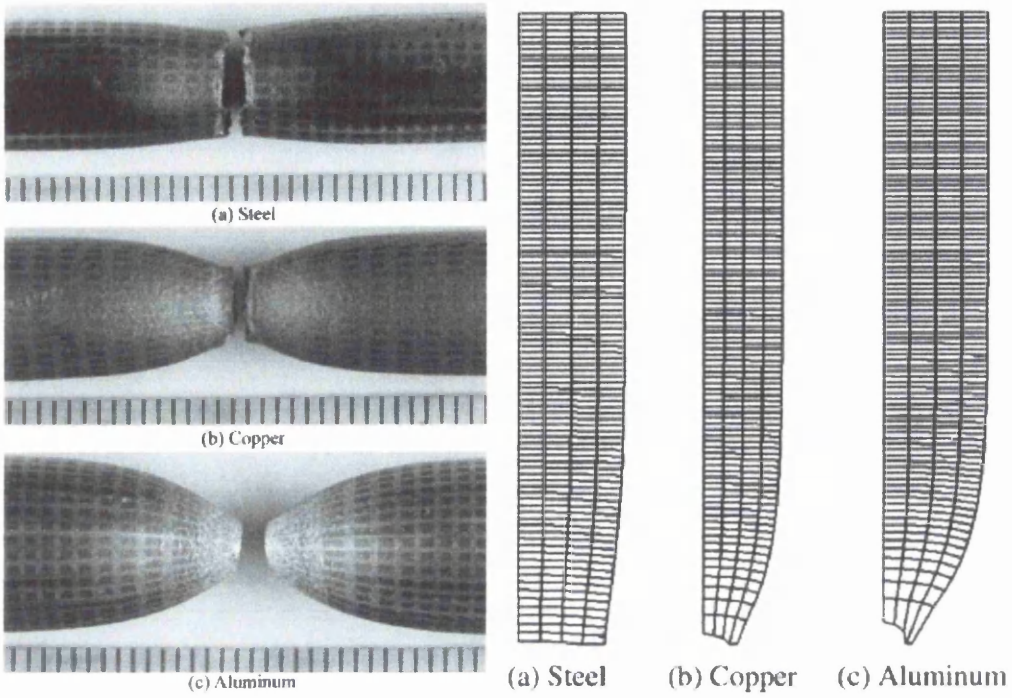

Figure 2.4 – [Left] Experimental Fracture mode [Right] Node Separation Method Deformed Mesh of a) Steel; b) Copper; c) Aluminium (K.Komori 2002)

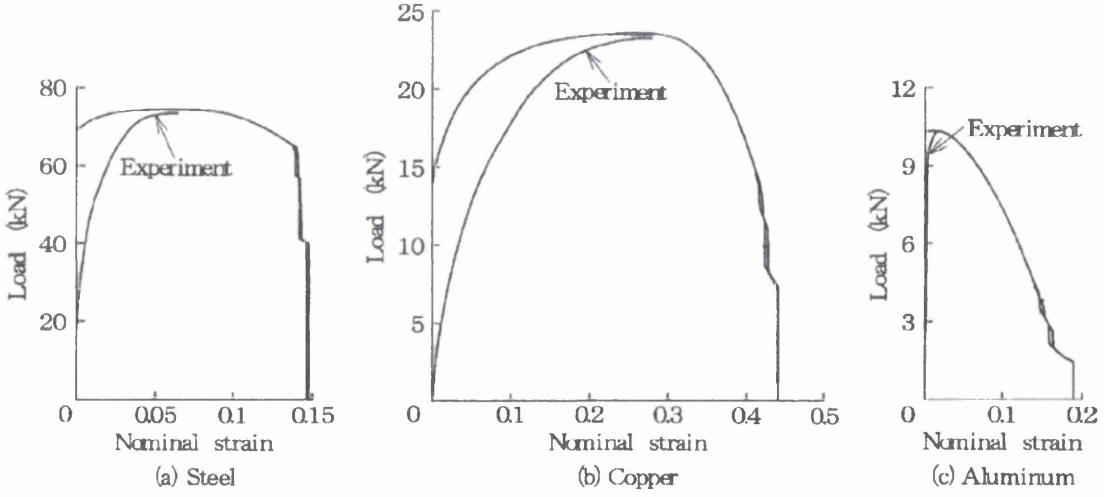

Figure 2.5 – The load-nominal strain relationship from experimental and the node separation approach for a) Steel b) Copper c) Aluminium (K.Komori 2002)

2.6 Saw-Tooth Continuum Model

A softening model based on sequentially linear saw-tooth continuum model has been proposed by Rots and Invernizzi (2004) using an adapted version of DIANA finite element package. This model, which was developed for concrete fracture is capable of capturing the nonlinear response via a series of linear steps, replacing the negative slope as the constitutive theory of softening plasticity would describe.

The incremental-iterative procedure is also replaced by a scaled sequentially linear procedure (Rots 2001). After a linear analysis, the critical element, i.e. the element for which the stress is most close to the current peak in the saw tooth diagram, is traced and the stiffness and strength of that element is reduced. This process is then repeated. The elements with reduced stiffness thus represent the softened areas. The curves were obtained by connecting the subsequent critical loads and the corresponding displacements at which the solution is executed.

One characteristic of the saw-tooth model is such that it is sensitive to mesh sizing and also the number of saw-teeth adopted in the discretization of the softening branch. The following load-displacement curves will demonstrate how these two factors affect the output of the analysis. A notched beam case with a four-point loading scheme was modelled.

In Figure 2.6, we can observe the deviation of the softening branches with the application of five, ten and twenty tooth approximations, along with a smooth reference curve from a nonlinear softening analysis (Rots 1993) for comparison purposes. The higher the number of tooth approximation, the lower the deviation is from the reference curve. Also, the predicted saw-tooth curves are better defined with increasing tooth approximation. The actual study by Rots examined five different mesh densities. In Figure 2.7, only three was presented for comparison purposes, i.e. very coarse, medium and very fine meshes. With increasing fineness of the mesh, the predicted curve paths become smoother. However, it is noticeable that there is an increasing underestimation of the curves' peak with respect to the peak of the reference curve. This is due to the sharper

stress peaks at the crack band tip with increasing mesh fineness such that the strength at the crack band tip is reached earlier for finer mesh (Rots and Invernizzi 2004).

As observed in the figures, the predicted load-displacement curve adopting this scheme follows an irregular and rough softening path. This owes to the fact that the process of which elements' becoming critical is discontinuous, i.e. the critical element at one step might not be the same critical element on the next step. This can be overlooked as long as the scheme is considered as a global measure of the overall model under consideration. Interestingly, the predicted saw-tooth curves underestimate the reference curve although the softening envelopes exhibit similar characteristic. In other words, it seems that the dissipated fracture energy is always less than those theoretical ones.

A mesh regularization procedure based on the adjustment of the tensile strength and the ultimate strain of the saw-tooth diagram was also proposed. The dissipated energy is kept invariant, which is represented by the area under the curve. Mesh-sensitivity is still applied but the approximation of the nonlinear reference result has found to be less accurate. Figure 2.8 show a solution adopting twenty-teeth, medium mesh which also includes the mesh regularization. Good agreement is reached.

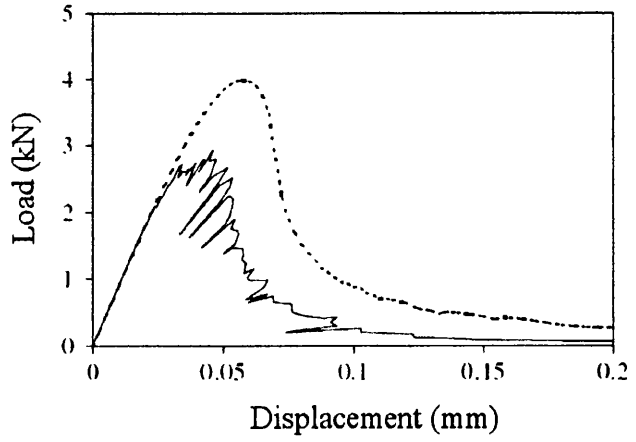

a)

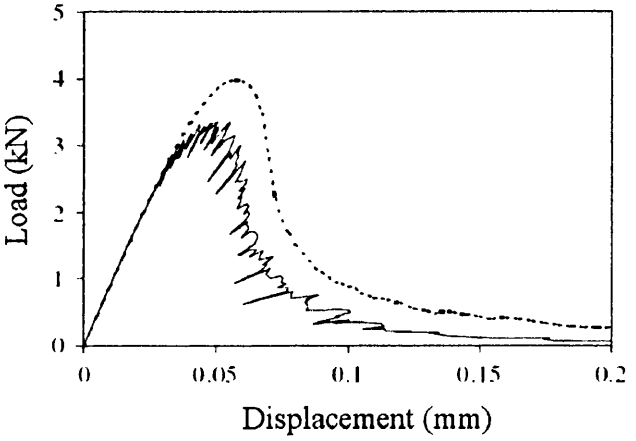

b)

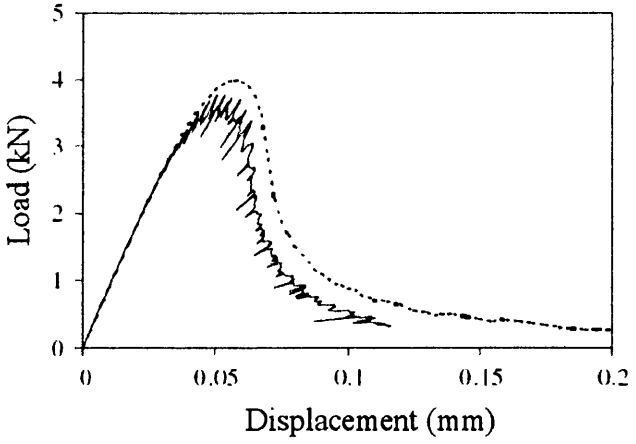

c)

Figure 2.6 – Load-displacement diagram, with medium mesh of unregularized a) 5-teeth b) 10-teeth c) 20-teeth (Rots and Invernizzi 2004)

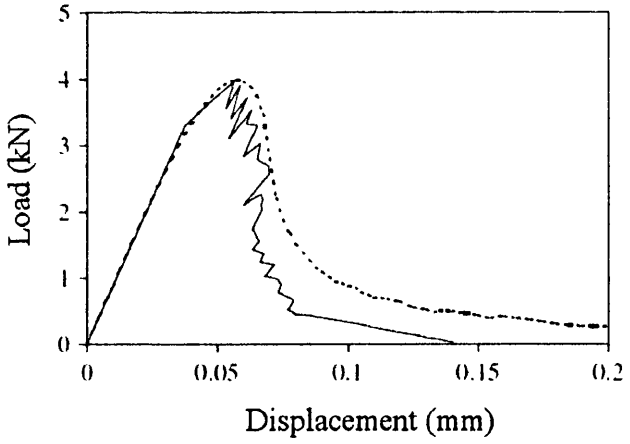

a)

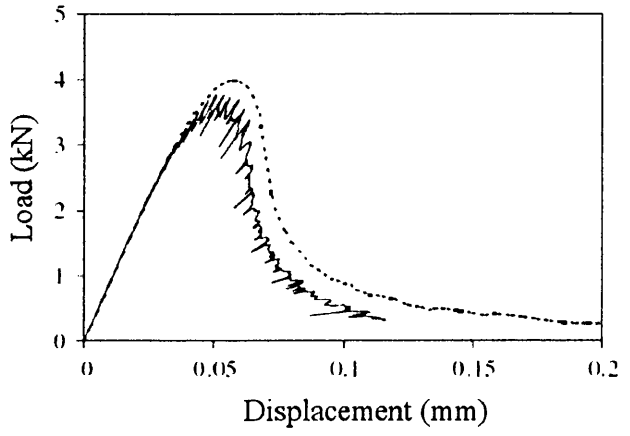

b)

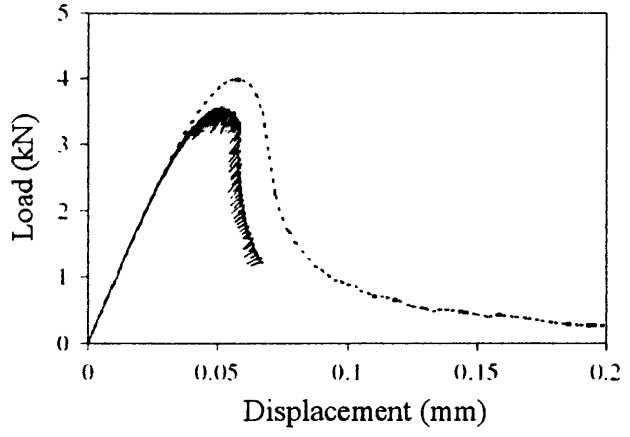

c)

Figure 2.7 – Load-displacement diagram, with unregularized 20-teeth of a) very coarse b) medium c) very fine meshes (Rots and Invernizzi 2004)

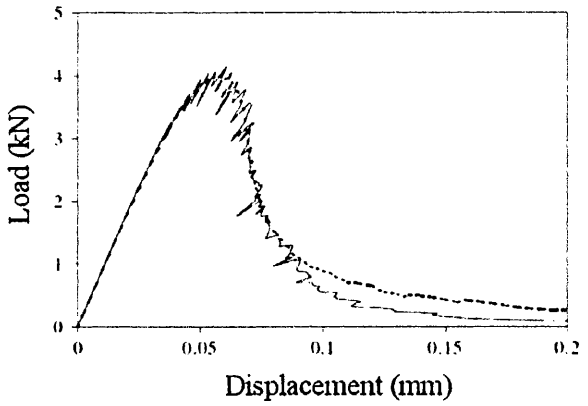

Figure 2.8 – A load-displacement response captured by adopting 20 teeth, medium mesh and the mesh regularization procedure (Rots and Invernizzi 2004)

The required computational time can be large, depending on the setting of the mesh, the number of saw-teeth adopted and also the amount of cracking and crushing that emerge. This approach utilizes a series of material properties updates and solution would always converge and the stiffness remains positive throughout.

2.7 Tension Softening Material Model

Attempts have been made by Xiao and Chin (2004) to develop a softening model capable of simulating the stress distribution including the post-cracking softening region for cementitious composites. In fact, two models were proposed as a result of their research, i.e. the Tension Softening Material (TSM) and Enhanced Multilinear Isotropic Softening (EMIS) (Xiao and Chin 2004; Chin 2006). The former is characterized by the nonlinear isotropic Voce hardening relation given by

$$\sigma = k_0 + R_0\varepsilon^{pl} + R_\infty(1 - e^{-b\varepsilon^{pl}}) \qquad \text{[Eq.2.4]}$$

where σ - stress $\left(N/mm^2\right)$, k_0 - elastic limit $\left(N/mm^2\right)$, R_0 - threshold stress $\left(N/mm^2\right)$, ε^{pl} - equivalent plastic strain, R_∞ - asymptotic stress $\left(N/mm^2\right)$and b - characteristic parameter. The latter, the EMIS model defines both the ascending and descending part of the stress strain curve with two separate equations as follows

Ascending branch; $$\left(\frac{\sigma}{f_t}\right)=1.20\left(\frac{\varepsilon}{\varepsilon_p}\right)-0.20\left(\frac{\varepsilon}{\varepsilon_p}\right)^6 \quad \text{[Eq.2.5]}$$

Descending branch; $$\left(\frac{\sigma}{f_t}\right)=\frac{\left(\frac{\varepsilon}{\varepsilon_p}\right)}{\alpha\left[\left(\frac{\varepsilon}{\varepsilon_p}\right)-1\right]^{\beta}+\left(\frac{\varepsilon}{\varepsilon_p}\right)} \quad \text{[Eq.2.6]}$$

where f_t - ultimate tensile stress $\left(N/mm^2\right)$, ε_p - the corresponding tensile strain and two dimensionless coefficients α and β which describes characteristic of the softening branch.

Both models (and also the saw-tooth continuum model in chapter 2.6) share similar principles, i.e. they consist of a series of material properties update procedures in the simulation of the softening response. However, they exhibit two main distinctions; Firstly, TSM is load-controlled while EMIS is displacement driven and secondly, EMIS has better capability of capturing the geometrical instability than the TSM model.

The following Figure 2.9 shows the validation results of the TSM and EMIS models. This is the only literature found which presents the numerical solution results in terms of stress-deformation response, which demonstrates its capability to capture the softening stress distributions. The captured stress distribution at peak stress and fracture of the finite element models were presented in Xiao and Chin (2004) and Chin (2006). It is interesting to note that in Chin (2006) the prediction of the EMIS model behaves almost identical in some way to the saw-tooth continuum model discussed above, with a smooth ascending branch followed by an irregular softening branch. In terms of capturing the post cracking stress distribution, the TSM model has indeed provided a better prediction, producing a smooth and well-defined softening branch. This model has since been further improved and developed for many validations and predictions of material behaviour.

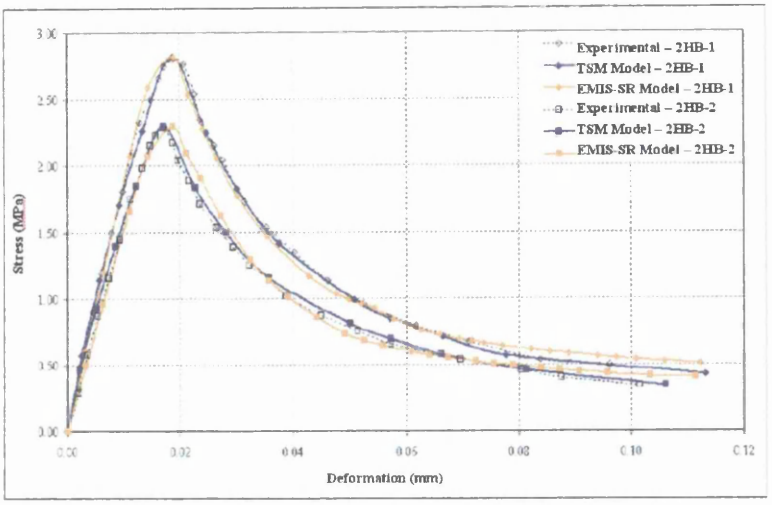
Experimental – 2HB-1
TSM Model – 2HB-1
EMIS-SR Model – 2HB-1
Experimental – 2HB-2
TSM Model – 2HB-2
EMIS-SR Model – 2HB-2
Stress (MPa)
Deformation (mm)

a)

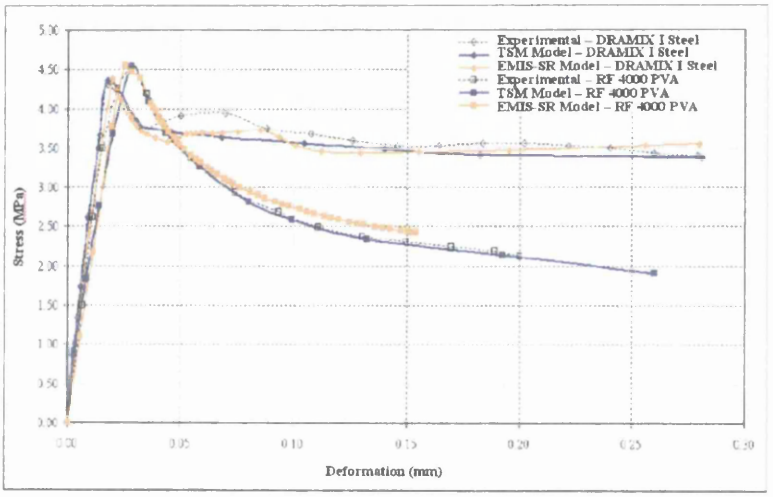
Experimental – DRAMIX I Steel
TSM Model – DRAMIX I Steel
EMIS-SR Model – DRAMIX I Steel
Experimental – RF 4000 PVA
TSM Model – RF 4000 PVA
EMIS-SR Model – RF 4000 PVA
Stress (MPa)
Deformation (mm)

b)

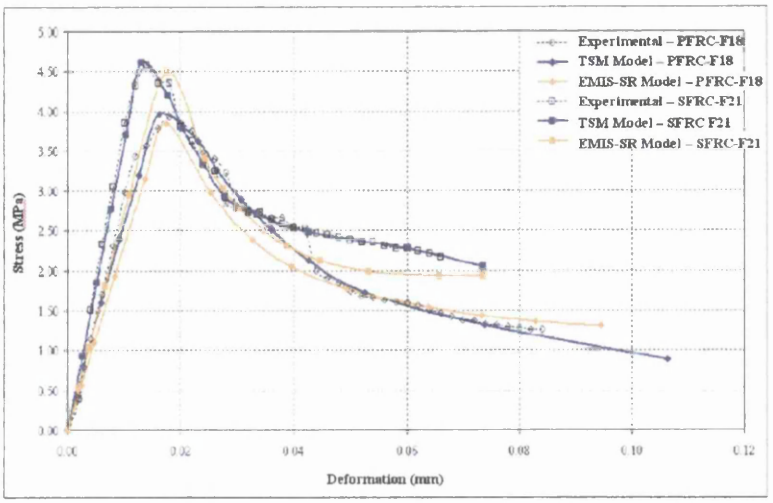

c)

Figure 2.9 – Experimental and Numerical models comparison of complete stress-deformation response of a) throated prismatic b) rectangular plate c) throated square plate specimens (Xiao and Chin 2004)

The failure mechanism for cementitious composites is distinguished by its post-cracking behaviour and does not exhibit large deformations as the EMIS model would predict. Therefore it seems that the EMIS model as being more suitable for predicting the softening response of ductile materials such as steel, copper etc. which exhibit significant geometrical deformation beyond the respective peak stresses.

2.8 Evaluation

The displacement-controlled (DCM) and arc-length methods are two options readily available in the ANSYS® software package though both are still incapable of simulating the post limit stress distributions. The execution of DCM can be done simply by replacing load with displacement as the driving force of the analysis, i.e. to assigning displacement onto boundary condition(s). On the other hand, the arc-length method requires trial and error procedures to obtain the suitable maximum and minimum radii and also adjustment for the reference arc-length which may be tedious especially to new and even moderate users. The determination of the limiting load or displacement value

within some known tolerance can also be difficult. Not to mention the computational run-time, with lengthy solution run even for a decent model.

What are the criteria then, to define a good softening model? Although many of the existing models have indeed been able to give a good prediction of the load-displacement response, the capability of these models to capture the stress states beyond the limit point remains generally unknown. Having this feature allows the critical element(s) to be identified and thus the ability to predict the weak link within the FE model when the maximum load is approached. The TSM and EMIS models have demonstrated this capability; whereby the post-cracking stress distribution of cementitious materials (Xiao and Chin 2004) are captured. Building up on that, it is always advantageous if the failure mechanism to fracture could also be captured. The importance to consider the geometrical instabilities could only be highlighted especially for ductile materials where necking is too significant to be ignored.

Although these models have been tested and validated to different extents, not all have been widely accepted, not to mention their implementation into finite element software for commercial application. Furthermore, debate exists over the pros and cons of different approaches (Borst et al. 1998) often in theoretical point of view. This reflects the need for more extensive research and development on both existing and new softening models which could well characterized post-limit behaviour for both tension and compression of various materials not only for material analysis, but also for structural analysis.

3.0 Numerical Modelling

3.1 Overview

Computational modelling implementing numerical method has made possible the simulation of an abstract model or models in a particular system. In this recent time, it has become a useful and important part of mathematical modelling of many natural and physical systems in computational physics, chemistry, biology, engineering and technology etc. to gain insight into the operations of those systems. The ultimate goal is to represent a real system with an abstract one and to observe, understand and predicts its response to certain combinations of disturbances and loadings under certain environment.

Traditionally, the formal modelling of systems has been via a mathematical model, which attempts to find analytical solutions to problems and enable the predictions of the behaviour of the system from a set of parameters and initial conditions. Computer simulations build on these and are a useful adjunct to purely mathematical models in small and large scale science and technology.

This study presents the application of numerical modelling on material behaviour, based on computer simulation of metallic tensile specimens. The experimental test

specimens were modelled and the predicted stress and deformation responses based on these computational simulations were validated against the corresponding experimental data.

3.2 The Elasto-Plastic (EP) Constitutive Relations for Plasticity

The theory of plasticity deals with the behaviour of materials at strains where Hooke's law is no longer valid, i.e. where the presence of non-recoverable strains upon load removal cannot be ignored. The following demonstrates the conventional elasto-plastic constitutive relations for 3-dimensional plasticity cases.

3.2.1 Additive split

The deformation in the plastic region can be subdivided into a standard manner where the incremental of total strain consists of the elastic and plastic components given by

$$\delta\varepsilon_{ij} = \delta\varepsilon_{ij}^{\ e} + \delta\varepsilon_{ij}^{\ p} \qquad \text{[Eq.3.1]}$$

Subsequently, the elastic component follows the Hooke's linear stress-strain relationship in the following form.

$$\delta\varepsilon_{ij}^{\ e} = [\mathrm{D}]^{-1}\delta\sigma_{ij} \qquad \text{[Eq.3.2]}$$

where [D] is the 3-dimensional uniaxial isotropic elasticity matrix defined by

$$[\mathrm{D}] = \frac{E}{(1+v)(1-2v)}\begin{bmatrix} (1-v) & v & v & 0 & 0 & 0 \\ v & (1-v) & v & 0 & 0 & 0 \\ v & v & (1-v) & 0 & 0 & 0 \\ 0 & 0 & 0 & \frac{(1-2v)}{2} & 0 & 0 \\ 0 & 0 & 0 & 0 & \frac{(1-2v)}{2} & 0 \\ 0 & 0 & 0 & 0 & 0 & \frac{(1-2v)}{2} \end{bmatrix} \qquad \text{[Eq.3.3]}$$

3.2.2 Failure/yield criterion

In most cases, structural components are subjected to multi-axial stress distribution and yielding does not always occur when the uniaxial yield point is attained. The yield criterion therefore determines the onset of plastic deformation i.e. the point at which the stress-strain behaviour deviates from linearity. Numerous yield criterions have been proposed and for ductile materials, the Tresca and in particular the von Mises criteria are the two most widely recognised.

The Tresca criterion, also known as the maximum shear stress criterion, is possibly the oldest formulation and was postulated by Henri Tresca in 1864. This criterion predicts that yield begins when the maximum shear stress distribution reached a critical value which is equivalent to the maximum shear stress occurred under a simple uniaxial tension test. The criterion, in its principle stress space is given by

$$f(\sigma) = \frac{1}{2}\max\left(|\sigma_1 - \sigma_2|, |\sigma_2 - \sigma_3|, |\sigma_3 - \sigma_1|\right) - \kappa_y(k) \qquad \text{[Eq.3.4]}$$

The critical value of the maximum shear stress, denoted by κ_y is half the yield stress σ_y in simple tension. It could be a function of expanding (or contracting) yield surface govern by a work hardening parameter k. This criterion can be represented by an infinitely long regular hexagonal cylinder as the yield surface in the 3-D principle axes, see Figure 3.1(a). The normal section where $\sigma_1 = \sigma_2 = \sigma_3$ is terms as the π plane.

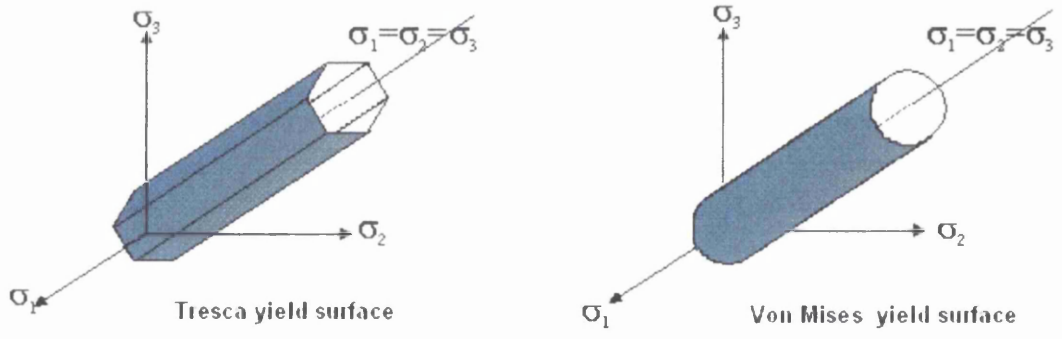

Figure 3.1 – a) Tresca and b) Von Mises Yield Surfaces

The von Mises criterion (also known as the maximum distortion energy criterion) states that failure occurs when the maximum octahedral shear stress reaches its critical value given by the yield stress in shear κ_y. The function is given by

$$f(\sigma)=\sqrt{\frac{1}{6}\left[(\sigma_1-\sigma_2)^2+(\sigma_2-\sigma_3)^2+(\sigma_3-\sigma_1)^2\right]}-\kappa_y(k) \qquad \text{[Eq.3.5]}$$

The von Mises yield surface is therefore an elliptical cylindrical surface parallel to the hydrostatic stress axis as shown in Figure 3.1(b). It can be observed that the yield locus is a circular cylinder, which is independent of the yield surface. The relationship between the uniaxial and shear yield stress is $\sigma_y=\sqrt{3}\kappa_y$.

3.2.3 Flow rule

To relate the incremental plastic strain with the corresponding increment in stress, an assumption of proportionality between the incremental plastic strain and the stress gradient of the plastic potential is described as follows

$$\delta\varepsilon_{ij}{}^{p}=d\lambda\frac{\partial Q}{\partial\sigma_{ij}} \qquad \text{[Eq.3.6]}$$

This equation is known as the flow rule and the constant $d\lambda$ introduced is termed as the plastic multiplier. If the yield function is equivalent to the plastic potential function $(Q=f)$, then the increment of plastic strain is associated with the yield surface, known as the associated (normal) flow rule. Hence, the equation above can be re-expressed as;

$$\delta\varepsilon_{ij}{}^{p}=d\lambda\frac{\partial f}{\partial\sigma_{ij}} \qquad \text{[Eq.3.7]}$$

3.2.4 Loading/unloading conditions

By assumptions that when $d\lambda=0$, $f<0$. It takes little effort to see that when plastic straining rate is zero, the failure criterion is not met. On the other hand, when the

plastic straining rate does exist, the failure criteria is met, i.e. $f = 0$. This implies the Kuhn-Tucker conditions where;

$$\begin{aligned} f < 0 &\Rightarrow d\lambda = 0 \\ f = 0 &\Rightarrow d\lambda > 0 \end{aligned} \qquad \text{[Eq.3.8]}$$

This could be expressed in a single equation $d\lambda f = 0$. The consistency condition is $d\dot{\lambda}\dot{f} = 0$, the rate form of the Kuhn-Tucker condition.

Upon unloading in a plastic deformation state, the unloading gradient is parallel to the elastic part of the elastic gradient. The elastic recovery strain is assumed to be $\varepsilon_{ij}^{\ e} = [D]^{-1}\sigma_{ij}$.

3.2.5 Isotropic hardening

We restrict here to the case of an associated flow rule and we can observe from experimental evidence that the elastic domain evolves in conjunction with continuous plastic straining. A parameter, α, which governs the evolution of elastic domain is introduced. With an isotropic material, the elastic domain evolves with its centre fixed at the $\sigma - \alpha$ space. The yield criterion representation of isotropic hardening is

$$f = \left|\sigma_{eff}\right| - \left[\sigma_{Y0} - H\alpha\right] \qquad \text{[Eq.3.9]}$$

where σ_{eff} - effective (von Mises) stress, σ_{Y0} - initial yield stress and H - plastic hardening modulus [Equivalent to R_0 in Voce's equation].

There exist several forms for α, notably;

$$\dot{\alpha} = \left|\dot{\varepsilon}^{p}\right| \text{ and } \dot{\alpha} = \sigma\left|\dot{\varepsilon}^{p}\right| \qquad \text{[Eq.3.10]}$$

which are termed as the strain and work hardening respectively.

3.2.6 Elasto-plastic stiffness matrix

The elasto-plastic (EP) modulus defines the stress-strain gradient in the plastic region. In computational procedures, the incremental total strain between two iterations is determined by the instantaneous modulus. Expressing equation [Eq.3.9] in a different form;

$$f(\sigma,\alpha) = \mathbf{g}(\sigma) - H(\alpha) = 0 \qquad \text{[Eq.3.11]}$$

where $\mathbf{g}(\sigma)$ is a function defining the effective stress and $H(\alpha)$ defines the expansion of the yield surface. To obtain the EP modulus, it is necessary to solve explicitly the parameter $d\lambda$. Differentiating equation [Eq.3.11] gives

$$df(\sigma,\alpha) = \frac{\partial f}{\partial \boldsymbol{\sigma}} d\boldsymbol{\sigma} + \frac{\partial f}{\partial \alpha} d\alpha = 0 \qquad \text{[Eq.3.12]}$$

or in expanded vector form,

$$\frac{\partial f}{\partial \sigma_x} d\sigma_x + \frac{\partial f}{\partial \sigma_y} d\sigma_y + \frac{\partial f}{\partial \sigma_z} d\sigma_z + \ldots + \frac{\partial f}{\partial \alpha} d\alpha = 0 \qquad \text{[Eq.3.13]}$$

which is also equivalent to

$$\left[\frac{\partial f}{\partial \boldsymbol{\sigma}}\right]^T d\boldsymbol{\sigma} + \frac{\partial f}{\partial \alpha} d\alpha = 0 \qquad \text{[Eq.3.14]}$$

Let the following representations

$$\mathbf{a} = \frac{\partial f}{\partial \boldsymbol{\sigma}} \text{ and } H = -\frac{1}{d\lambda}\frac{\partial f}{\partial \alpha} d\alpha \qquad \text{[Eq.3.15]}$$

Therefore substitution of [Eq.3.15] into equation [Eq.3.14] gives

$$\mathbf{a}^T d\boldsymbol{\sigma} - H d\lambda = 0 \qquad \text{[Eq.3.16]}$$

The term **a** is also known as the flow vector and H being the plastic hardening modulus which can be obtained from the uniaxial stress-strain by the following relation

$$H = \frac{\partial \sigma}{\partial \varepsilon^p} = \frac{E_T E}{E - E_T} \qquad \text{[Eq.3.17]}$$

where E and E_T are the Young's (elastic) and tangent elasto-plastic (EP) modulus respectively. By employing equations [Eq.3.2] and [Eq.3.7] into [Eq.3.1], we get

$$d\boldsymbol{\varepsilon} = [\boldsymbol{D}]^{-1} d\boldsymbol{\sigma} + d\lambda \frac{\partial \boldsymbol{f}}{\partial \boldsymbol{\sigma}} \qquad \text{[Eq.3.18]}$$

Now let,

$$\boldsymbol{d}_D^T = \mathbf{a}^T \boldsymbol{D} \qquad \text{[Eq.3.19]}$$

Multiply equation [Eq.3.18] with equation [Eq.3.19]

$$\boldsymbol{d}_D^T d\boldsymbol{\varepsilon} = \mathbf{a}^T [\boldsymbol{D}]^{-1} \partial \boldsymbol{\sigma} + \mathbf{a}^T \boldsymbol{D} d\lambda \frac{\partial \boldsymbol{f}}{\partial \boldsymbol{\sigma}} \qquad \text{[Eq.3.20]}$$

$$= \mathbf{a}^T \partial \boldsymbol{\sigma} + \mathbf{a}^T \boldsymbol{D} d\lambda \mathbf{a} \qquad \text{[Eq.3.21]}$$

Recall the consistency condition $d\dot{\lambda} \dot{f} = 0$ and equation [Eq.3.16] then implies

$$d\lambda = \frac{\boldsymbol{d}_D^T d\boldsymbol{\varepsilon}}{H + \mathbf{a}^T \boldsymbol{D} \mathbf{a}} \qquad \text{[Eq.3.22]}$$

Consider a separate development on equation [Eq.3.18] that gives;

$$d\boldsymbol{\varepsilon} = [\boldsymbol{D}]^{-1} d\boldsymbol{\sigma} + d\lambda \mathbf{a} \qquad \text{[Eq.3.23]}$$

Rearranging yields

$$d\boldsymbol{\sigma} = [\boldsymbol{D}](d\boldsymbol{\varepsilon} - d\lambda \mathbf{a}) \qquad \text{[Eq.3.24]}$$

Substitute equation [Eq.3.22] into equation [Eq.3.24] and simplifications gives

$$d\boldsymbol{\sigma} = [\boldsymbol{D}]\left(d\boldsymbol{\varepsilon} - \frac{1}{H + \mathbf{a}^T \boldsymbol{D}\mathbf{a}} \mathbf{a} \boldsymbol{d}_D^T d\boldsymbol{\varepsilon} \right)$$

$$= \left[\boldsymbol{D} - \frac{\boldsymbol{D}\mathbf{a}\boldsymbol{d}_D^T}{H + \mathbf{a}^T \boldsymbol{D}\mathbf{a}} \right] d\boldsymbol{\varepsilon} \qquad \text{[Eq.3.26]}$$

And,

$$\boldsymbol{d}_D = \boldsymbol{D}\mathbf{a} \qquad \text{[Eq.3.27]}$$

Substitution into equation [Eq.3.26]

$$d\boldsymbol{\sigma} = \left[\boldsymbol{D} - \frac{\boldsymbol{d}_D \boldsymbol{d}_D^T}{H + \boldsymbol{d}_D^T \mathbf{a}} \right] d\boldsymbol{\varepsilon} \qquad \text{[Eq.3.28]}$$

Or in a simpler form of;

$$d\boldsymbol{\sigma} = \boldsymbol{D}_{ep} d\boldsymbol{\varepsilon} \qquad \text{[Eq.3.29]}$$

where

$$\boldsymbol{D}_{ep} = \boldsymbol{D} - \frac{\boldsymbol{d}_D \boldsymbol{d}_D^T}{H + \boldsymbol{d}_D^T \mathbf{a}} \qquad \text{[Eq.3.30]}$$

Equation [Eq.3.30] is known as the elasto-plastic stiffness matrix which varies with each load increment. In the mathematical solution, this stiffness matrix takes a negative form beyond the limit point in the softening region. However, the finite element computational procedure has been limited by its inadequacy in handling this non-positivity form with its conventional N-R procedure and will lead to non-convergence when the limit stress is exceeded.

3.3 General purpose ANSYS® software package

3.3.1 Introduction

ANSYS® v11.0 is a general purpose finite element analysis software for solving numerically a wide variety of mechanical problems in different engineering disciplines. The nature of the problems could include static or dynamic, linear and non-linear structural analysis, heat transfer, fluid, acoustic, electro-magnetic and biomedical problems. This software includes a platform, i.e. the unified graphical user interface (GUI) which gives an easy and interactive access to program functions, commands, documentations, etc. The GUI contains several analysis tools in particular the pre-processing (for geometry and mesh generation), solver and post processing modules.

The ANSYS® software enables engineers to perform many tasks as follows:

1. Build abstract models or export and import CAD models of structures, products, or components to different compatible analysis programs.
2. Apply operating loads or other design performance conditions.
3. Study physical responses, such as stress levels, temperature distributions, etc.
4. Optimization of a design in the initial development process to reduce production costs.
5. Perform prototype testing in environments where it would otherwise be undesirable or impossible.

The basic steps involved in any typical FEA in ANSYS® consist of the following.

3.3.2 Preprocessing

The model is created using a combination of keypoints, lines, areas and volumes. Mesh can be generated either by manual settings or using the default mesh controls, which are appropriate for many models. The initial material properties are assigned at this stage.

3.3.3 Solver

The boundary conditions are applied onto the model. The solution options are set such that the type of analysis, substeps, solver type and other desirable options are defined accordingly. As the term itself suggests, the solution is solved in this stage. Also, for the proposed modelling technique to be discussed in chapter 4, the modified material properties must be reassigned in the solver interface.

3.3.4 Postprocessor

In the postprocessor interface, the desired results of the solution can be obtained for viewing purposes. There are two options available. In the General Postprocessor, ANSYS® could display the solution results over the entire model at a specific load or sub step while the Time-History Postprocessor offers the viewing of the variation of a particular result in respect to time.

4.0 Methodology of the Proposed Modelling Technique

4.1 Introduction

The proposed softening technique was built based on the credible laboratory observations on material behaviour in a series of cyclic loading and unloading stages. When the peak points of each cyclic loop are joined, they form an almost identical hardening and softening path as a single monotonic test would follow (Chun et al. 2001); see Figure 4.1. This principle of increasing (and decreasing) stress path with increasing load cycles was adapted in this model for the softening analysis, as the hardening branch could be numerically solved in a straight forward manner by selecting the available nonlinear options.

The material stress-strain curve in this modelling technique is in general characterized by the Voce exponential strain-hardening function (Voce 1948). The original form of this equation was first proposed in 1948, resulting from the experimental observations that the alloy materials tested by Cook and Larke (1945) exhibit a similar load-deformation response, differing only in a constant which describes the characteristic of each material. Further discussion on the Voce equation was reported in (Voce 1955);

particularly on the overall advantages of this strain hardening function over the well-known power function of Ludwick (See Appendix 2).

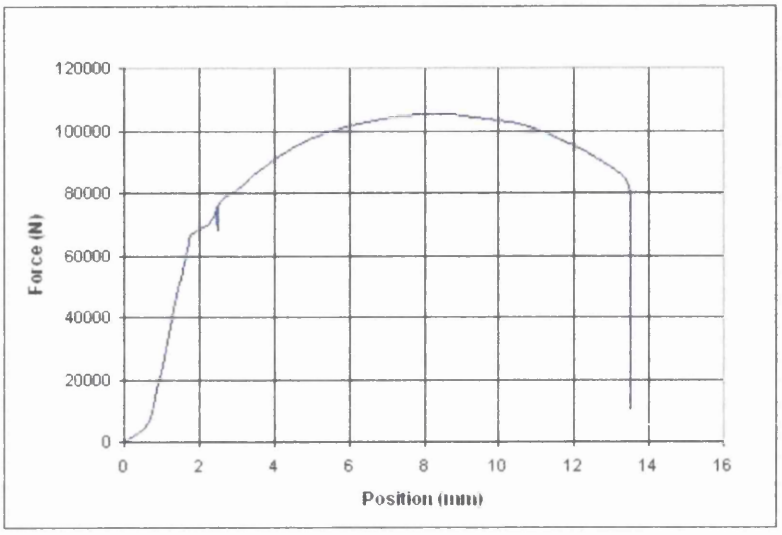

a)

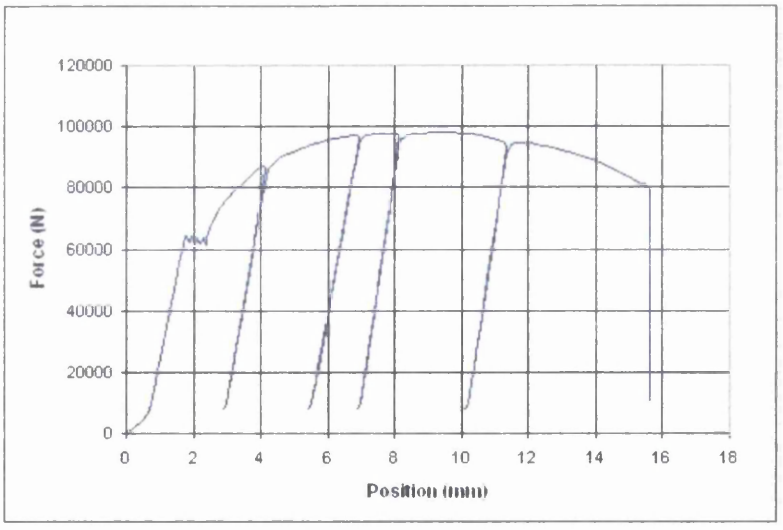

b)

Figure 4.1 – Force-displacement diagram of a) monotonic and b) cyclic loaded steel bar

The early work on Voce exponential function was based on the true stress σ_t vs. strain ratio R curve although several terms for the abscissa have also been suggested, e.g. logarithmic strain and percentage of deformation. A typical $\sigma_t - R$ curve is such a way that the stress path always ascends even beyond the maximum load, approaching an

asymptotic stress as shown in Figure 4.2. In an event of experimental testing where the actual test is discontinued before fracture, a free-hand extrapolation could well indicate the final horizontal asymptotic stress attained at 100% deformation (infinite strain).

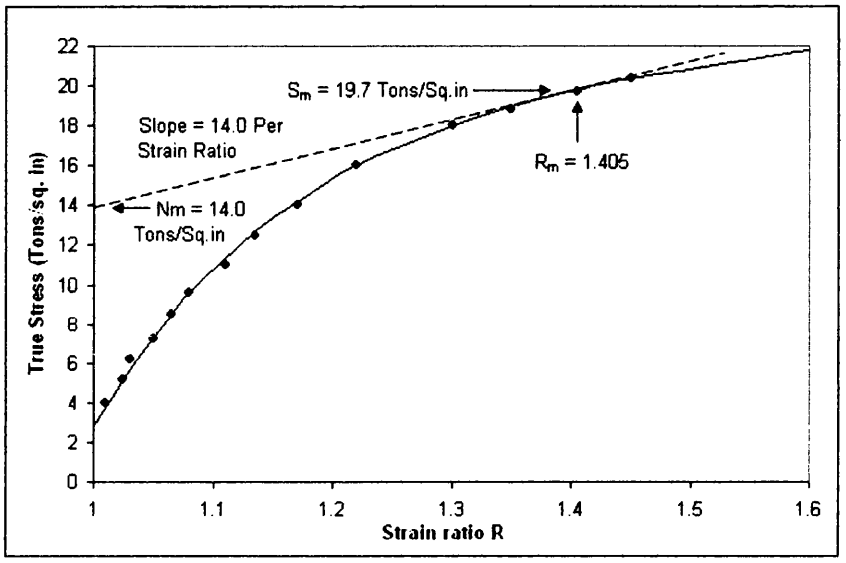

Figure 4.2 – A typical $\sigma_t - R$ curve, obtained from tensile tests on Electrolytic and Phosphorus Deoxidised Coppers

One characteristic of such $\sigma_t - R$ curve is that the tangential slope of the curve at maximum applied load is numerically equal to the engineering ultimate tensile strength. In fact, the gradient at every point along the curve corresponds to the engineering stress at that particular point. This relationship is true for the case of true $\sigma_t - R$ curve. Refer to Appendix 3 for derivations.

4.2 The Constitutive Theory of the Proposed Softening Model

The Voce exponential function which is governed by four parameters can be expressed as

$$\sigma = k_0 + R_0 \varepsilon^{pl} + R_\infty (1 - e^{-b\varepsilon^{pl}}) \qquad \text{[Eq.4.1]}$$

where k_0 - elastic limit$\left(N/mm^2\right)$, R_0 - plastic hardening modulus$\left(N/mm^2\right)$, R_∞ - asymptotic stress$\left(N/mm^2\right)$and a constant b (dimensionless) which controls the elastic-plastic transition fillet. σ is the current stress state$\left(N/mm^2\right)$ and ε^{pl} the corresponding equivalent plastic strain (dimensionless).

This equation characterizes the hardening portion of the stress-strain curve up to the ultimate tensile stress. Apparently, it is also necessary for a function to define the softening branch of the curve to simulate the complete monotonic stress-strain response. Hence, equation [Eq.4.2], computed from direct modification from the original Voce hardening term was proposed for this necessity.

$$\sigma = \sigma_{ult} + R_0^{soft}\left(\varepsilon^{pl} - \varepsilon_{peak}^{pl}\right) + R_\infty^{soft}\left[1 - e^{b^{soft}\left(\varepsilon^{pl} - \varepsilon_{peak}^{pl}\right)}\right] \qquad \text{[Eq.4.2]}$$

where the notations; σ_{ult} - ultimate tensile strength$\left(N/mm^2\right)$, R_0^{soft} - plastic softening modulus$\left(N/mm^2\right)$, R_∞^{soft} - asymptotic softening modulus $\left(N/mm^2\right)$ and a constant b^{soft}. ε_{peak}^{pl} is the equivalent plastic strain at peak stress. This equation was constructed from the original Voce equation by replacing k_0 with σ_{ult}, ε^{pl} with$\left(\varepsilon^{pl} - \varepsilon_{peak}^{pl}\right)$ and a negative term of R_0^{soft}. Therefore, these two independent equations, [Eq.4.1] and [Eq.4.2] define the ascending and descending branches of the monotonic tensile stress-strain curve respectively.

A polynomial function [Eq.4.3] could also be adopted for the nonlinear elasto-plastic region. This function consists of seven polynomial constants, C_i which describes the non-linearity from the onset of plastic deformation to the fracture point.

$$\sigma = C_6\varepsilon^6 + C_5\varepsilon^5 + C_4\varepsilon^4 + C_3\varepsilon^3 + C_2\varepsilon^2 + C_1\varepsilon + C_0;\ C_i \text{ where } 0 < i < 7 \qquad \text{[Eq.4.3]}$$

As previously discussed, this proposed softening model utilizes the loading-unloading-reloading principle to simulate the softening behaviour of a material. At each

reloading phase, the Voce equation is reassigned with a new set of parameters. By employing such approach of material properties modification at each subsequent step, the solution process would avoid non-convergence due to negative stiffness. The element stiffness matrix would remain positive definite throughout.

4.3 Determination of Parameters

In general, the parameters in equation [Eq.4.1] can be obtained through the following practices. The elastic limit k_0 can be estimated from the experimental stress strain curve as the stress when the plastic deformation first occurs. R_0 is taken as $\frac{EE_T}{E-E_T}$; E being the initial Young's modulus and E_T the instantaneous elasto-plastic tangent modulus near peak stress. This condition allows a steady transition from the hardening to the softening regime. R_∞ is obtained through the following simple arithmetic.

$$R_\infty = \sigma_{ult} - R_0\varepsilon^{pl}_{peak} - k_0 \qquad \text{[Eq.4.4]}$$

Different materials are possible to exhibit (almost) similar elastic limit and ultimate tensile strength but yet follow different transition paths (Figure 4.3), i.e. the elasto-plastic hardening paths for the respective materials. Based on this argument, it does not seem to give a physical meaning to compute a derivation for b and thus this constant is estimated through fitting of the experimental curve. Figure 4.4 shows the Voce representation of a hardening material curve adopted in ANSYS®.

The parameters for the monotonic softening equation for [Eq.4.2] are generally obtained through curve fitting. The ultimate tensile strength σ_{ult} can be obtained from the uniaxial tensile stress-strain curve as the maximum stress the material could reach before the onset of necking. From the many trials dedicated into this equation, it is suggested to specify $R_0^{soft} = 0$ as the initial trial. This condition works well in most cases. The parameter b^{soft}

could then be adjusted with little effort. R_{∞}^{soft} is assigned only if required and in many cases, can be ignored.

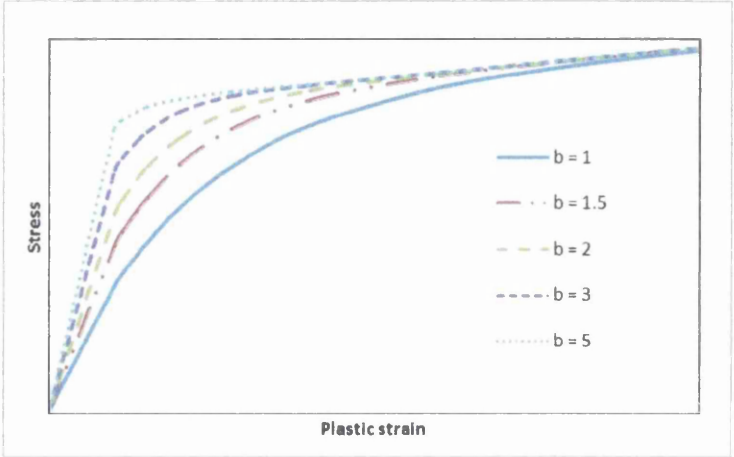

Figure 4.3 – Elasto-plastic hardening fillets due to variation of constant b

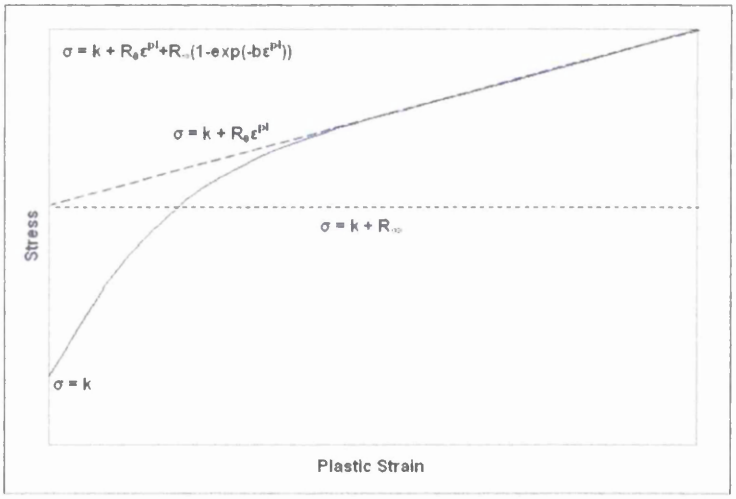

Figure 4.4 – Voce Nonlinear Hardening Stress- Plastic Strain Curve

Equation [Eq.4.3] provides an easier determination of material parameter procedures for the stress – strain relation. It utilizes the capability of the Microsoft Excel package to define a trendline which best fit the elasto-plastic experimental stress – strain pairs. For consistency, the polynomial function is kept to the seventh order, although in some cases, a good stress – strain relation could be obtained with a smaller order. The constants then could be viewed and obtained by selecting the 'display equation on chart'

option. These constant parameters are imported to an ANSYS® macro (Appendix 4) to determine the required internal variables.

When the ultimate tensile strength is attained, the reloading Voce equation takes the same expression but a slightly different definition than previously defined. Since we have little interest with the possible paths in which the reloading could follow apart from its peak point, R_0 can be considered as redundant. This is replaced by a negative constant R_0^* which no longer is the plastic hardening modulus. This serves as a dummy value to give rise to the bifurcation point in the Voce equation. For each subsequent reloading procedure, the pair of stress-strain state corresponds to a certain point along the monotonic softening branch, i.e. equations [Eq.4.2] or [Eq.4.3]. The asterisks (*) were assigned to distinguish the parameters notation for the softening region from those for the hardening region. Therefore, in the softening region we have the reloading Voce equation as

$$\sigma = k_0^* + R_0^* \varepsilon^{pl} + R_\infty^* (1 - e^{-b^* \varepsilon^{pl}}) \qquad \text{[Eq.4.5]}$$

At each subsequent softening (peak) point, the condition $\frac{\partial \sigma^*}{\partial \varepsilon^{pl}} = 0$ has to be met, i.e.

$$\frac{\partial \sigma^*}{\partial \varepsilon^{pl}} = R_0^* + R_\infty^* b e^{-b^* \varepsilon^{pl}} = 0 \qquad \text{[Eq.4.6]}$$

Rearranging,

$$R_\infty^* = -\left(\frac{R_0^* e^{b^* \varepsilon^{pl}}}{b^*} \right) \qquad \text{[Eq.4.7]}$$

Substituting [Eq.4.7] into [Eq.4.5] gives;

$$\sigma = k_0^* + R_0^* \varepsilon^{pl} - \left(\frac{R_0^* e^{b^* \varepsilon^{pl}}}{b^*} \right) (1 - e^{-b^* \varepsilon^{pl}}) \qquad \text{[Eq.4.8]}$$

which represents the reloading path in the softening region, where $k_0^* = \psi\sigma = \frac{k_0}{\sigma_{ult}}\sigma$ and R_0^* is kept consistent with a value of -100.

Equating [Eq.4.2] or [Eq.4.3] with [Eq.4.8] solves for parameter b^*. Substituting b^* into [Eq.4.7] gives R_∞^* and along with k_0^* and R_0^* as defined above are the updated set of Voce parameters. The new set of material properties is then assigned to the material elements for the subsequent loadstep.

4.4 Numerical Simulation: ANSYS® Input Commands and Solution Options

In this section, the ANSYS® input commands will be demonstrated and where relevant, the command usage will only be briefly discussed. For descriptions on more command usage and reference, refer (ANSYS 2007).

4.4.1 Element type

All the models were modelled using SOLID185 elements. This element type is used for the 3-D modelling of solid structures. Defined by eight nodes and having three degrees of freedom at each node, i.e. translations in the nodal x, y, and z directions, its element has plasticity, hyperelasticity, stress stiffening, creep, large deflection and large strain capabilities. The geometry and node location of the element are shown in Figure 4.5.

For the modelling of the dumbbell tensile specimens of circular cross-sectional gauge area, the choice of higher order elements with mid-side nodes would probably be more suitable due to the curvy nature of the structure. However, the SOLID185 element type was adopted because it is required for the future implementation of user programmable subroutines. Such programmable feature is only compatible with the 18x family of elements.

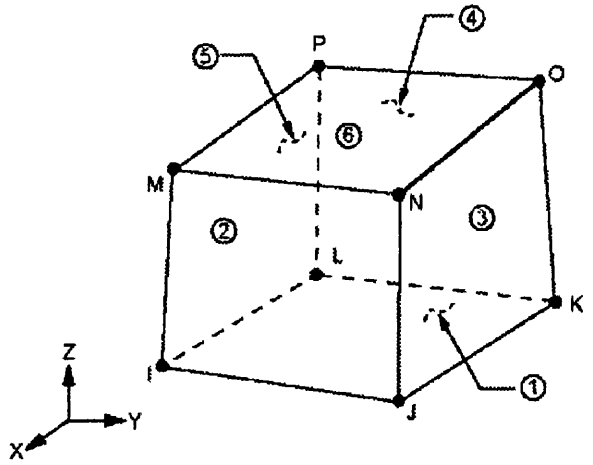

Figure 4.5 – SOLID185 Structural solid geometry; Alphabets I - P and the circled integers represents the nodes and element surfaces respectively

4.4.2 Material Properties

The initial material properties are assigned for the pre-peak limit analysis. As the peak stress is approached, a new set of updated material properties is re-assigned to the selected elements or element components within the FE model. Therefore, the complete analysis consists of a series of material properties update procedures at each subsequent softening loadsteps. The linear elastic properties, i.e. (elastic) Young's modulus and Poisson's ratio remain consistent and unchanged throughout the analysis.

The ANSYS® FE software package adopts the Voce exponential function for its nonlinear isotropic hardening option (NLISO). This option is activated by employing the TB command and the four Voce parameters, e.g. K0, R0, RASM and B, which characterize the elasto-plastic hardening and each softening points, are assigned. The MPCHG command reassigns the selected elements to a new defined set of material properties as follows

...
TB,NLIS,I,1,4,
TBTEMP,0
TBDATA,, K0 , R0, RASM, B,,

MPCHG, MAT, ELEM

...

The following ANSYS® input commands demonstrate how the Voce parameters are determined and stored for each reloading loadstep; I being the *n*th set number of material properties (also the number of loadstep) while K0, R0, RASM and B, corresponding to k_0^*, R_0^*, R_∞^* and b^*, are the updated set of Voce parameters. They are stored for each loadstep in a 2-dimensional table array, defined by *DIM which is given the term SIGEPS. The command abbreviations are; SPTS – number of softening points, EPSPL – equivalent plastic strain, SIGULT – softening peak stress, TOL – tolerance, PSI - ψ (refer chapter 4.3).

*DIM,SIGEPS,TABLE,6,SPTS,1,,, } Defines a 6 x SPTS table-type array

*DO,I,1,SPTS,1
EPSPL = SIGEPS(1,I,1)
SIGULT = SIGEPS(2,I,1)
K0 = SIGULT/PSI
R0 = -100
} Determination of k_0^* and R_0^*

LHS = (SIGULT-K0-R0*EPSPL)/R0
*DO,B,1,1200,0.1
RHS = -EXP(B*EPSPL)*(1-EXP(-B*EPSPL))/B
DIFF = ABS(LHS-RHS)
*IF,DIFF,LE,TOL, EXIT
*ENDDO
} Determination of b^*

RASM = -R0*EXP(B*EPSPL)/B } Determination of R_∞^*

*SET,SIGEPS(3,I,1) ,K0
*SET,SIGEPS(4,I,1) ,R0
*SET,SIGEPS(5,I,1) ,B
*SET,SIGEPS(6,I,1) ,RASM
} Store the updated Voce parameters in table array

*ENDDO

The command lines for the setting of the analysis environment and determination of the softening parameters are written in separate functional macros as shown in Appendix 4.

4.4.3 Loadings and Boundary Condition

The settings of the boundary conditions for the finite element models are rather straight forward. One end of the tensile specimens was constrained in the x, y and z directions while the pressure (surface) loads were applied at the other end of the specimens. The loads and boundary conditions were applied to the finite elements entities (nodes and elements) so as the unloading response could be captured. Similar runs with application of loads and boundary condition on the geometric entities (keypoints and areas) seem not to be able to capture the unloading path. For the unloading operations, the load is scaled to a small scaling factor such that the loads are reduced to virtually zero. Removing the loads or applying a zero scaling factor results in unchanged stress distribution. The following demonstrates the load scaling command; the scaling of the surface load on all elements with a scaling factor of 0.001.

...
SFSCALE,ALL,0.001,1,
...

4.4.4 Solution Option

The intrinsic TIME at which the model specimen reaches peak stress is set to unity as a common practice. As for materials which exhibit significant nonlinearity and/or small tangent modulus with respect to the Young's modulus, the iteration point tends to follow a large jump after which the elastic limit has been exceeded. This applies for a solution within the first loadstep, given that a load-controlled (force or pressure loading) analysis is adopted where the solution is stress-increment sensitive rather than of strain-increment sensitive. Therefore, to capture a smooth and gradual increment stress-

deformation response, the pre-peak stress responses for these cases are solved through several loadsteps with a gradual increment of applied load within the hardening branch until the peak stress is attained. Displacement driven analyse do not encounter this problem and can always be solved within one loadstep with good convergence.

The frequency of the solution data is such that the unloading and intermediate reloading paths are not written to the database apart from the bifurcation points of each reloading branch, i.e.

At TIME values during unloading;

```
...
OUTRES,ERASE
OUTRES,ALL,NONE
...
```

and, at TIME during reloading;

```
...
OUTRES,ERASE
OUTRES,ALL,LAST
...
```

As a matter of the real time for solution, it is uneconomical if the solution control option for each subsequent loadstep is kept consistent throughout based on the initial pre-peak loadstep(s) settings. For this reason, it is more advantageous to set the substep to one (unity) during the unloading phases such that the unloading is solved in one iteration, as the reduction in stress during unloading would follows a straight descending path parallel to the initial elastic Young's modulus. During reloading phrases, a substep of three or four is assigned so that the nonlinear paths can be captured when desired.

4.4.5 Reduced-load Optimization

Apparently, as the load is increased such that the peak stress is approached, the load capacity at which the FE model could withstand will decrease. Hence, it is therefore necessary to reduce the load to a value which corresponds to the optimum capacity of the FE model at that specific point. A macro was written to perform an optimization operation to compute the respective optimum load at each loadstep. This optimization procedure adopts the bisection method between the upper and lower bound load capacities whereby the accuracy of the prediction depends on the tolerance TOL2; where $0 \leq TOL2 \leq 1$, which was set by the author to 0.999 for optimum accuracy for all analysis. Lowering the value of TOL2 will result in considerable over or under estimation of deformation with respect to applied load/stress.

```
AVE = (UB + LB)/2 } Initial average of upper and lower bounds load value
...
*DO,A,1,50,1
FINISH
/SOL
SFSCALE,ALL,AVE,1, } Scaling down of load value
/STATUS,SOLU
SOLVE

*GET,CNVG,ACTIVE,0,SOLU,CNVG,, } Retrieving convergence status
```

```
SFSCALE,ALL,(1/AVE),1,
RATIO = LB/AVE
TOL2 = 0.999
*IF,RATIO,GE,TOL2,THEN
*EXIT
*ELSEIF,CNVG,EQ,1,THEN
UB = UB
LB = AVE
*ELSE
UB = AVE
LB = LB
*ENDIF
AVE = (UB + LB)/2
*ENDDO
```

Updating scaling down factor

5.0 Results: Validation Cases

5.1 Introduction

Several validation tests have been carried out to determine the feasibility and efficiency of the proposed modelling technique. The tests were done against some experimental test data obtained from available sources and presented in the following sub-chapters. The specimens are of dumbbell, circular tube and rectangular shapes and note that the test data selected were those without a yield plateau.

All the models were built within the ANSYS® platform. The deformations are taken as the net incremental displacement between two nodes which correspond to the experimental gauge positions. Both the cyclic and monotonic stress paths were presented for comparisons, although the softening model concerns primarily the monotonic response only. Whilst Case 1 will discussed more thoroughly, the other validation cases will be presented in the sequence of tabulated material properties and gauge dimensions, element mesh and boundary condition, stress-deformation response, and the stress distribution plot at peak point and fracture.

5.2 Case 1: Circular Solid Steel; Specimen G1X1A

Table 5.1 tabulates the material properties, i.e. Young's modulus, yield stress tensile ultimate strength and the gauge area dimensions of the circular solid steel specimen G1X1A. The source at which the reference curve was obtained is also stated. This validation test adopts the polynomial softening equation [Eq.4.3] to simulate the post limit response where C_6 = -15,119, C_5 = 305,250, C_4 = 237,320, C_3 = 89,818, C_2 = 18097, C_1 = 2,470 and C_0 = 55.

Source	Properties				
	Material			Gauge Area	
	Young's modulus	Yield Stress	Ultimate Tensile Strength	Length	Diameter
(Barret 1999)	205,000 *MPa*	125 *MPa*	350 *MPa*	25.4 *mm*	5.0 *mm*

Table 5.1: Material properties and gauge dimension of circular solid steel specimen

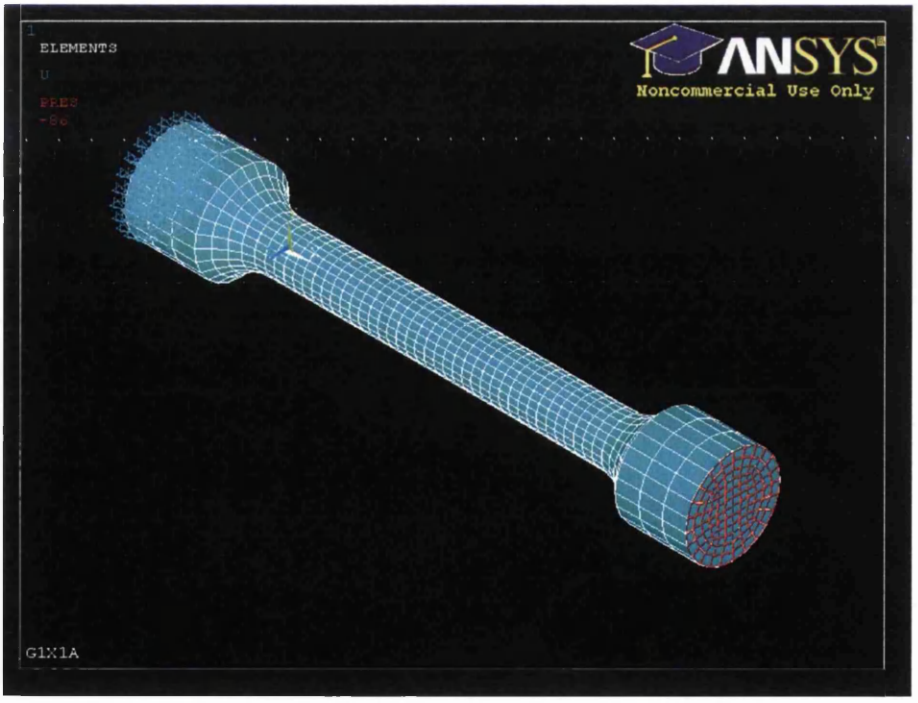

Figure 5.1 –The Element Mesh of specimen G1X1A with its applied boundary condition(s).

Figure 5.1 shows the element mesh of the tensile test specimen along with the boundary condition and applied load. The corresponding stress-deformation response after solution is presented in Figure 5.2(a) and (b). These two curves were obtained from the same solution with different data frequency being written. In Figure 5.2(a), the complete loading and unloading stress paths which are captured throughout the solution can be observed. When these peak points of each reloading path are joined, they form the monotonic stress-deformation response, as in Figure 5.2(b).

The output data at each loadstep can be observed in the general post-processing module. The stress contour at the peak and fracture stress state are displayed in Figure 5.3, with the conventions SMN and SMX being the minimum and maximum stresses in the longitudinal (axial) direction respectively. DMX is the maximum displacement between the ends of the specimen and does not correspond to the displacement of the gauge length.

As expected, the concentration of stresses occurred in the reduced cross sectional gauge area. The reduction of the stresses can be seen from the two plots captured at different TIME values. It can also be observed that the necking phenomenon, which accompanies ductile materials, was not captured due to the geometrically perfect finite element model. In any real materials, geometric imperfections will be present in some extent to initiate localisation of deformation; i.e. necking in a tensile test.

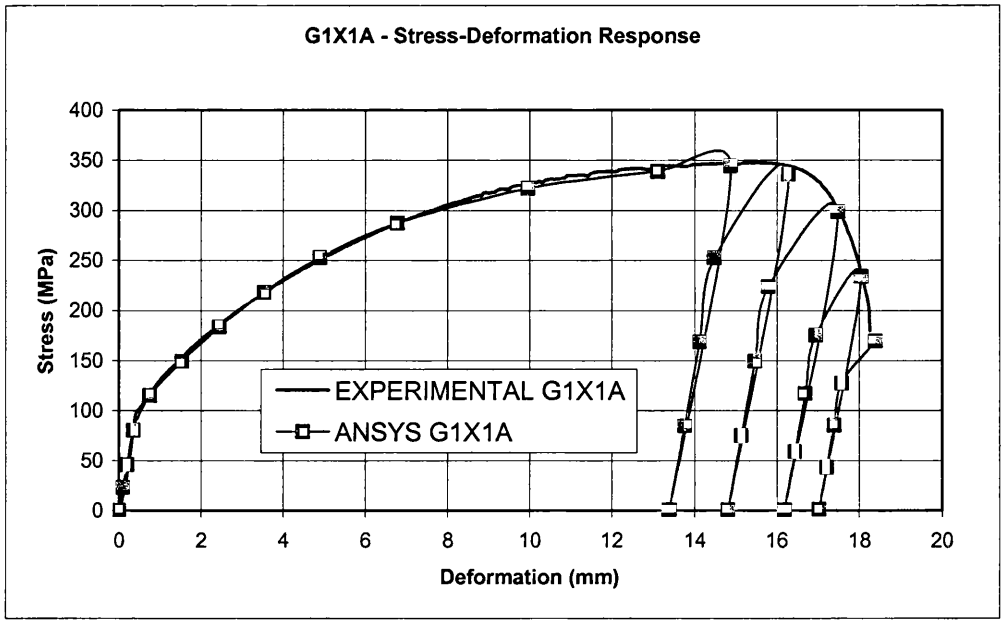

a)

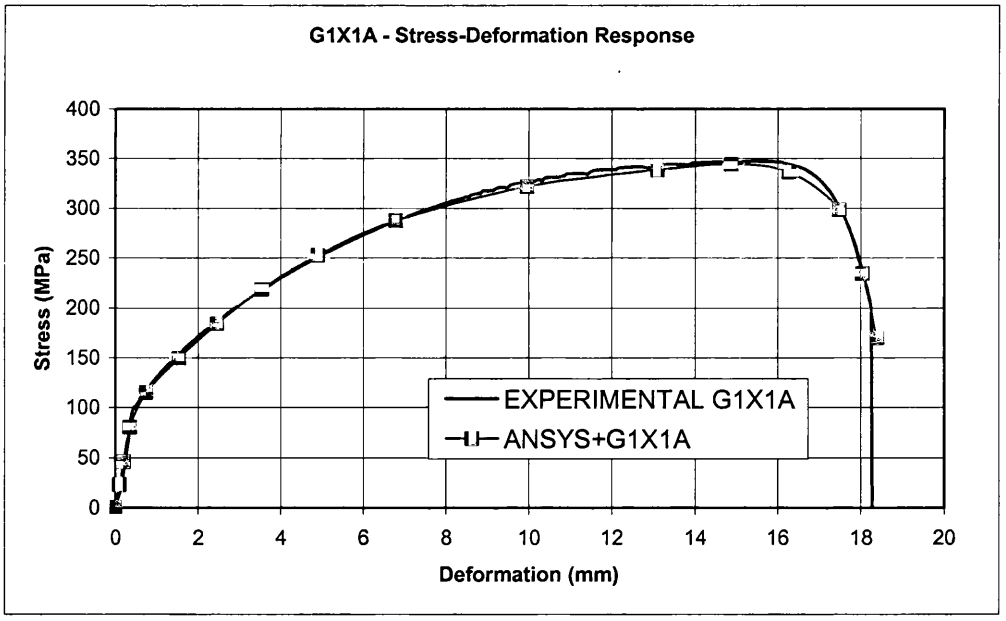

b)

Figure 5.2 – Stress-Deformation Response of specimen G1X1A Steel a) cyclic and b) monotonic representations; Experimental curve from Barret (1999)

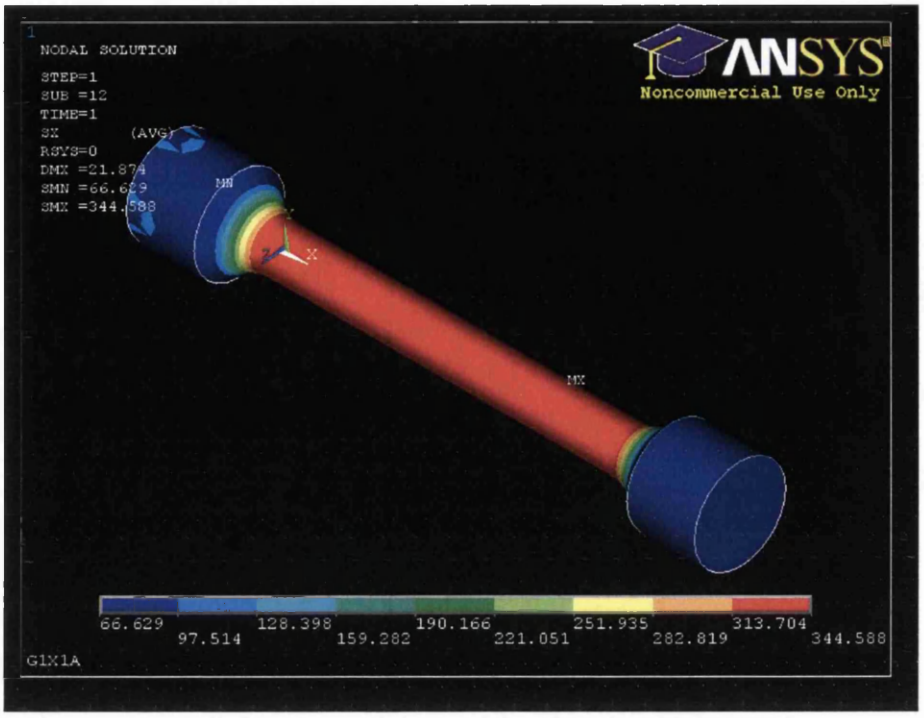

a)

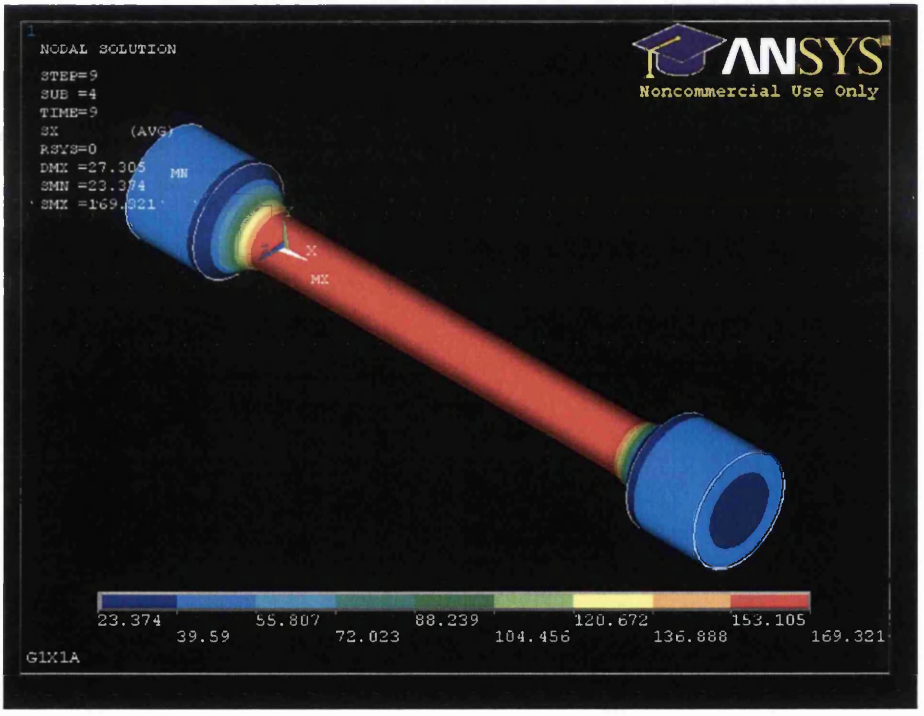

b)

Figure 5.3 – The stress distribution of specimen G1X1A a) Time=1 @ peak stress and b) Time=9 @ fracture stress

5.3 Case 2: VHS Circular Steel Tube; Specimen FTS2A

This validation test adopts modified Voce softening equation [Eq.4.2] where σ_{ult} $= 1485\,N/mm^2$, $R_0^{soft} = 0$, $R_\infty^{soft} = 175\,N/mm^2$ and $b^{soft} = 5.5$.

Source	Properties					
	Material			Gauge Area		
	Young's modulus	Yield Stress	Ultimate Tensile Strength	Length	Outer Diameter	Thickness
(Jiao and Zhao 2001)	200,000 *MPa*	1350 *MPa*	1500 *MPa*	320 *mm*	38.3 *mm*	1.84 *mm*

Table 5.2 - Material properties and gauge dimension of VHS circular steel tubes

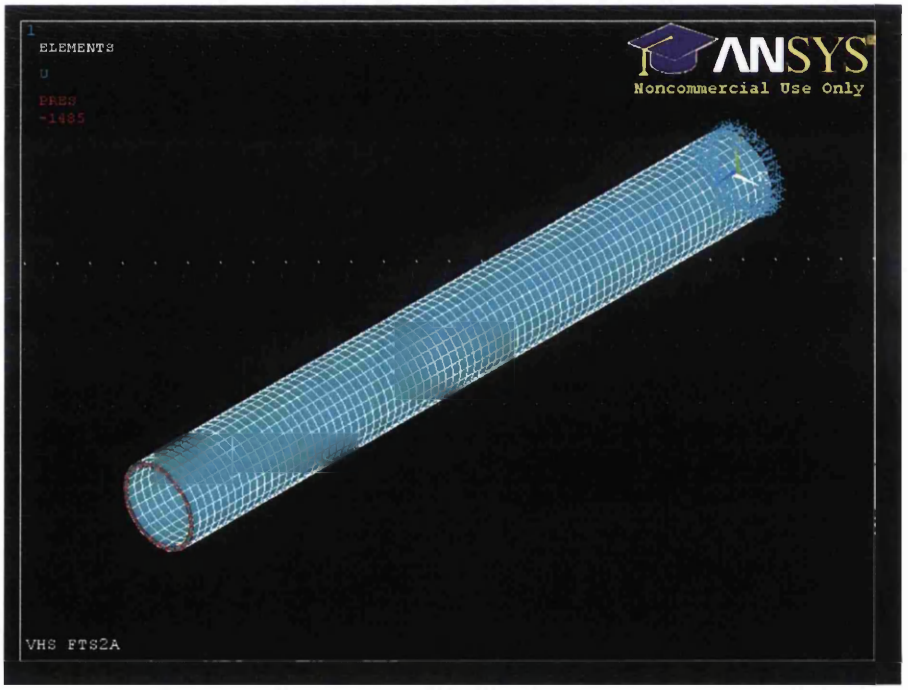

Figure 5.4 –The Element Mesh of VHS FTS2A with its applied boundary condition(s).

Note: This analysis utilizes several loadsteps to solve the initial pre-peak stress branch to capture a smooth and continuous response in the nonlinear hardening region (refer to chapter 4.4.4).

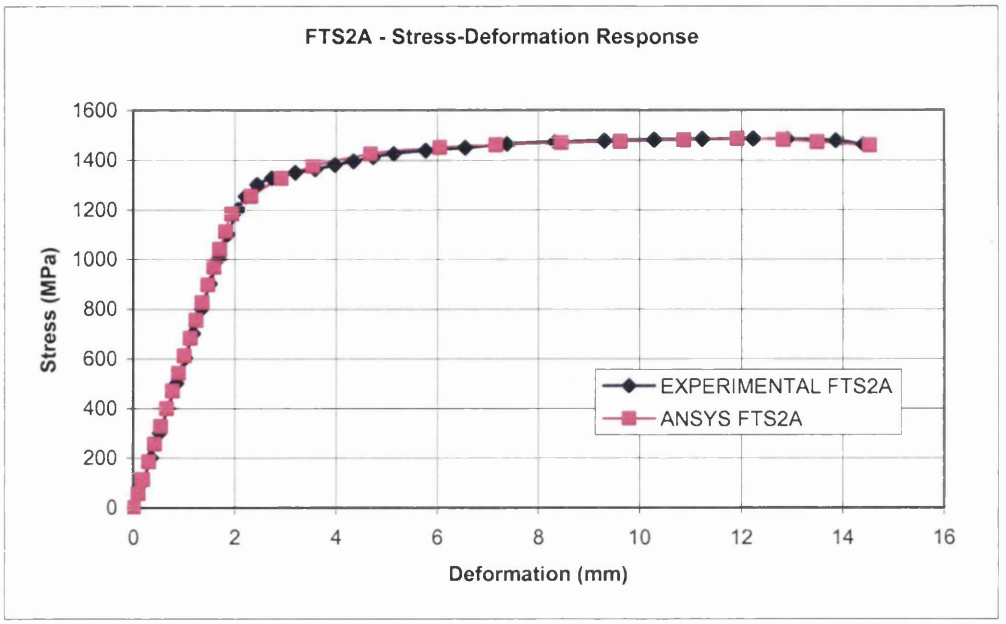

a)

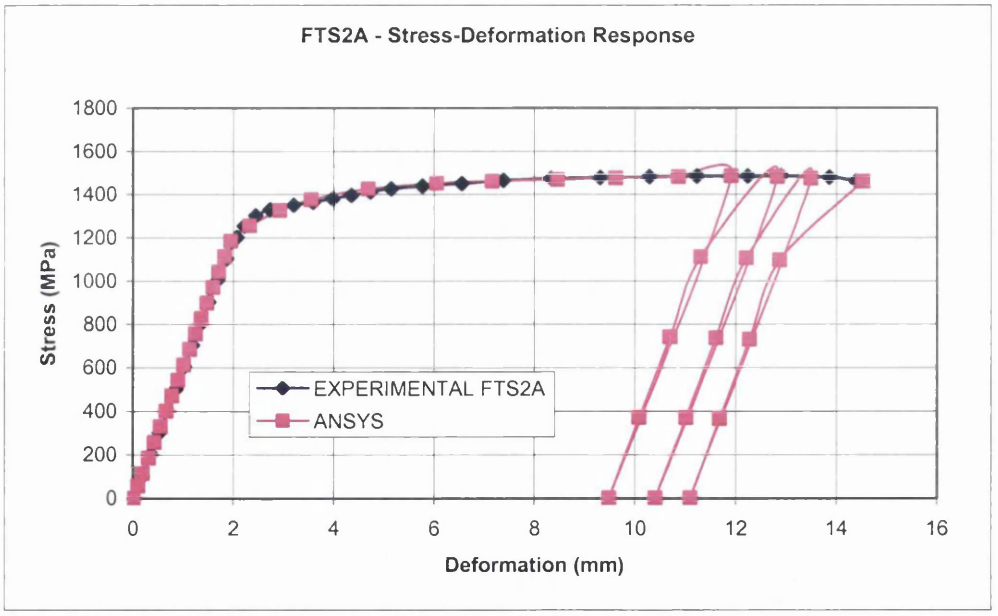

b)

Figure 5.5 – Stress-Deformation Response of VHS Circular Steel Tubes a) cyclic and b) monotonic representations; Experimental curve from Jiao and Zhao (2001)

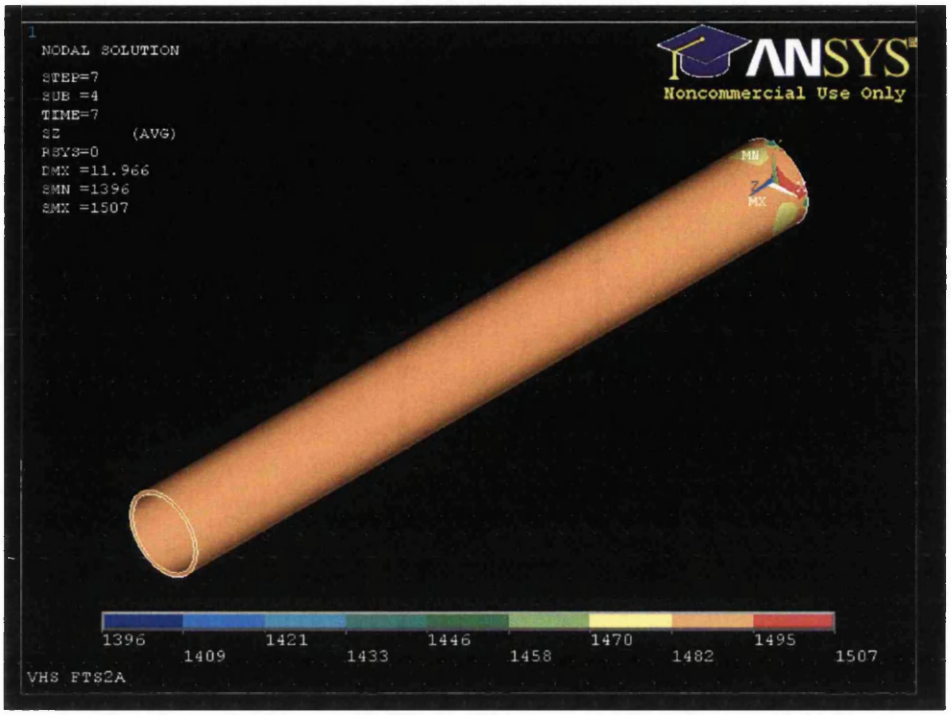

a)

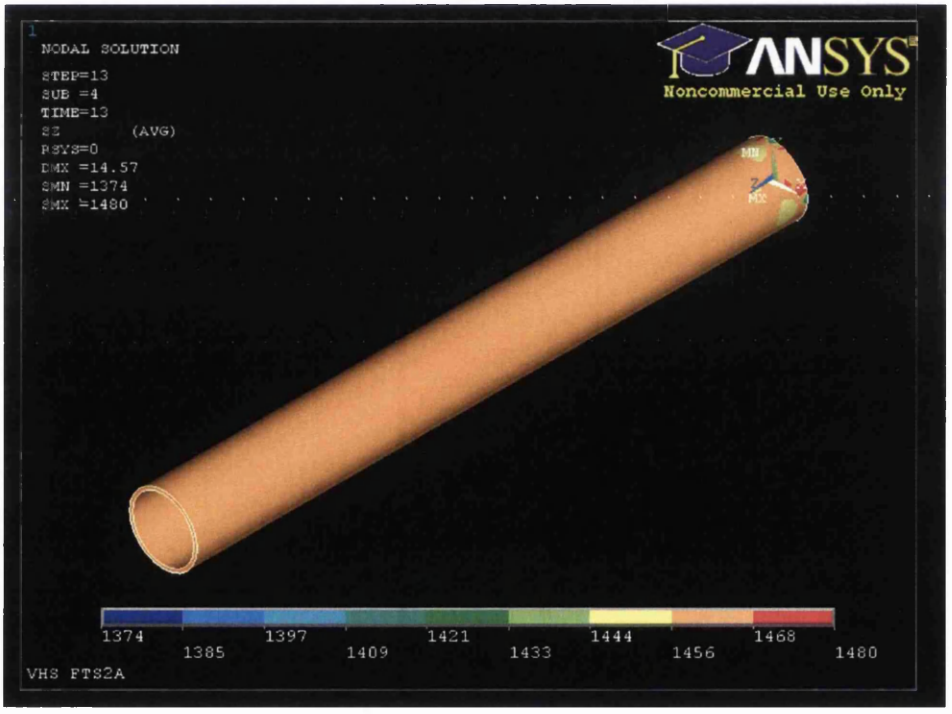

b)

Figure 5.6 – The stress distribution of specimen VHS FTS2A a) Time=7 @ peak stress and b) Time=13 @ fracture stress

5.4 Case 3: NHT CHS; Specimen FTS1A

This validation test adopts the polynomial softening equation [Eq.4.3] where C_6 = -44,951,970,336,640, C_5 = 4,736,033,063,734, C_4 = 196,183,053,669, C_3 = 4,050,011,174, C_2 = 43,618,047, C_1 = 231,847 and C_0 = 5.

Source	Properties					
	Material			Gauge Area		
	Young's modulus	Yield Stress	Ultimate Tensile Strength	Length	Outer Diameter	Thickness
(Jiao and Zhao 2001)	198600 *MPa*	200 *MPa*	486 *MPa*	320 *mm*	38.1 *mm*	1.58 *mm*

Table 5.3 - Material properties and gauge dimension of NHT CHS Specimen

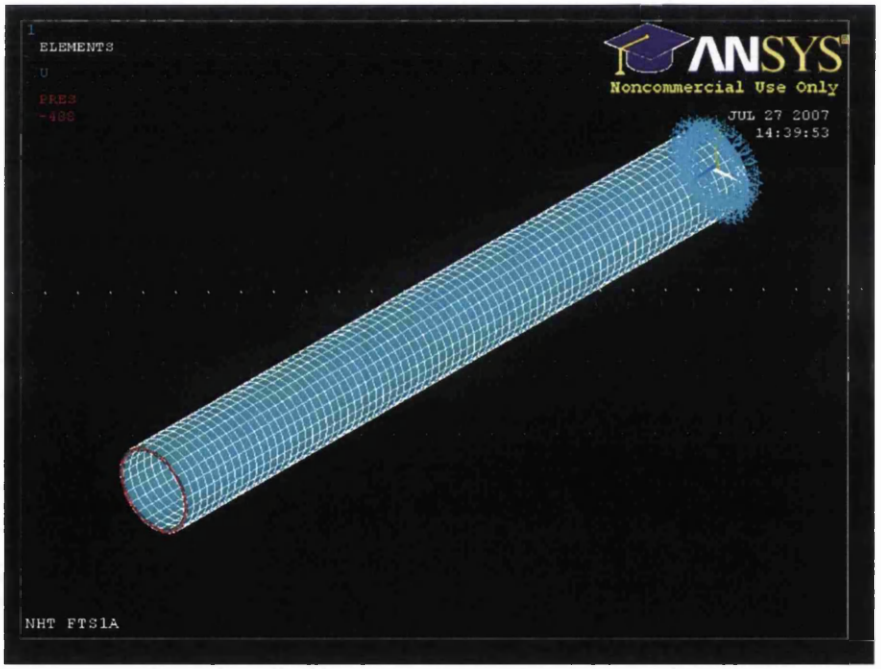

Figure 5.7 –The Element Mesh of NHT FTS1A with its applied boundary condition(s).

Note: The NHT CHS is the parent metal of VHS tubes, with different chemical composition. The end portion of the curves in Figure 5.8(a) and (b) represents the unloading operation after the specimen was stretched until near fracture. In FEA, similar operations were simulated where the unloading operation was solved in one iteration,

represented by the huge jump in the reduction of stress to virtually zero. The point at which this line intersects the x-axis represents the total plastic strain at the end of the analysis, with some residual degree of elasticity.

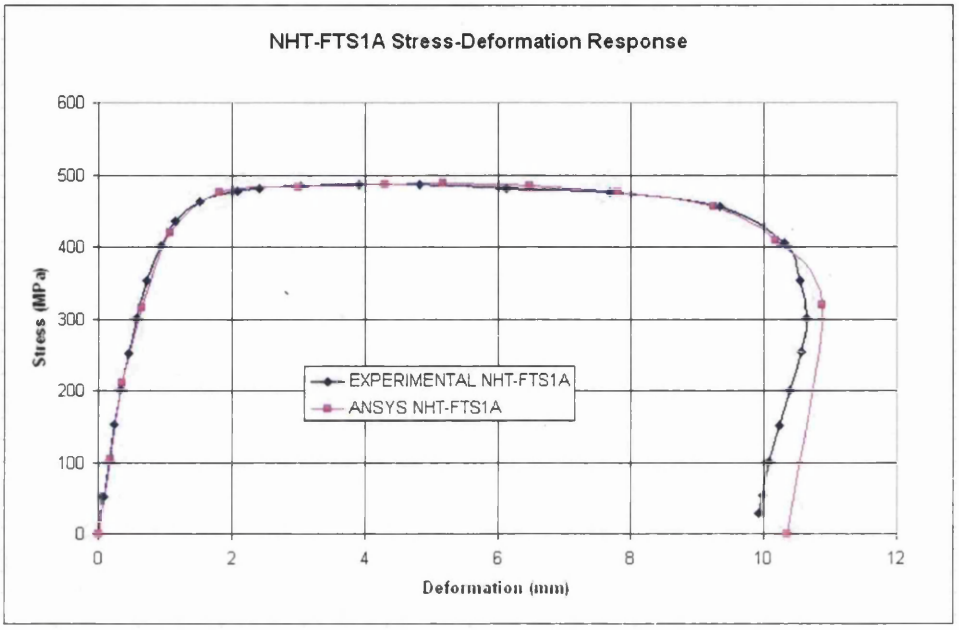

a)

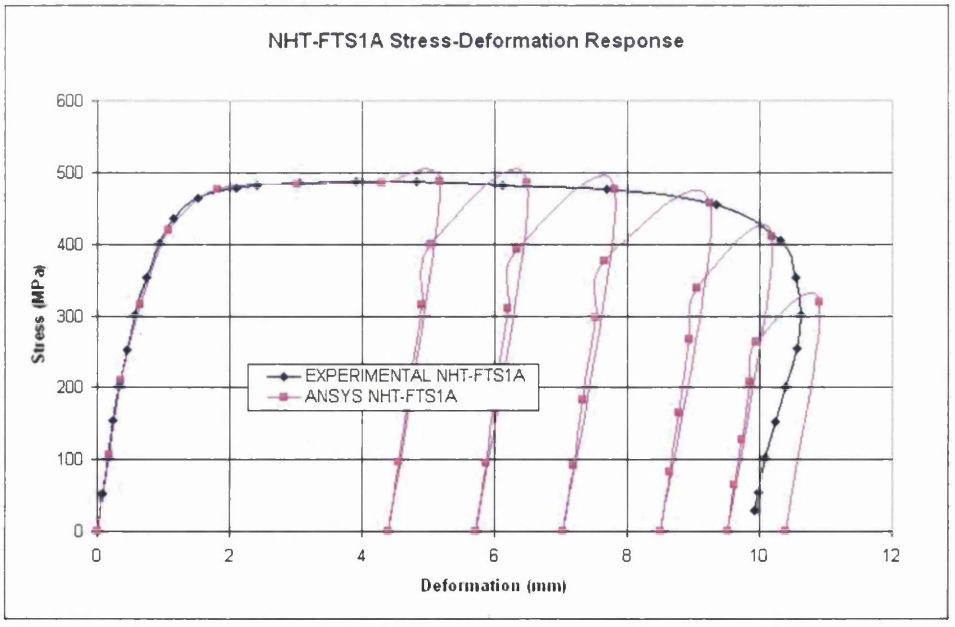

b)

Figure 5.8 – Stress-Deformation Response of specimen NHT-FTS1A a) cyclic and b) monotonic representations; Experimental curve from Jiao and Zhao (2001)

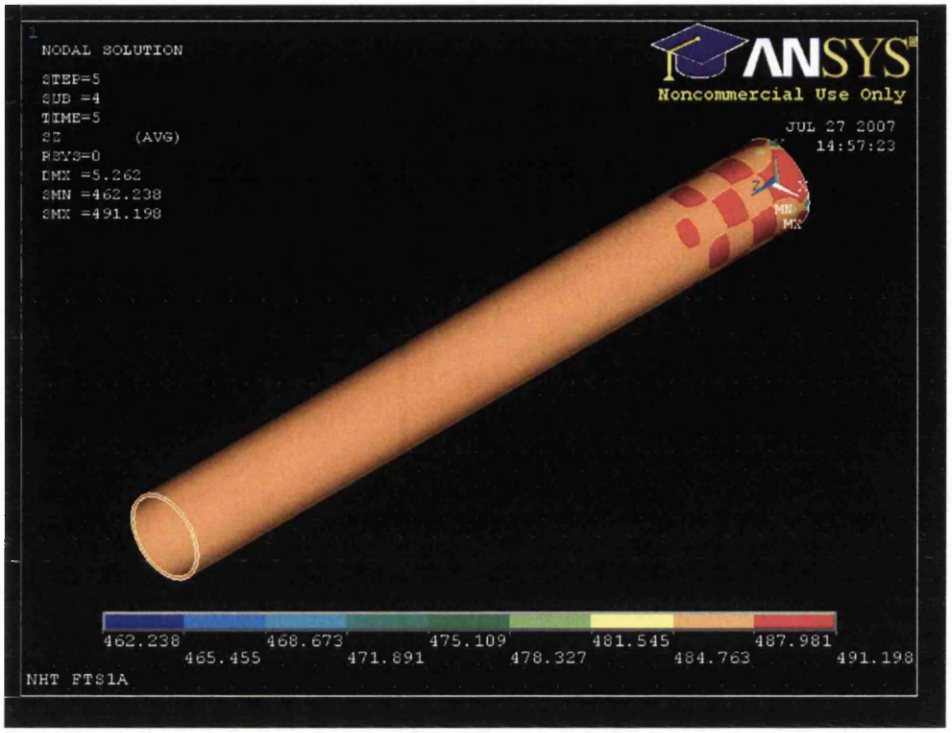

a)

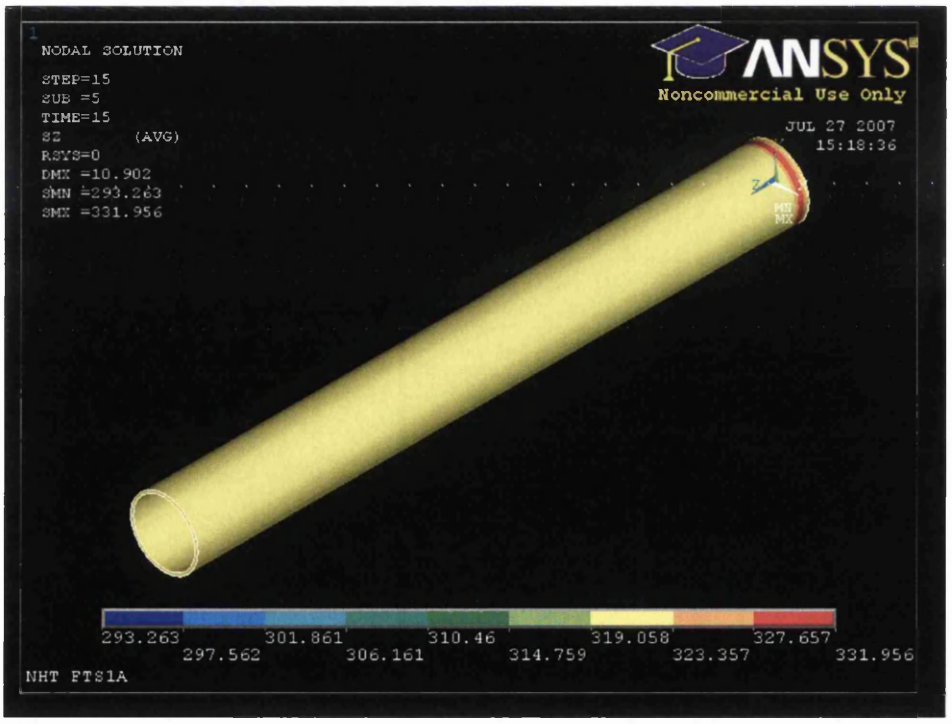

b)

Figure 5.9 – The stress distribution of specimen NHT FTS1A a) Time=5 @ peak stress and b) Time=15 @ (near) fracture stress

5.5 Case 4: A Ductile Material; Specimen DUCMAT

This validation test adopts the polynomial softening equation [Eq.4.3] where C_6 = 0, C_5 = 0, C_4 = -51,406, C_3 = 47,945, C_2 = 16,522, C_1 = 2,508 and C_0 = 137.

Source	Properties				
	Material			Gauge Area	
	Young's modulus	Yield Stress	Ultimate Tensile Strength	Length	Diameter
(ASMI 2004)	200,000 *MPa*	135 *MPa*	280 *MPa*	50.0 *mm*	12.5 *mm*

Table 5.4 – Material properties and gauge dimension of a Ductile Material (DUCMAT)

Note: This material was unnamed in the source. However, given the stress-strain curve, with an elastic modulus approximately 200,000 *MPa* and exhibiting significant ductility in the elastic-plastic region, it was suggested that it may be from the steel family. For convenience, this material was referred as the ductile material, DUCMAT.

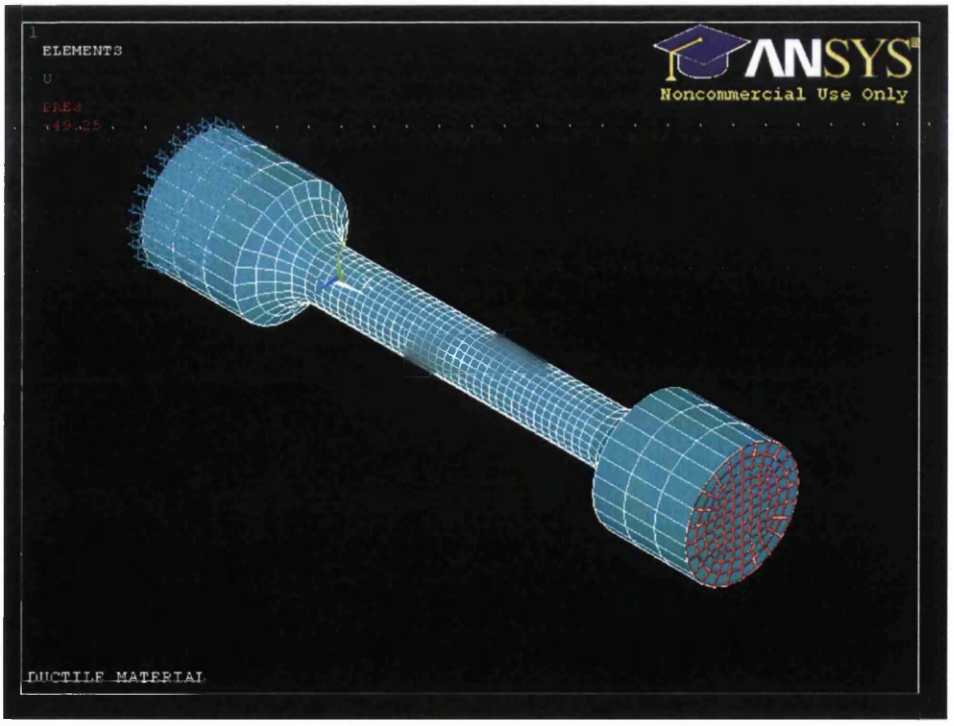

Figure 5.10 –The Element Mesh of a Ductile Material (DUCMAT) with the applied boundary condition(s)

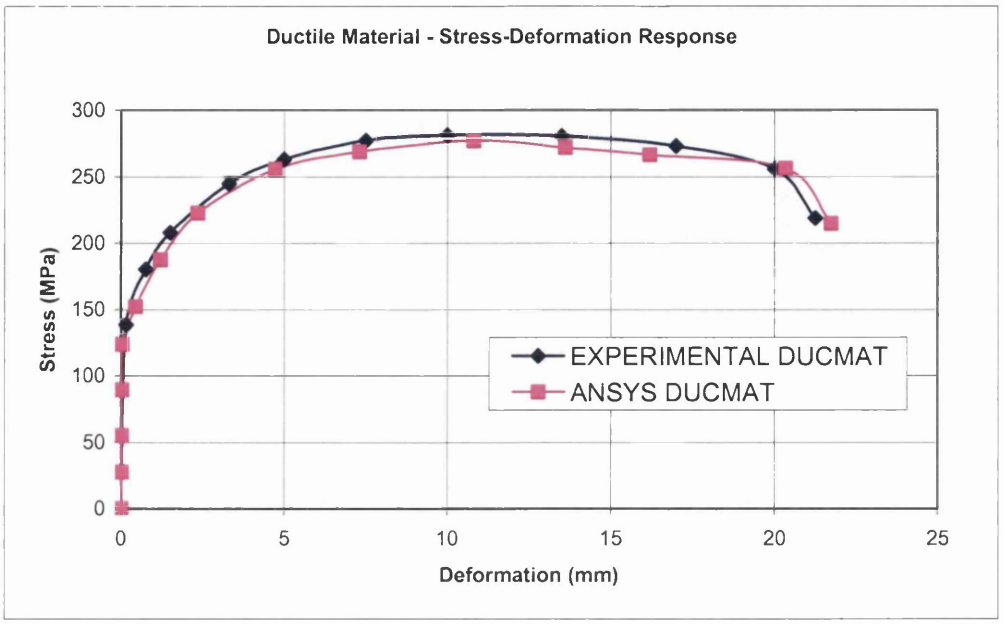

a)

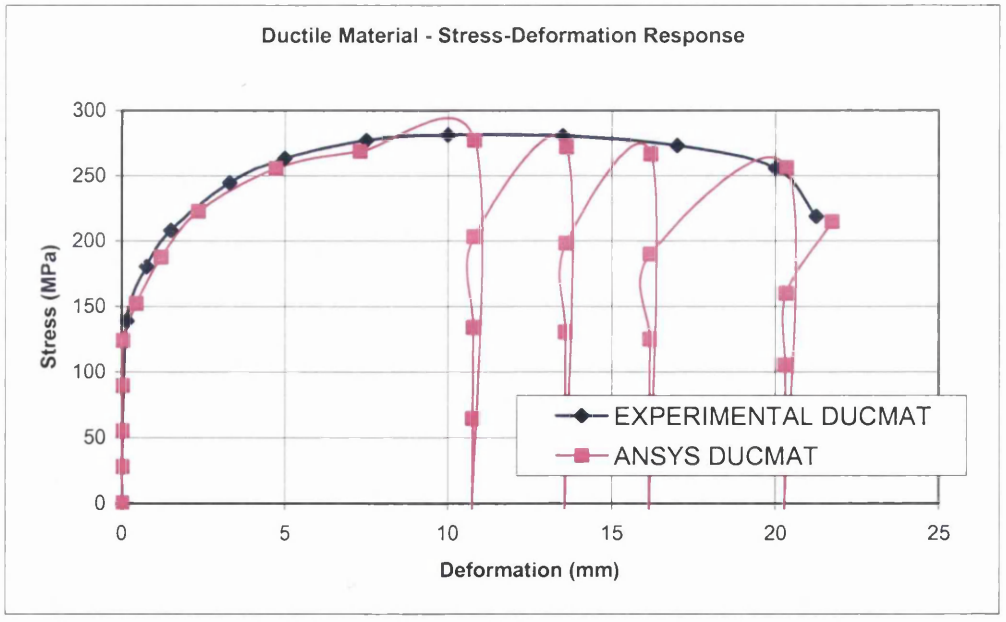

b)

Figure 5.11 – Stress-Deformation Response of specimen DUCMAT a) cyclic and b) monotonic representations; Experimental curve from ASM International (2004)

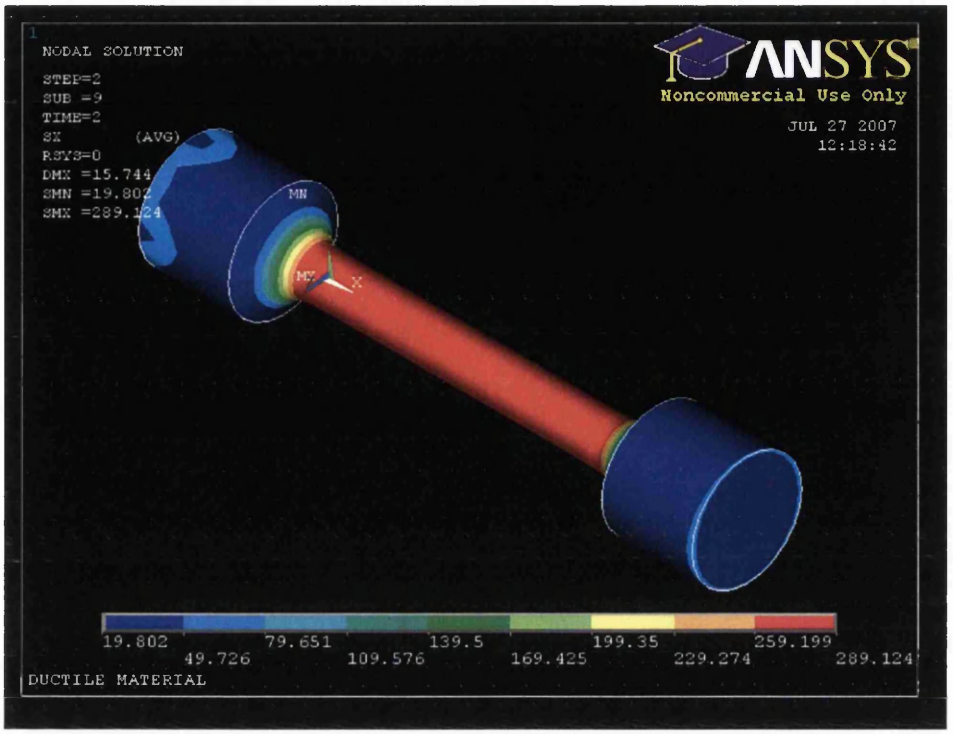

a)

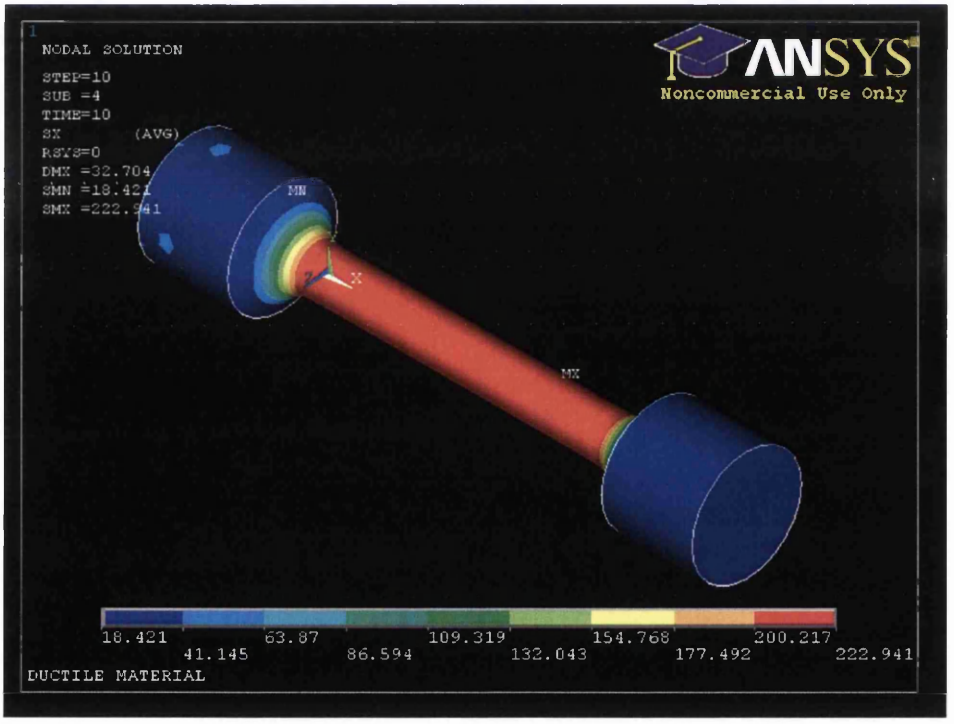

b)

Figure 5.12 – The stress distribution of specimen DUCMAT a) Time=2 @ peak stress and b) Time=10 @ fracture stress

5.6 Case 5: Dual Phase Steel Strip; Specimen DP800

This validation test adopts modified Voce softening equation [Eq.4.2] where σ_{ult} = $770\,N/mm^2$, $R_0^{soft} = 0$, $R_\infty^{soft} = 10\,N/mm^2$ and $b^{soft} = 35$.

Source	Properties				
	Material			Gauge Area	
	Young's modulus	Yield Stress	Ultimate Tensile Strength	Length	Width
(Xin 2005)	205,000 *MPa*	500 *MPa*	780 *MPa*	40.0 *mm*	20.0 *mm*

Table 5.5 – Material properties and gauge dimension of DP800 Dual Phase Steel Strip Specimen

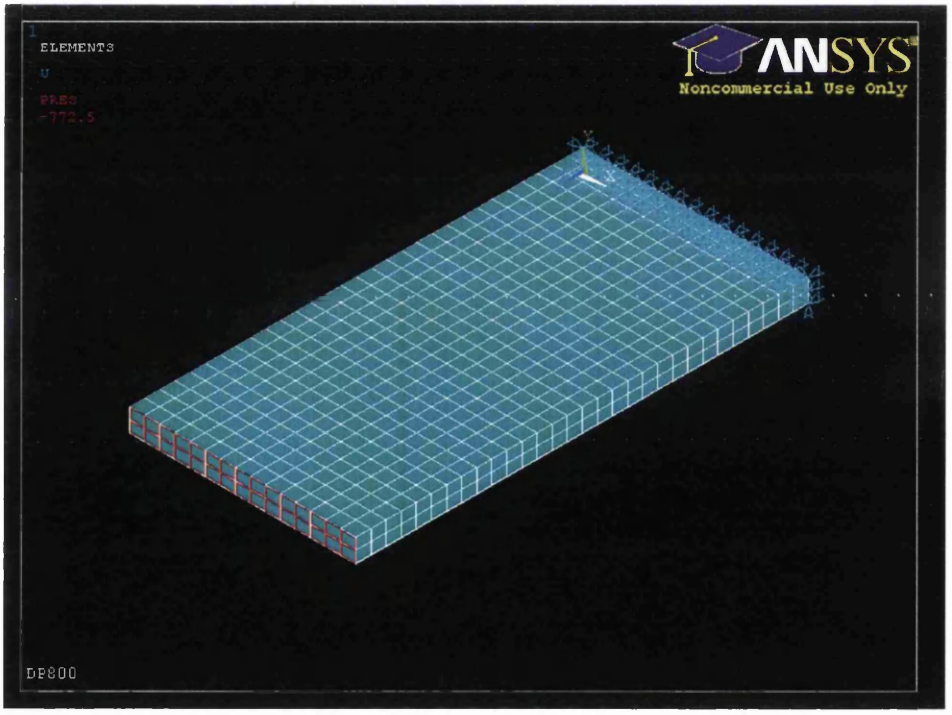

Figure 5.13 –The Element Mesh of DP800 steel plate with the applied boundary condition(s)

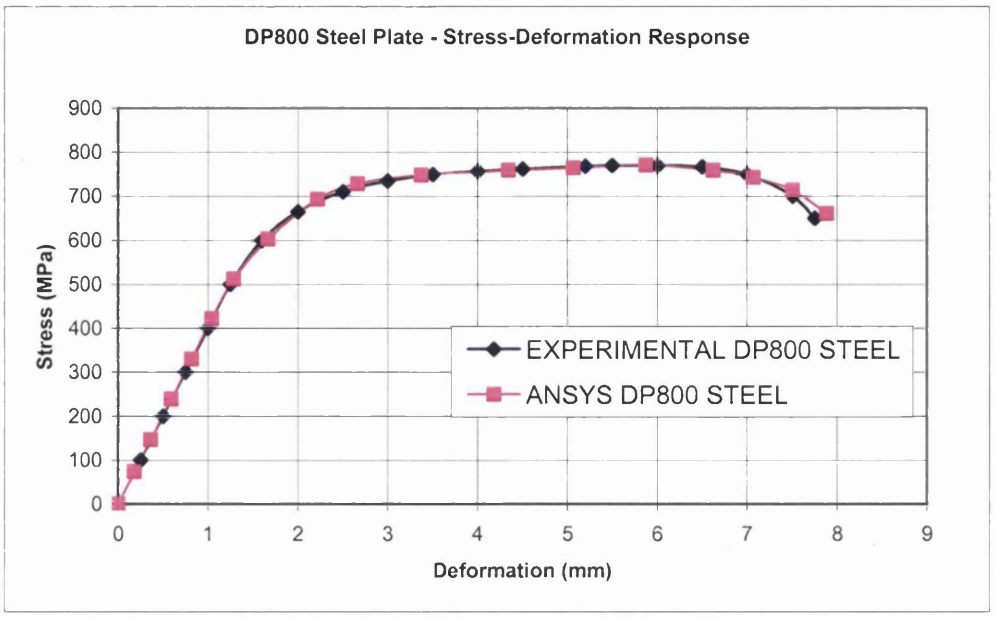

a)

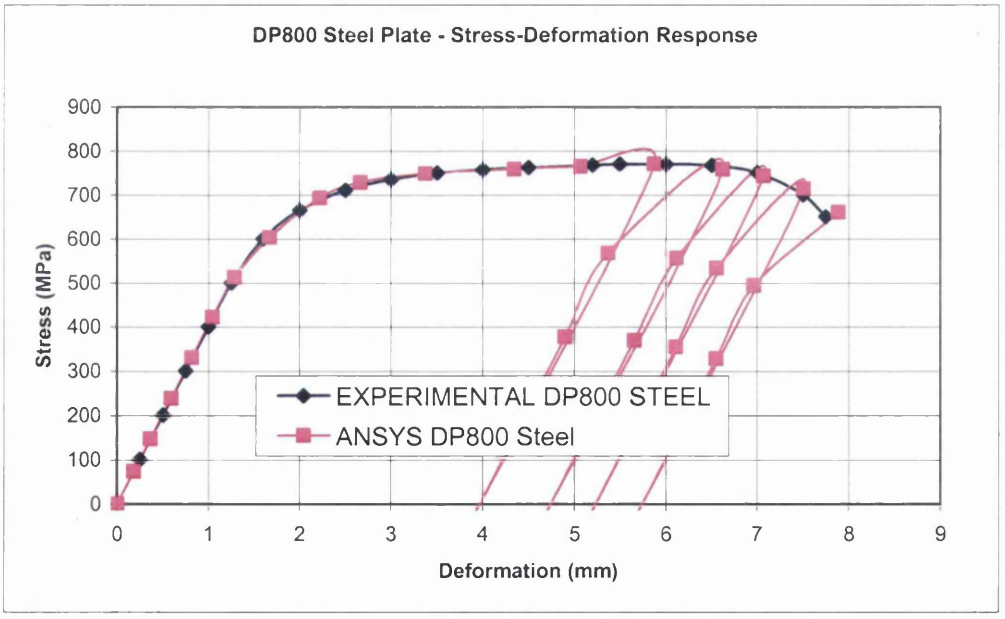

b)

Figure 5.14 – Stress-Deformation Response of specimen DP800 plate a) cyclic and b) monotonic representations; Experimental curve from Xin (2005)

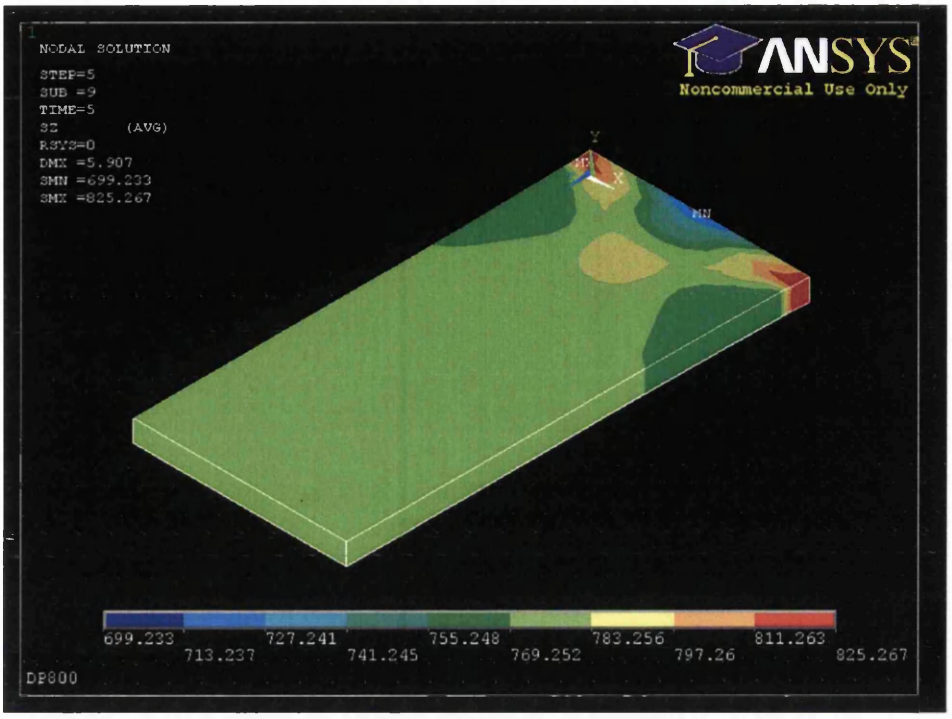

a)

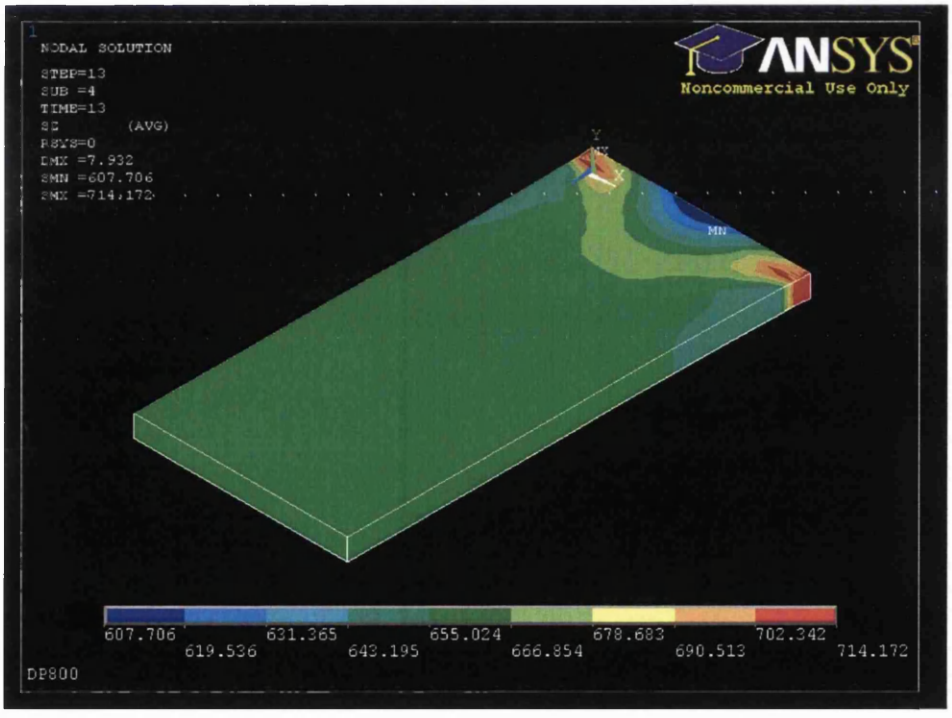

b)

Figure 5.15– The stress distribution of specimen DP800 steel a) Time=5 @ peak stress and b) Time=13 @ fracture stress

5.7 Case 6: Circular Solid Copper; Specimen G1WA

This validation test adopts the polynomial softening equation [Eq.4.3] where $C_6 = -8x10^7$, $C_5 = 6x10^7$, $C_4 = -2x10^7$, $C_3 = 2x10^6$, $C_2 = 188{,}186$, $C_1 = 6{,}939$ and $C_0 = 209$.

Source	Properties				
	Material			Gauge Area	
	Young's modulus	Yield Stress	Ultimate Tensile Strength	Length	Diameter
(Barret 1999)	14000 *MPa*	300 *MPa*	305 *MPa*	26.14 *mm*	5.03 *mm*

Table 5.6 – Material properties and gauge dimension of a Circular Solid Copper Specimen G1WA

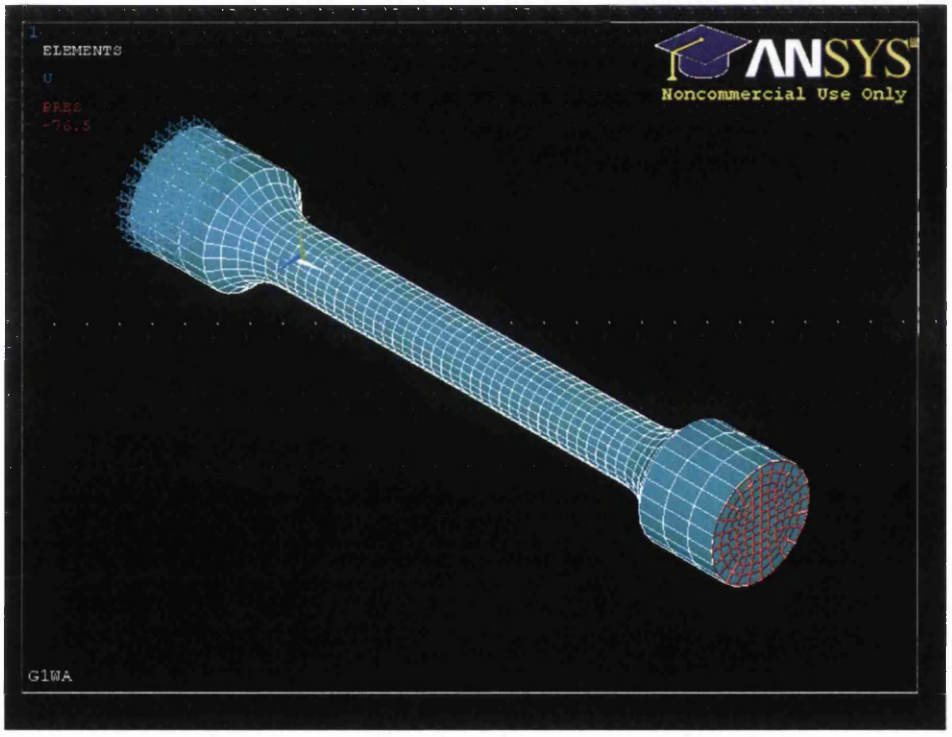

Figure 5.16 –The Element Mesh of specimen G1WA with the applied boundary condition(s)

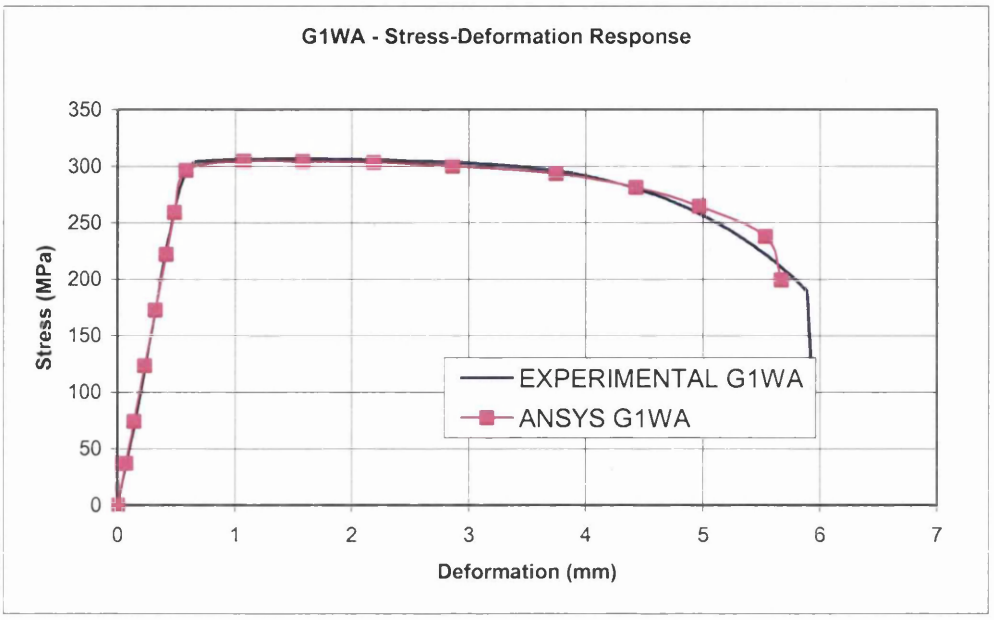

a)

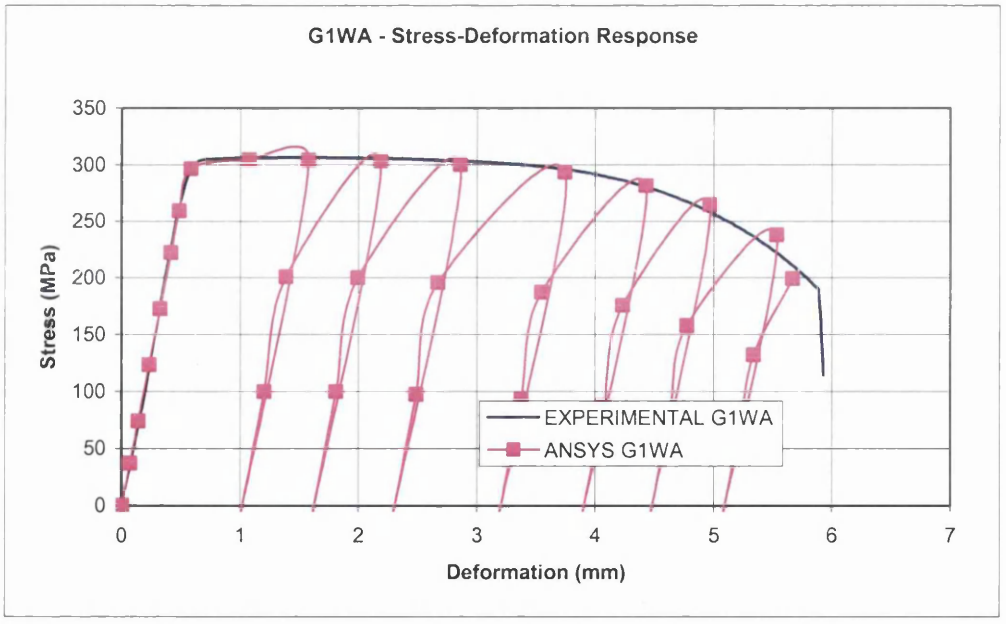

b)

Figure 5.17 – Stress-Deformation Response of specimen G1WA a) cyclic and b) monotonic representations; Experimental curve from Barret (1999)

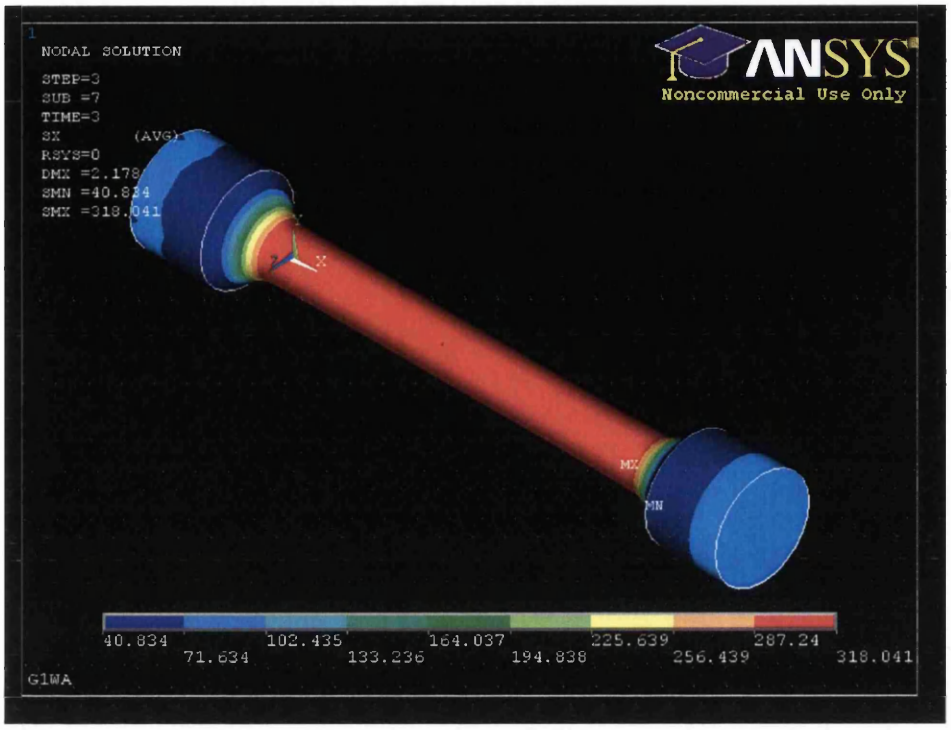

a)

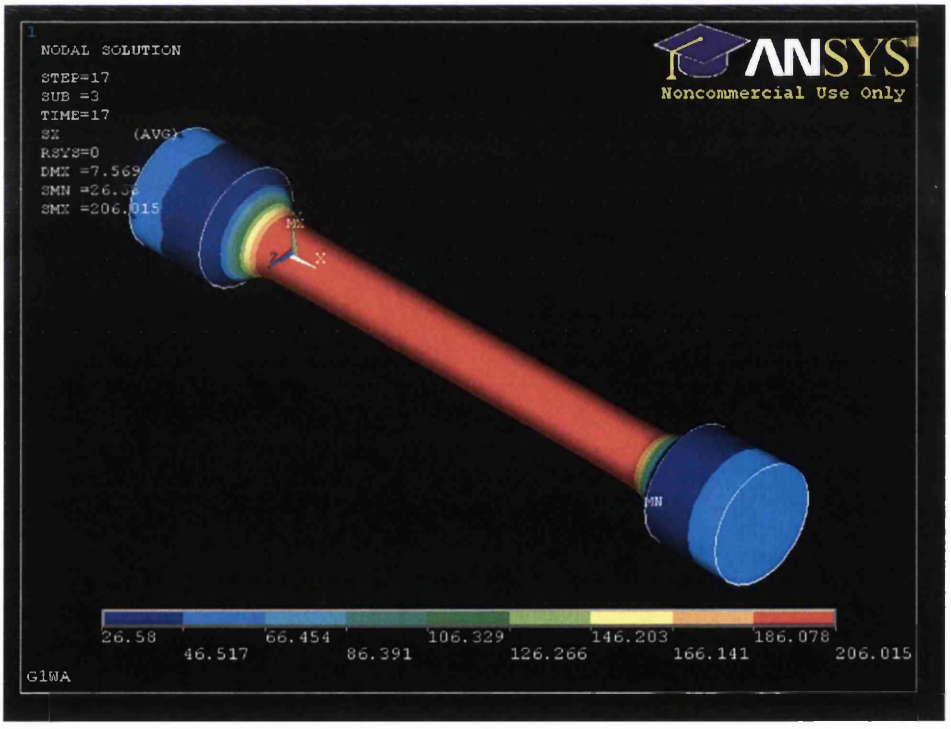

b)

Figure 5.18 – The stress distribution of specimen G1WA a) Time=3 @ peak stress and b) Time=13 @ fracture stress

6.0 Discussions

6.1 The material stress-strain curve

The input of true or (probably) experimental stress-strain values in FEA is somewhat obscure, at least to the author. Lindle (2007) stated that material stress-strain properties must be ascribed in terms of true stress-true strain for large strain analysis, and since the true and engineering values have little or negligible differences in small strain analysis, it can be safely implied that the true values should always be used for all analysis. The complication arises from which true stress values is defined for softening analysis; being dependant to the cross sectional area of the material. The fact that many metallic materials exhibit at least some extent of ductility leads to the need to consider localisation of geometric effect in large strain deformation and thus results in different true stress-true strain relationships throughout the section of the material.

Consider a ductile material in a tensile test. In the critical localised necking region, the reduction in cross-sectional area is significant, giving rise to a higher and always increasing (true) stress. If these true values are used for FEA, a softening model would be unnecessary, as the plastic flow branch in the nonlinear curve will always increase, i.e. stiffness matrixes remain positive and increasing throughout (deceiving at

times because when material softens, the stiffness decreases) and this could be easily represented by adopting the available nonlinear option. If instead, the stress-strain values of the other extreme (i.e. in areas of negligible or small cross-section change) are used, the stress states at the neck region will be underestimated. This condition merely assumes the necking phenomenon being non-existence.

The approach adopted in the study to rectify this ambiguity is by taking the average between the true values at the critical necking and non-necking regions as the global measure. There is no direct derivation for this average known to the author. Nonetheless, common sense would recognise that these averaged true values would fall above the engineering values and below the critical true values at necking, and thus some form of function that would yield values between these (upper and lower) bounds is required. Many experimental stress-strain curves are presented in term of engineering values and the simple true-engineering relations in Appendix 1 provides the required true values, which are assumed to be the averaging values of the stress-strain relation of the material for FE softening analysis. These averaging values exhibit a descending softening stress-strain branch, giving rise to need of the proposed non-local (averaging) modelling technique.

6.2 Determination of parameters

Curve fitting of the monotonic hardening and softening portions of the stress-strain curve provides a simple workable solution to determine the characteristic parameters. Although procedures were suggested for the determination of parameters and could well match the experimental stress-strain curve to satisfactory accuracy, it seems to be impractical in the longer term as it provides no consistency on the accuracy and tolerance performed by different users and could yield scatters of parameter sets on the same material analysis. This applies notably to the softening branch, in which the parameters R_0^{soft} and R_∞^{soft} in equation [Eq.4.2] do not really represent any definite physical meaning to the characteristic of the material. This provokes two arguments; first, parameters without any physical meaning, especially when the standard deviation of the parameters determination could be large. Secondly, the parameters do not have any

relation to the material characteristic, but rather in a mathematical point of view, simply define the shape of the curve. Hence, a future research is proposed in Chapter 8 (1) to develop a new softening function which is defined based on material characteristic parameters (e.g. tensile yield stress, ultimate tensile strength, etc.).

Recall that in chapter 4.3, it was mentioned that the parameter R_0^* has little or negligible effect on the final softening stress-strain points and only serves to control the reloading paths which are of little importance to the monotonic stress-deformation response. However, it is speculated that this parameter might has its influence in determining the tolerance of the subsequent final peak-points. One reason at which it is much desirable for the incremental displacement being a less sensitive variable with respect to stress increment is that; for a load-controlled analysis, the convergence of the analysis near peak point (the unstable region), i.e. when $\frac{\partial \sigma^*}{\partial \varepsilon^{pl}}$ approaching zero becomes more difficult. If the reloading operations follow a steep path, then a smaller stress increment (or decrement) stress would result in a smaller displacement increment. Otherwise, it would result in a large displacement jump and the stress-deformation response would seem discontinuous. However, the exactitude of this hypothesis has yet to be clarified; if proven true, then a larger value of R_0^* is suggested. Its corresponding determination procedure would also be required.

6.3 Evaluations

6.3.1 The capability of geometrical effect

In laboratory experimental tensile testing, localised necking phenomena would be expected for many metallic materials which exhibit considerable ductility. To simulate this geometrical effect, there are two considerations that should be made. First, the effect of large deformation should be activated. In the current study, preliminary runs with large deformation activated have resulted in early non-convergence well before the peak stress is attained. Taking validation case 3 for example, it can be observed that there is a concentration of stress within the proximity of the constrained boundary end; see Figure

5.9(b). Activating the large deformation options will results in over excessive stress and deformation localisation comprehended in this region and results in premature non-convergence. Although this could be overcome by increasing the stiffness in the boundary region, the large deformation option is kept deactivated in this study for simplicity.

Secondly, it is necessary to develop an approach at which necking is first initiated within the locality of the material. The stiffness of the critical elements could be reduced such that these elements exhibit lower resistance to deformation compared to the non-critical elements. Furthermore, fracture simulation, an on-going research, is also possible by exploiting the use of the 'element birth and death' feature in ANSYS®.

6.3.2 Adaptability

This modelling technique has proved to be adequate for simulating the post limit stress-deformation response of metallic materials; assuming uniform deformation (homogeneity) along the loaded section. In terms of capturing the localisation of geometric instability, further developments and modifications are required to the existing proposed modelling technique. This model however, seems to be more suitable and adequate to simulate brittle materials that exhibit little geometrical changes upon fracture. The stress-strain relation of most brittle (usually high strength) metallic material characterizes a near perfectly plastic behaviour with trivial softening response (e.g. validation case 2: VHS steel tubes). Also this model could potentially be applied for cementitious composite materials which exhibit significant (exponential) softening behaviour yet minimal geometrical deformation, e.g. cracking.

7.0 Concluding Remarks

The computational finite element simulation of the softening response is not possible to be solved in a direct manner by applying the softening theory of plasticity and the conventional computational algorithm. Hence, an attempt was made to overcome this problem which gave birth to the proposed modelling technique.

The Voce hardening function [Eq.4.1] and two other softening equations [Eq.4.2 and 4.3] were proposed to define the complete stress – strain behaviour of the materials. The softening response is governed by a set of parameters which defines the monotonic descending branch. A reduced-load optimization code was also implemented into the model to control the material load capacity in the softening region. This modelling technique adopts the cyclic loading and unloading principles, as observed in an experimental cyclic test, whereby the reloading materials properties are updated at each cycle and reassigned for the selected component of elements.

This study has presented a demonstration of the capability of the proposed technique to capture the softening response of some materials under consideration. It has so far been tested on several solitary uniaxial tensile test material specimens and the results have been encouraging. It has yet to be implemented to more complicated multi-axial structural problems.

At this preliminary stage, it remains to its preferred term as a modelling technique. However, this could serve to stimulate further improvements to develop this technique into a complete structural softening model based on the demonstrated methodology. The ultimate goal is to develop a universal and reliable softening model implemented into the finite element software to solve major structural problems.

8.0 Future Research

Having worked considerably on this modelling technique, the author has come to appreciate that there is indeed much room for developments and improvements to be explored and implemented into the technique. The current study has demonstrated a softening model operating within the graphical user interface (GUI) of the ANSYS® FE software. However, with the intention to build a complete, comprehensive and user-friendly model, the following are suggested for future research on the proposed modelling technique. They are listed in a suggested sequence of precedence.

1. An improved functional derivation to define the complete stress-strain curve. It is favourable to define the full stress – strain curve of a material governed by elementary material characteristic, e.g. tensile yield stress and ultimate tensile strength being the governing parameters that defines the shape of the curve.

2. Strain limit. The setting of the limit of analysis at which the solution is said to be achieved till fracture. This limit could be set such that solution is solved when asymptotic strain is attained (may require computational extrapolation) or at which the fracture strain is achieved (a definition for fracture strain is then necessary)

3. Implementations of user-programmable subroutines. An on-going preliminary research to implement the modelling technique into the user programmable subroutines, e.g. USERMAT, USERPL etc. This involves modifications on the computational algorithms and update procedures to characterize the material behaviour.

4. A localised softening model to accommodate geometric effects. Simulation of the necking phenomenon is possible for observable geometric deformations in FE softening analysis by reducing the elasticity and/or the 'killing' of the critical elements.

5. Application to metallic materials with yield plateau. The adaptability of metallic materials with yield plateau to the proposed modelling technique could also be investigated. The direct simplification is to replace the yield plateau with a smooth hardening fillet connecting between the linear elastic and the hardening segment. The corresponding yield point in the smooth curve is then taken as the yield in the former curve with yield plateau. Else, a function which defines the complete monotonic stress-strain curve, including yield plateau is could also be used.

With the suggested future work as discussed above, it can be seen that this proposed modelling technique has great potential and versatility. Although static cases have been tested with the model, its use in transient and harmonic analysis could be explored. Ultimately, the intention of the research on this modelling technique is to develop one which could be implemented into the commercial FE softwares for material and structural analysis.

References

(2007). ANSYS Release 11.0 Documentation. Structural Guide Chapter 8.4 Nonlinear Structural Guide.

(2007). ANSYS Release 11.0 Documentation. Command Reference.

Arya, C. (2003). Design of Structural Element, Concrete, steelwork, masonry and timber designs to British Standards and Eurocodes. London; New York, Spon Press.

ASM International, Introduction to tensile testing (2004). A. M. I. Society.

Barret, Z. (1999). The tensile test and the stress strain curves. Swansea, Swansea University.

Bathe, K. J. (1996). "Finite Element Procedures."

Batoz, J. L. and G. Dhatt (1979). "Incremental displacement algorithms for nonlinear problems." Short communications.

Bazant, Z. P. and P. C. Pratt (1988). "Microplane model for brittle plastic material." Journal of Engineering Mechanics (ASCE).

Belnoue, J. P., G. D. Nguyen, et al. (2007). "A one-dimensional nonlocal damage plasticity model for ductile materials." Int J Fract (2007)(144).

Bergan, P. G. and T. H. Soreide (1978). "Solution of large displacement and instability problems using the current stifness parameter." Finite Elements in Nonlinear Mechanics 2.

Borst, R. d., N. Bicanic, et al. (1998). Computational Modelling of Concrete Structures. Proceedings of EURO-C 1998, Balkema.

Borst, R. d. and P. Nauta (1986). "Non-orthogonal cracks in a smeared finite element model." Engineering Computation(2).

BSI (1992). Tensile Testing of Metallic Material. B. E. 10002-5:1992, BSI.

Cerini, M. and B. G. Falzon (2005). "Use of arc-length method for capturing mode jumping in postbuckling aerostructures." AIAA Journal 43(3).

Chin, C. S. (2006). Experimental and computational analysis of fibre reinforced cementitious composites. Civil & Computational Engineering Centre. Swansea, University of Wales Swansea. Ph.D.

Chun, L., P. Knutzen, et al. (2001). Cyclic load testing of steel bars.

Clift, S. E., P. Hartley, et al. (1990). "Fracture prediction in plastic deformation processes." Int. J. Mech. Sci. 32.

Clough, R. W. (1960). The finite element method in plane stress analysis. 2nd Conference on Electronic Computation A.S.C.E. Structural Division, Pittsburgh, Pennsylvania.

Cook, M. and E. C. Larke (1945). "Resistance of copper and copper alloys to homogenous deformation in compression." J. Ins. Metals 71.

Crisfield, M. A. (1991). Nonlinear finite element analysis of solids and structures, John Wileys & Sons.

Crutchley, D. A. and M. Zwonlinski (2004). DC Operating Point Analysis using Evolutionary Computing. Proc. 24th International Conference on Microelectronics (MIEL 2004), Serbia and Montenegro.

D.J. Celentano, E.E. Cabezas, et al. (2004). "Characterization of the mechanical behaviour of materials in the tensile test: experiments and simulation." Modelling and Simulation in Materials Science and Engineering 12.

Feenstra, P. H. and R. d. Borst (1996). "A composite plasticity model for concrete." International Journal of Solids and Structures(33).

Feenstra, P. H., J. G. Rots, A. Arnesen, J.G. Teigen & K.V. Hoiseth (1998). A 3D constitutive model for concrete based on a co-rotational concept. Proceedings of EURO-C 1998.

Forde, W. R. B. and S. F. Stiemer (1987). "Improved Arc Length Orthogonality Methods for Nonlinear Finite Element Analysis." Computers & Structures 27(5).

Gurson, A. L. (1977). "Continuum theory of ductile rapture by void necleation and growth." Trans. ASME J. Eng. Mater. Technol. 99.

Haisler, W. E. and J. A. Stricklin (1977). "Structural analysis by the self-correcting method." International Journal for Numerical Methods in Engineering(11).

He, J. H. (2004). "A modifed Newton Raphson method." Commun. Numer. Meth. Engng(20): 801–805.

Hrennikoff, A. (1941). "Solution of problems of elasticity by the frame-work method." ASME J. Appl. Mech.(8): A619–A715.

J.Argyris (1954). "Energy Theorems and Structural Analysis." Aircraft Engineering.

Jefferson, A. D. (2003). "Craft - a plastic-damage-contact model for concrete II. Model implementation with implicit return-mapping algorithm and consistent tangent matrix." International Journal of Solids and Structures(40).

Jiao, H. and X. L. Zhao (2001). "Material ductility of very high strength (VHS) circular steel tubes in tension." Thin-Walled Structures 39.

Kaw, A. K. (2007). Newton-Raphson Method of Solving Nonlinear Equations.

Key-to-Steel (2007). Key to Steel Knowledge Base; Mechanical Testing - Engineering Stress-Strain Curve, Key to Steel - The World's Most Comprehensive Steel Database.

Kim, H. S., Y. T. Im, et al. (1999). "Prediction of ductile fracure in cold forging of aluminium alloy." Trans. ASME J. Manuf. Sci. Eng. 121.

Komori, K. (1999). "Simulation of chevron crack formulation and evolution in drawing." Int. J. Mech. Sci. 41(12).

Komori, K. (2001). "Simulation of shearing by node separation method." Comput. Struct. 79(2).

Komori, K. (2002). "Simulation of tensile test by node separation method." Journal of material processing technology.

Lindle, M. XANSYS - Ansys User Community Forum.

Ling, Y. (2004). "Uniaxial true stress-strain after necking." AMP Journal of Technology 5.

Lourenco, P. and J. G. Rots (1997). "A multi-surface interface model for the analysis of masonry structures." Journal of Engineering Mechanics (ASCE)(123).

Mallardo, V. and C. Alessandri (2004). "Arc-length procedures with BEM in physically nonlinear problems." Engineering Analysis with Boundary Elements 28.

May, I. M. and Y. Duan (1997). "A local arc-length procedure for strain softening." Computers & Structures 64.

Mazars, J. and G. Pijaudier-Cabot (1989). "Continuum damage theory - application to concrete." Journal of Engineering Mechanics of cohesive-frictional materials (ASCE)(115).

Memon, B. A. and X. Z. Su (2004). "Arc-length technique for nonlinear finite element analysis." Journal of Zhejiang University SCIENCE(5).

Nayak, G. C. and O. C. Zienkiewicz (1972). "Elasto-plastic stress analysis. A generalisation for various constitutive relations including strain softening." International Journal of Numerical Methods in Engineering(5): 113-135.

Nayak, G. C. and O. C. Zienkiewicz (1972). "Note on the 'alpha' - constant stiffness method for the analysis of nonlinear problems." International Journal of Numerical Methods in Engineering(4).

Nour-Omid, B., C. Rodrigues, et al. (1983). Solution Techniques in Finite Element Analysis, Dept. of Civil Engineering, University of California.

O.C.Zienkiewicz and R. L. Taylor (2000). The Finite Element Method, Butterworth-Heinemann.

Pimanmas, A. and K. Maekawa (2001). "Multi-directional fixed crack approach for highly anisotropic shear behaviour in precracked RC members." Journal of Materials and Concrete Structures Pavements (JSCE)(669).

Ponthot, J. P. (2002). "Unified stress update algorithms for the numerical simulation of large deformation elasto-plastic and elasto-viscoplastic processes." International Journal of Plasticity 18.

R.Courant (1942). "Variational methods for the solution of problems of equilibrium and vibrations." Trans. Amer. Math. SOC.: 1-23.

Reddy, N. V., P. M. Dixit, et al. (2000). "Ductile fracture criteria and its prediction in axisymmetric drawing." Int. J. Mach. Tools Manuf. 40.

Riks, E. (1972). "The application of newtons method to the problem of elastic stability." Journal of Applied Mechanics 39.

Riks, E. (1979). "An incremental approach to the solution of snapping and buckling problems." International Journal of Solids and Structures 15.

Rots, J. G. (1993). "The smeared crack model for localized mode-I tensile fracture." Numerical Models for Fracture Mechanics.

Rots, J. G. (2001). "Sequentially linear continuum model for concrete fracture." Fracture Mechanics of Concrete Structure.

Rots, J. G. and S. Invernizzi (2004). "Regularized sequentially linear saw-tooth softening model." International Journal of Numerical And Analytical Methods in Geomechanics.

Rots, J. G., P. Nauta, et al. (1985). "Smeared crack approach and fracture localization in concrete." HERON(30).

Sabir, A. B. and A. C. Lock (1972). The application of Finite elements to the large deflection geometrically nonlinear behaviour of cylindrical shells. Conference on Variational Methods in Engineering. Southampton University.

Simo, J. C. and R. L. Taylor (1985). "Consistent tangent operators for rate-independant elastoplasticity." Computer Methods in Applied Mechanics and Engineering(48): 101-118.

Stankowski, T., K. Runesson, S. Sture (1993). "Fracture and slip of interfaces in cementituous composites. I. characteristics, and II: implementation." Journal of Structural Engineering (ASCE)(119).

Suidan, M. and W. C. Schnobrich (1973). "Finite element analysis of reinforced concrete." Journal of Structural Division (ASCE)(99).

Teng, J. G. and Y. F. Luo (1988). "A user-controlled arc-length method for convergence to predefined deformation states." Communications in Numerical Methods in Engineering 14.

Turner, M. J., R. W. Clough, et al. (1956). "Stiffness and Deflection Analysis of Complex Structures." Journal of Aerospace Science.

Voce, E. (1948). "The relationship between stress and strain for homogeneous deformation." Metallurgist.

Voce, E. (1955). "A practical strain-hardening function." Metallurgica.

Wemper, G. (1971). "Discrete approximation related to nonlinear theories of solids." International Journal of Solids and Structures 7.

Wifi, A. S., A. A. Hamid, et al. (1998). "Computer-aided evaluation of workability in bulk forming processes." J. Mater. Process. Technol. 77.

Wright, E. W. and E. H. Gaylord (1968). "Analysis of unbraced multistorey steel rigid frames." International Journal of Structural Division ASCE(94).

Xiao, R. Y. and C. S. Chin (2004). Fracture and Tension Softening of High Performance Fibrous Concrete. Proceedings of the Seventh Interntaional Conference on Computational Structures Technology, Stirling Scotland, Civil-Comp Press.

Xiao, R. Y. and C. S. Chin (2004). Nonlinear finite element modelling of the tension softening of conventional and fibrous cementitious composites. ACME Association of Computational Mechanics in Engineering, United Kingdom.

Xin, Y. (2005). Optimisation of the microstructure and mechanical properties of DP800 strip steel. Material Research Centre. Swansea, Swansea University. MPhil.

Zhang, K. S. and Z. H. Li (1994). "Numerical Analysis of the Stress-strain Curve and Fracture Initiation for Ductile Material." Engineering Fracture Mechanics 49.

Zheng, H., D. F. Liu, et al. (2005). "Displacement-controlled method and its application to material non-linearity." International Journal for Numerical and Analytical Methods in Geomechanics(29).

Zhu, J.-f. and X.-t. Chu (2002). "An improved arc-length method and application in the post-buckling analysis for composite structures." Journal Applied Mathematics and Mechanics (23).

Zienkiewicz, O. C. (1971). "Incremental displacement in nonlinear analysis." International Journal for Numerical and Analytical Methods in Geomechanics(3).

Zienkiewicz, O. C. and R. L. Taylor (1989). The Finite Element Method, McGraw-Hill Book Company.

Appendix

Appendix 1: True and engineering stress strain conversion

True stress can be related to the engineering stress with the assumption that there is no volume change in the specimen. This condition leads to the conservation of volume, i.e.

$$AL = A_0 L_0 \qquad \text{[A.1.1]}$$

Recall from equation [Eq.1.2]:

$$\sigma_t = \frac{P}{A} = \frac{P}{A_0}\frac{L}{L_0} \qquad \text{[A.1.2]}$$

Hence,

$$\sigma_t = \sigma_e\left(1+\varepsilon_e\right) \qquad \text{[A.1.3]}$$

The true strain can be defined as the sum of all the instantaneous engineering strains. Letting

$$d\varepsilon = \frac{dL}{L} \qquad [A.1.4]$$

Then the true strain is

$$\varepsilon_t = \int d\varepsilon = \int_{L_0}^{L_f} \frac{dL}{L} = \ln\left(\frac{L_f}{L_0}\right) \qquad [A.1.5]$$

where L_f is the final length when the loading is removed. True strain can also be related back to the engineering strain, through the manipulation

$$\varepsilon_t = \ln\left(\frac{L_f}{L_0}\right) = \ln\left(\frac{L_0 + \Delta L}{L_0}\right) \qquad [A.1.6]$$

$$\varepsilon_t = \ln(1+\varepsilon_e) \qquad [A.1.7]$$

As the strain increases, the cross-sectional area of the specimen decreases and for a constant load P, and recalling equations [Eq.1.1] and [Eq.1.2] the true strain is always larger than the engineering strain.

Appendix 2: The Ludwick power law relation

Ductile metals often exhibit true stress-strain relations that can be characterized by a simple power law relation of the form of:

$$\sigma = K\varepsilon^n \qquad [A.2.1]$$

where n is the strain-hardening exponential and K is the strength coefficient. A log-log plot of true stress-true strain up to the maximum applied load will result in a straight-line (Figure A.1). The linear slope of this line is n and K is the true stress attained at $\varepsilon = 1.0$. The strain-hardening exponent may have values from $n = 0$ (perfectly plastic solid) to $n = 1$ (elastic solid). Most metals has n values between 0.10 and 0.50

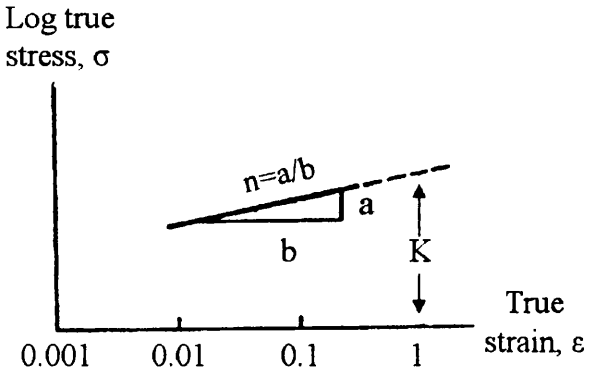

Figure A.1 – The log-log plot of true stress-strain curve

Appendix 3: The properties of Voce $\sigma_t - R$ curve

The strain ratio R is the ratio between the final and the original sectional area or length. It is arranged such that the greater area or length, whether before or after deformation, appears in the numerator of the fraction. Therefore the strain ratio is always greater than unity and the true strain is kept positive. Recall equations [Eq.1.1] and [Eq.1.2]. Hence, for the tension case;

$$R = \frac{L}{L_0} = \frac{A_0}{A} = \frac{\sigma_t}{\sigma_e} \qquad [A.3.1]$$

Simple rearrangement yields

$$\sigma_e = \frac{\sigma_t}{R} \qquad [A.3.2]$$

By equation [A.3.2], it follows that the condition of maximum engineering stress (at maximum load or necking point) is such that

$$d\sigma_e = \frac{\sigma_t^m dR^m - R^m d\sigma_t^m}{\left[R^m\right]^2} = 0 \qquad [A.3.3]$$

Since by definition the strain ratio is never less than unity, the denominator is not equal to zero and therefore:

$$\left(\frac{d\sigma_t}{dR}\right)^m = \frac{\sigma_t^m}{R^m} = \sigma_e^m \qquad [A.3.4]$$

Thus the slope of the curve at the maximum load, when strain ratios are used as the abscissa, is numerically equal to the engineering tensile strength σ_e^m of the material. This can be illustrated as shown in Figure A.2, in which any straight line drawn from the origin satisfies equation [A.3.1], the slope of the line being the applied engineering stress σ_e. Such a line can therefore be used to indicate the variations of true stress from point to point along a specimen, the sectional area of which may vary owing to necking or other causes, while it is subjected to the constant engineering stress σ_e.

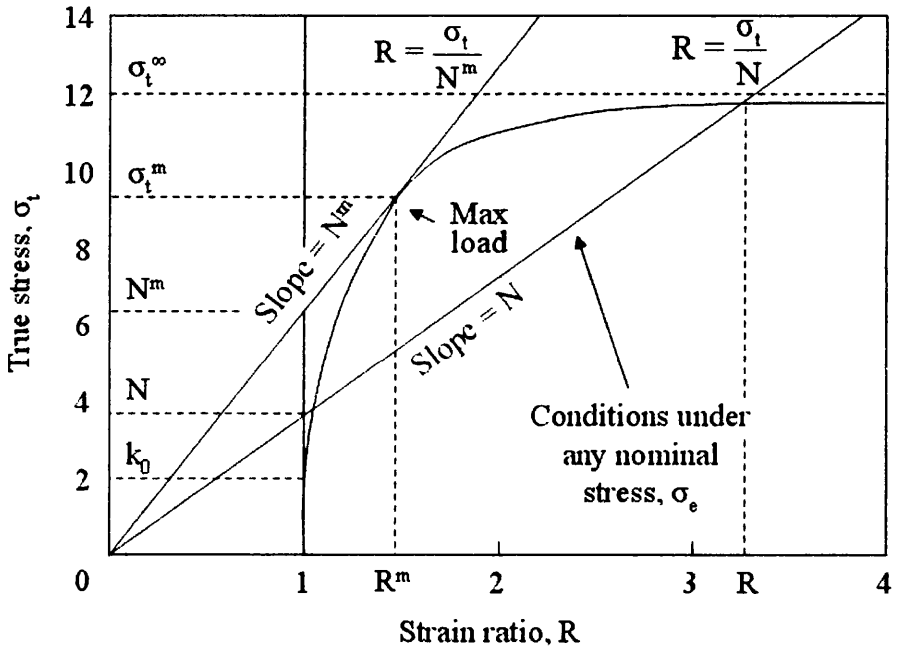

Figure A.2 – True stress-strain ratio $\sigma_t - R$ relation

The slope of the straight line is clearly at a maximum when it becomes tangent to the curve, and this tangent therefore defines the conditions at the maximum load; its slope being the engineering tensile strength σ_e^m while the coordinates of its point of contact

with the curve are respectively the true stress σ_f^m and the strain ratio R^m at the maximum load.

Appendix 4: Macros for the Setting of Analysis Environment

```
!*** Parameter input ***

MULTIPRO,'START',2
*CSET,1,3,EPEAK,'ENTER THE STRAIN @ PEAK STRESS',
*CSET,4,6,EPSFRAC,'ENTER THE STRAIN @ FRAC. STRESS',
MULTIPRO,'END'

MULTIPRO,'START',7
*CSET,1,3,CONST6,'ENTER CONSTANT6',
*CSET,4,6,CONST5,'ENTER CONSTANT5',
*CSET,7,9,CONST4,'ENTER CONSTANT4',
*CSET,10,12,CONST3,'ENTER CONSTANT3',
*CSET,13,15,CONST2,'ENTER CONSTANT2',
*CSET,16,18,CONST1,'ENTER CONSTANT1',
*CSET,19,21,CONST0,'ENTER CONSTANT0',
*CSET,22,24,SPTS,'ENTER THE NO. SOFT. POINTS', 5
MULTIPRO,'END'

!*** Setting environment for hardening analysis ***

*DIM,SIGEPS,TABLE,8,SPTS,1, , ,
*DO,I,1,SPTS,1
SIGEPS(0,I,1)=I
*ENDDO
*DO,I,1,8,1
SIGEPS(I,0,1)=I
*ENDDO
*DO,I,1,4,1
*GET,SIGEPS(I+2,1,1),NLISO,1,TEMP, ,CONST,I,
*ENDDO
*GET,YOUNG,EX,1,TEMP, ,
*GET,POSN,PRXY,1,TEMP, ,
RHS1 = CONST6*(EPEAK**6)+CONST5*(EPEAK**5)+CONST4*(EPEAK**4)
RHS2 = CONST3*(EPEAK**3)+CONST2*(EPEAK**2)+CONST1*EPEAK+CONST0
SIGULT = RHS1 + RHS2
*SET,SIGEPS(1,1,1) , SIGULT
*SET,SIGEPS(2,1,1) , (EPEAK - SIGULT/YOUNG)
*SET,SIGEPS(7,1,1) , 1.0
*SET,SIGEPS(8,1,1) , 1.0
```

```
! *** Setting environment for softening analysis ***

BETA = SIGULT/SIGEPS(3,1,1)
EPSINT = (EPSFRAC - EPEAK)/(SPTS-1)
*DO,I,2,SPTS,1
*SET,SIGEPS(2,I,1) , EPEAK + EPSINT*(I-1)
RHS1 = CONST6*(SIGEPS(2,I,1)**6)+CONST5*(SIGEPS(2,I,1)**5)+
CONST4*(SIGEPS(2,I,1)**4)
RHS2 = CONST3*(SIGEPS(2,I,1)**3)+CONST2*(SIGEPS(2,I,1)**2)+
CONST1*SIGEPS(2,I,1)+CONST0
SIGEPS(1,I,1) = RHS1 + RHS2
*SET,SIGEPS(2,I,1) , SIGEPS(2,I,1) - SIGEPS(1,I,1)/YOUNG
*SET,SIGEPS(3,I,1) , SIGEPS(1,I,1)/BETA
*SET,SIGEPS(4,I,1) , -100
LHS = SIGEPS(1,I,1)-SIGEPS(3,I,1)-SIGEPS(4,I,1)*SIGEPS(2,I,1)
TOL = 0.5
*DO,B,0.01,1000,0.01
RHS = -SIGEPS(4,I,1)*EXP(B*SIGEPS(2,I,1))*(1-EXP(-B*SIGEPS(2,I,1)))/B
ERROR = ABS(LHS-RHS)
*IF,ERROR,LT,TOL,*EXIT
*SET,SIGEPS(6,I,1) , B
*SET,SIGEPS(5,I,1) , -
SIGEPS(4,I,1)*EXP(SIGEPS(6,I,1)*SIGEPS(2,I,1))/SIGEPS(6,I,1)
*ENDDO
*ENDDO

!*** Setting environment for reduced-load optimization ***

*DIM,BISO,TABLE,3,SPTS,1, , ,
*DO,I,1,SPTS,1
BISO(0,I,1)=I
*ENDDO
*DO,I,1,3,1
BISO(I,0,1)=I
*ENDDO
*SET,BISO(1,1,1) , SIGEPS(3,1,1)
*SET,BISO(2,1,1) , (SIGEPS(1,1,1)-SIGEPS(3,1,1))/SIGEPS(2,1,1)
*SET,BISO(3,1,1) , (YOUNG*BISO(2,1,1))/(YOUNG - BISO(2,1,1))
*DO,I,2,SPTS,1
*SET,BISO(1,I,1) , SIGEPS(1,I,1)/(((BETA-1)/3)+1)
*SET,BISO(2,I,1) , (SIGEPS(1,I,1)-BISO(1,I,1))/SIGEPS(2,I,1)
*SET,BISO(3,I,1) , (YOUNG*BISO(2,I,1))/(YOUNG - BISO(2,I,1))
*ENDDO
```